DELIVERABLE D5.5
DATABASE OF PETROPHYSICAL AND FLUID PROPERTIES AND RECOMMENDATIONS FOR MODEL PARAMETRIZATION OF THE FOUR VARISCAN RESERVOIR TYPES

WP5: VARISCAN GEOTHERMAL RESERVOIRS (GRANITIC AND METAMORPHIC ROCKS)

Contractual delivery date:	M24
Actual delivery date:	M26

PROJECT INFORMATION

Grant Agreement n°	792037
Dates	1st May 2018 – 31 October 2021

This project has received funding from the European Union's Horizon 2020 research and innovation programme under grant agreement No 792037

DOCUMENT INFORMATION

Version	V5	**Dissemination level**	PU
Editor	Kristian Bär (TUDa)		
Other authors	Kristian Bär, Rhadityo Arbarim, Aysegül Turan, Katja Schulz, Saeed Mahmoodpour (TUDa), Bernd Leiss (UEG, UGOE), Bianca Wagner (UGOE, UEG), Graciela Sosa (UGOE), Katherine Ford (UGOE), Ghislain Trullenque (ULS), Johanne Klee (ULS), Yves Vanbrabant (GSB), Erik Rybacki, Harald Milsch, Johannes Herrmann, Wenxia Wang (GFZ), Xavier Sengelen, Ronan Hébert, Beatrice Ledésert (CYU)		

DOCUMENT APPROVAL

Name	Position in project	Organisation	Date	Visa
ALBERT GENTER ELEONORE DALMAIS	Project Coordinator	ES GEOTHERMIE	29/06/2020	OK
John Reinecker	Internal Reviewer	GeoT	22/06/2020	OK
JEAN HERISSON	Project Manager Officer	AYMING	29/06/2020	OK

DOCUMENT HISTORY

Version	Date	Modifications	Authors
V1	12/03/2020	Initial draft with request for contributions from partners	K. Bär / TUDa
V2	09/04/2020	Compiled contributions of TUDa, UEG, UGOE, GSB	See above
V3	29/04/2020	Reviewed V2	K. Bär / TUDa
V4	18/06/2020	Compiled contributions from ULS, CYU, GFZ, reviewed	See above
V5	24/06/2020	Completely restructured version after internal review by JRe	K. Bär / TUDa
VF	30/06/2020	Compiled contributions for Cornwall, internal review from A.Genter and J. Herisson included	K. Bär / TUDa

LIST OF FIGURES

LIST OF TABLES

PUBLIC SUMMARY

Deliverable D5.5 presents the current results of all petrophysical and hydrochemical investigations of the samples taken from the four Variscan demo sites and their respective outcrop analogues within MEET. In total 540 samples have been analyzed for their petrophysical properties summing up to more than 4000 single measurements. The geochemical or mineralogical characteristics were determined with thin section analysis or XRD and XRF measurements on 264 of the abovementioned samples to understand the key parameters controlling the rock properties in more detail. Further investigation is still ongoing.
All results are stored in one specifically designed comprehensive database. D5.5 furthermore provides a statistical analysis of the properties to parameterize numerical models of the different geotectonic settings encountered within MEET.

CONTENT

1. EXECUTIVE SUMMARY

Deliverable D5.5 presents the current results of all petrophysical and hydrochemical investigations of the samples taken from the four Variscan demo sites and their respective outcrop analogues within MEET. In total 540 samples have been analyzed for their petrophysical properties summing up to more than 4000 single measurements. The geochemical or mineralogical characteristics were determined with thin section analysis or XRD and XRF measurements on 264 of the abovementioned samples to understand the key parameters controlling the rock properties in more detail. Further investigation is still ongoing.

All results are stored in one specifically designed comprehensive database. D5.5 furthermore provides a statistical analysis of the properties to parameterize numerical models of the different geotectonic settings encountered within MEET.

1.1 DESCRIPTION OF THE DELIVERABLE CONTENT AND PURPOSE

This deliverable D5.5 '*Database of Petrophysical and fluid physical properties and recommendations for model parametrization of the four Variscan reservoir types*', is part of the EU MEET project and sums up the (preliminary) results of all petrophysical, rock mechanical and hydrochemical investigations within Task 5.1 (Characterization of the four Variscan Reservoir types) and Task 3.2 (*Structural reservoir geometry and petrophysical characterization for optimizing geothermal production from fractured crystalline rocks*). It is intended to provide the necessary input for Task 5.2 (*EGS Reservoir numerical simulation and validation*) in one comprehensive database. Based on the collected data recommendations it will give suggestions on how to statistically deal with the measurements to process them for model parametrization. This will also be the basis for the evaluation of rock heterogeneities and can allow for stochastic evaluation or modelling of the four Variscan reservoir types.

However, since MEET focusses mainly on fractured reservoirs of the Variscan basement of Europe, the petrophysical, rock mechanical and hydrochemical parameters presented in this deliverable only cover part of the reservoir characterization. The structural situation of the reservoirs including features like faults, folds, damage zones and fracture networks (as described in D5.4) are also key for reservoir characterization and will be more in the focus of D5.7 (*Strategies and recommendations for stimulation operations for the four Variscan reservoir types*) and D5.9 (*Field-based characterisation of the four reservoir types completed*).

In the present deliverable, section 2.1 presents the structure and internal design of the database, which groups all acquired data describing the meta-information of each sample collected at the different demo- and analogue sites. This includes petrophysical and rock mechanical data, petrographical data (hand specimen, thin section, XRD), geochemical data (XRF) and thermobarometric data (XRD, fluid inclusions). Section 2.2 presents first the sample material, the workflow of investigation and measurements methods, especially concerning petrophysical investigations. Secondly, it presents the preliminary results for the respective demo- and outcrop

analogue sites. Finally, section 2.3 presents some recommendations for model parameterization by providing exploratory statistics of the property measurements for all relevant rock types for each site respectively.

Although all petrophysical rock properties presented here were analyzed at laboratory conditions and therefore deviate from in situ properties at reservoir conditions, the presented dataset enhances the knowledge of petrophysical rock properties within the study area for further geothermal applications. To estimate the in-situ reservoir conditions, this dataset will be enlarged in future investigations by considering the increasing pressure, temperature and salinity at reservoir conditions. Alternatively, generic equations implemented in most numerical simulation codes can be used for correction (e.g. Bär 2012).

1.2 BRIEF DESCRIPTION OF THE STATE OF THE ART AND THE INNOVATION BREAKTHROUGHS

The state of the art is described in section 2.1 in detail.

The innovation breakthrough of this deliverable is given by the fact that except for the Soultz sous Forêts project, no comprehensive data on petrophysical or rock mechanical properties is available for the MEET demo sites. This deliverable thus presents the present state of the investigation results of the MEET partners following their aim to characterise the different reservoir rock types in more detail. These results provide a much better dataset for the parametrisation of numerical simulations of the different test, which can be generally applied for the characterisation of the Variscan basement of Europe. The dataset furthermore provides the basis for task 5.2 (*EGS Reservoir numerical simulation and validation*) of the MEET project.

1.3 CORRECTIVE ACTION (IF RELEVANT)

Two corrective actions were necessary for D5.5 due to the impact of the COVID19 pandemic.

The first concerns the UDDGP project, which had its wells finished already in July 2019. The third phase of the program focus on the workover operations, which include downhole logging, the collection of side-wall cores (SWC) and hydraulic testing, was initially planned for end of March 2020 had to be postponed and are now planned for end of July / beginning of August 2020. Therefore, the only available reservoir samples available for D5.5 are the drill cuttings from the well UD-1. Investigation and characterization of the SWCs will therefore only be possible from August onward and will complete the rock property determination for the UDDGP demosite.

The second corrective action concerned the whole MEET project since due to the COVID-19 lockdown of the lab facilities of all partners, no lab investigations where possible between March and May 2020. D5.5 had thus to be postponed by two months and due to the ongoing impact does still not contain the final results from all partners and demo- and outcrop analogue sites

respectively. The final results will be included into D5.9 and the excelfile P³2MEET will be continuously updated on Aymingsphere. The current results presented here however, are providing a significant improvement compared to the state of the art before MEET.

1.4 IPR ISSUES (IF RELEVANT)

NA

2. DELIVERABLE REPORT

2.1 GENERAL DESCRIPTION OF THE DATABASE P³2MEET

2.1.1 Summary

Petrophysical and fluid properties are key parameters to populate local and/or regional numerical models and to interpret results from geophysical investigation methods. Searching for rock property values measured on samples from a specific rock unit at a specific location might become a very time-consuming challenge given that such data are spread across diverse compilations and that the number of publications on new measurements is continuously growing and data are of heterogeneous quality. Profiting from existing laboratory data to populate numerical models or interpret geophysical surveys at specific locations or for individual reservoir units, is often hampered if information on the sample location, petrography, stratigraphy, measuring method and conditions are sparse or not documented.

Within the framework of the EC funded project IMAGE (Integrated Methods for Advanced Geothermal Exploration, EU grant agreement No. 608553), an open-access database of lab measured petrophysical properties has been developed (Bär *et al.*, 2019: P³ - Database, http://dx.doi.org/10.5880/GFZ.4.8.2019.P3), which has been extended significantly by additional data types for the purpose of the project MEET.

The goal of this hierarchical database is to provide easily accessible information on physical rock and fluid properties as well as geochemistry and fluid inclusions relevant for geothermal exploration and reservoir characterization in a single compilation. Collected data include 'classical' petrophysical, thermophysical and mechanical properties and, in addition, electrical conductivity and magnetic susceptibility and is now complemented by bulk rock geochemistry, thin sections and fluid inclusion analyses for MEET.

Each measured value is complemented by relevant meta-information such as the corresponding sample location, petrographic description, chronostratigraphic age, if available, and original citation. The original stratigraphic and petrographic descriptions are transferred to standardized catalogues following a hierarchical structure ensuring inter-comparability for statistical analysis (Bär *et al.*, 2019: P³ - Petrography, http://dx.doi.org/10.5880/GFZ.4.8.2019.P3.p, Bär *et al.*, 2019: P³ - Stratigraphy, http://dx.doi.org/10.5880/GFZ.4.8.2019.P3.s).

In addition, information on the experimental setup (methods) and the measurement conditions are listed for quality control. Thus, rock properties can directly be related to in-situ conditions to derive specific parameters relevant for simulating subsurface processes or interpreting geophysical data.

We have updated this P³ database as part of the MEET project to the P²2MEET version which includes some additional properties and information. In the following, we describe the structure, content and status quo of the database and discuss its limitations and advantages for the end-user.

2.1.2 Introduction

The characterisation and utilisation of subsurface reservoirs generally relies on applying geophysical investigation methods and/or numerical simulations– both requiring, in turn, the knowledge of petrophysical properties at depth. The strategy of populating numerical models with petrophysical properties can differ. For local-scale models, laboratory data from individual samples collected from the geological unit of interest may exist. In this case, this direct information should be used together with physical and empirical laws to populate the entire geological unit. For regional and continental-scale models, in contrast, parameters have to be generalised with respect to the spatial and physical variability of the investigated lithological units.

Individual rock types typically exhibit a variability in petrophysical properties due to anisotropic mineral composition, variable texture and porosity distribution (Schön, 2015). Existing compilations of rock properties reflect the high variability and the different purposes of such databases (e.g. Cermak and Rybach, 1982, Clark, 1966, Clauser and Huenges, 1995, Landolt-Börnstein, PetroMod, Schön, 2004, 2011, 2015, Mortimer, 2005, Hantschel and Kauerauf, 2009, Lilios and Exadaktylos, 2011, Descamps *et al.*, 2013, Aretz *et al.*, 2015). Most compilations are published with limited meta-information, and it is difficult to extract data for formations of interest. Additionally, existing compilations are often focused on distinct rock types and/or geographic regions (e.g. Germany: FIS Petrophysik hosted by the Leibniz Institute of Applied Geophysics (LIAG) (http://www.fis-geophysik.de), Great Britain: BritGeothermal (http://www.britgeothermal.org) hosted by the British Geological Survey (BGS), USA: National Geothermal Data System (NGDS) hosted by a federate infrastructure including national organizations and academia (e.g., the United States Geological Survey, Southern Methodist University, Association of American State Geologists, U.S. Department of Energy's Geothermal Data Repository, http://geothermaldata.org), Ireland: IRETherm project (http://www.iretherm.ie/), Australia: Rock Properties Explorer (http://www.ga.gov.au/explorer-web/rock-properties.html), New Zealand: PETLAB: National Rock and Geonalytical database(http://pet.gns.cri.nz/#/, and many more).

Furthermore, exploration data availability often depends on national legislation. In some countries industrial exploration data, including petrophysical properties measured on cores of deep wells, may be made public after a certain time period and then usually is incorporated in national information systems. In other cases exploration data remains confidential for longer time periods or even infinitely resulting in scarce data availability if no budget for acquisition of such data is available.

Due to the current publication policy of international research institutions where a high number of peer-reviewed publications become more and more important for the individual scientific career, the amount of petrophysical data recorded worldwide increased dramatically. These publications however, are spread over many different geoscientific journals and are dispersed in many hundreds of publications. Given the rate of newly published property data combined with

the multitude of publishing journals, countries and authors, the research for and collection of data can be incredibly time-consuming. Recent studies show that domain experts spend nearly 80% of their working hours into collecting, cleansing and managing their domain specific data (CrowdFlower, 2016). An effective, comprehensive collection, collation and dissemination of this data are deemed critical to promote rapid, creative and accurate research (Gard *et al.*, 2019).

To facilitate (i) efficient search for and research on measured rock physical properties, (ii) further evaluation of the property data using complementing meta-information, and (iii) adequate property generalisation for specific units, a comprehensive database was developed within the framework of the project IMAGE project. The aim of this database is to compile, store and publicly provide petrophysical property data from published laboratory test results on rock samples of any kind including as much meta-information as possible. So far, literature data and laboratory data collected during the IMAGE project were fed into this novel PetroPhysical Property (P^3) Database (Bär *et al.*, 2019: P³ - Database, http://dx.doi.org/10.5880/GFZ.4.8.2019.P3).

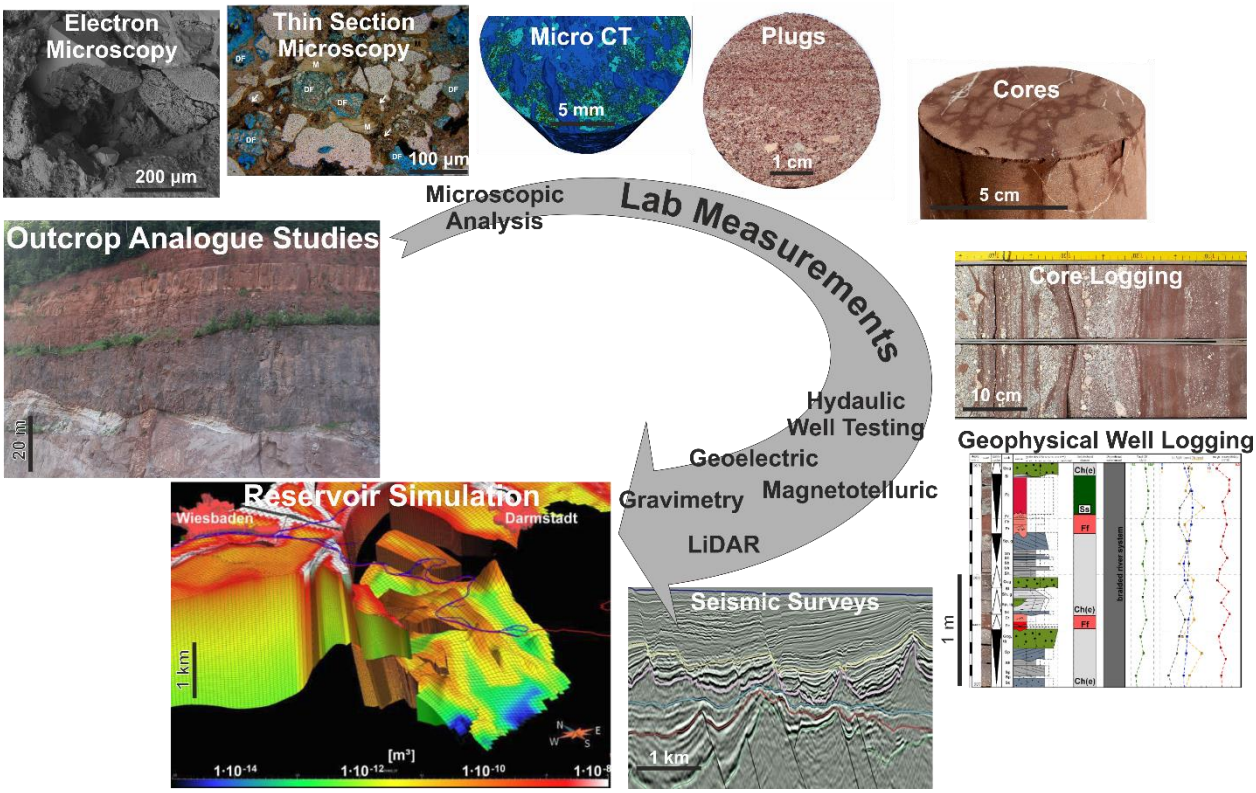

Figure 1: Concept of multiscale characterisation of geological reservoirs with (examples of) integrated petrological, petrophysical or geophysical methods bridging outcrop analogue studies to numerical reservoir simulations.

2.1.3 Contents and Structure of the Database

P³ is publicly accessible and contains physical rock properties measured in laboratory experiments. It is licensed under a creative commons (CC-BY 4.0) license and its structure follows the FAIR guiding principles for scientific data management and stewardship (Wilkinson *et al.* (2016). All data are selected to represent the characteristic scale of rock samples in the range of a few centimetres to decimetres, depending on the measurement methods for the different properties (as described by numerous norming institutions or committees as e.g. the International Society for Rock Mechanics and Rock Engineering (ISRM), European Committee for Standardization (C)EN, International Organization for Standardization (ISO), American Society for testing and Materials (ASTM international) and many more). Within P³ we aimed at homogenising measurement method descriptions to increase the inter-comparability between individual reported values. Larger-scale data from geophysical well logging, hydraulic well testing, integrating geophysical methods or other field-scale measurements, which integrate over larger rock volumes or several rock types, are not yet included in the database (Figure 2). This shall ensure to reduce sampling bias introduced by heterogeneities within larger geobodies including discontinuities like fractures, bedding or schistosity. In addition, judged based on the lithological description, we did not include data from very small scale samples, where the volume of interest is likely smaller than the minimum representative elementary volume (REV) (e.g. Ringrose and Bentely, 2015) for the investigated rock type. The full range of the scale-dependency of petrophysical properties as described in previous studies (e.g. Enge *et al.*, 2007, Rühaak *et al.*, 2015) is thus not yet reflected by the database but is planned to be incorporated in future versions.

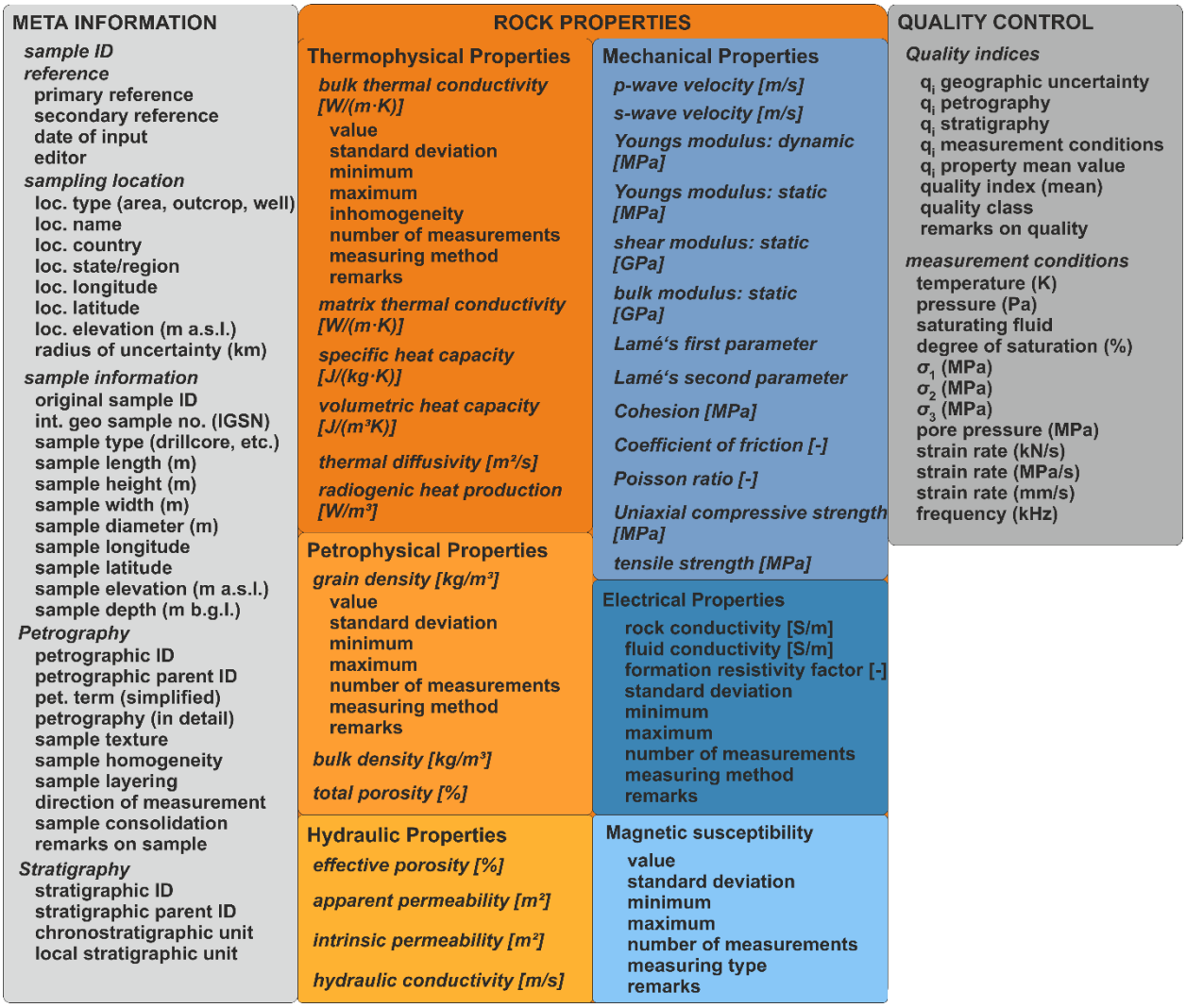

Figure 2: Schematic structure of P³ illustrating the three sections or super entities: 'meta information', 'rock properties' and 'quality control'. Different input parameters (small font) are grouped according to entities or property sub-tables (italics) they belong to.

To ensure that source data are publicly available to researchers, only data from scientific publications (books or peer reviewed journals) or proceedings (e.g. IGA Geothermal Papers/Conference Database) as well as published research reports (e.g. dissertations, master theses, project reports) were included in P³. We have only included data for which a minimum amount of meta-information is documented in order to allow reasonable interpretations, generalisations, or simulations based on the collected data. The minimum meta-information necessary is the reference to the data origin (citation) and information about the petrography / lithotype. If available, additional meta-data were included, such as the sampling location (potentially including its type, e.g. outcrop, abandoned or active quarry, vertical or deviated well), the affiliation to a registered sample set (e.g. International Geo Sample Number (IGSN, cf. Devaraju *et al.*, 2016, Lehnert *et al.*, 2006)), stratigraphy, sample dimensions, measurement method or device and measurement conditions (pressure, temperature, stress) including degree

of saturation and type of saturating fluid. Conversion to SI units as well as correction of some minor errors or omissions from previous databases as they are identified is an ongoing process during the data curation.

The database was developed as flat-file format using Microsoft Excel to keep it as simple and easy to handle as possible, even by the unexperienced user. Other database structures may be much more efficient, their database management schemes however may be too difficult to render for users not familiar with SQL to recover the desired information. However, the internal design of P³ with multiple tables is structured following a relational database management system (RDBMS, Codd, 1970) so that it could easily be transferred to e.g. the well-established structured query language (SQL, Chamberlin and Boyce, 1974). Following this relational structure the database could easily be organised into multiple tables using the names of the tables as unique keys as links to other sub-tables. The main advantages of a relational database over a flat file format are that data is uniquely stored just once, eliminating data duplication, as well as performance increases due to greater memory efficiency and easy filtering and rapid queries (Gard *et al.*, 2019). This current structure allows for easy modification and extensions as new requirements emerge, as for example by adding more sub-tables for newly developed property measurements not fitting to any of the already included properties could be added at later stages. On the other hand, filtering and quality control to ensure that data is entered into the database only once and that no duplicates exist had to be done manually. In our case data duplicates where removed by checking the coordinates of each data point with a radius of uncertainty of 1 km and, if necessary, manually removing every double entry identified.

Following the minimum requirements, the database is structured into three main sections or super entities (Figure 2), which are sets of data tables (described in more detail in the following parts of the paper). The first, named ‘meta information’, contains all meta-information on the sample including the sampling location, the sample type and dimensions as well as information on its petrography and stratigraphy and thus acts as primary table for unique sample identification. The second section or super entity contains the measured property value(s) of the unique rock samples. This section is sub-grouped into thermo-physical properties, ‘classical’ petrophysical properties, mechanical properties as well electrical and magnetic properties and fields for property specific remarks. Finally, the third section or super entity named ‘quality control’ includes all information relevant for the quality assessment of each data record (property measurement of the unique samples). Here, especially information on the measurement conditions (methodology, pressure and temperature conditions, degree of saturation etc.) are documented and used for the implemented semi-automatic quality control and assessment.

The first super-entity ‘meta-information’ consists of five tables or entities: sample ID, reference, sampling location, sample information, petrography and stratigraphy. A description of each of these tables is included in the following sub-chapters. The tables for petrography and stratigraphy are available separately. The super-entity ‘rock properties’ contains 28 separate sub-tables for all properties included so far into the database each following a similar internal structure. For many samples measurements of multiple properties were available and included into the database, which results in multiple documentation of the ‘meta-information’ of these samples in the current file structure. The super-entity ‘quality control’ contains two tables or

entities, the first one for documentation of the measurement conditions and the second one for the automated quality assessment of the entries.

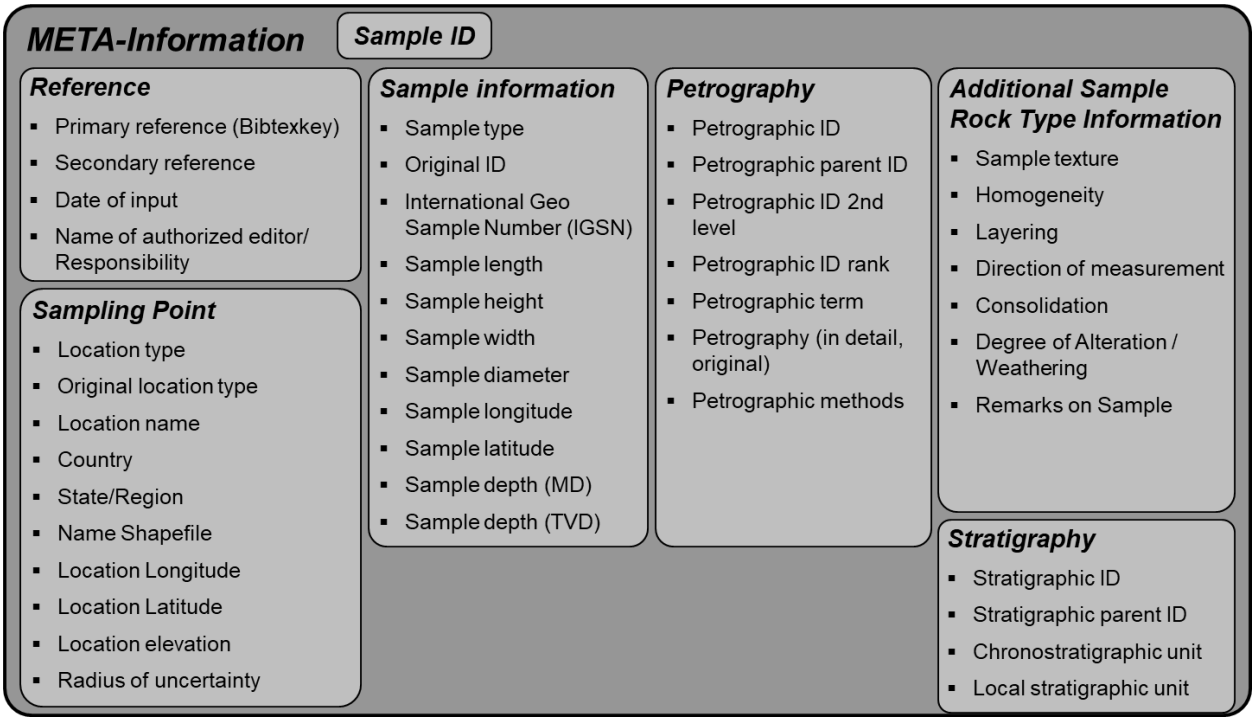

Figure 3: Structure of the metadata sub-tables for each measured value in P³ corresponding to the individual rock sample.

2.1.3.1 Sample Information

To distinguish measurements of different properties on a single sample or of the same properties performed at varying measurement conditions, every measurement is listed in a separate row. To group measurement data from individual samples, every sample receives a unique sample ID, which acts as the primary key of each record and links multiple measurements conducted on a single rock sample. The sample ID consists of the surname of the first author and the year of publication, together with a sequential number for the particular rock sample presented in the respective publication. In case of several references per author and year an additional letter (a, b, …) is introduced after the year.

For example, Fourier1822_1 stands for sample 1 within a publication of Fourier, J.B.J. (1822). In case of more than one publication per year Fourier1822a_1 would represent sample 1 within a publication of Fourier, J.B.J. (1822a). The sample ID is linked to an accompanying reference database, compatible to all major reference management tools (e.g. EndNote, Citavi, BibTeX, JabRef, etc.), which contains the full information (Co-Authors, full title, journal, volume, pages, etc.) on the reference. The references are abbreviated in a Bibtexkey according to the terminology used for individual samples. At best, only primary references are given. In case the primary reference is unavailable, while the data point is published as part of a review (or the like), a secondary reference was introduced.

Additionally, the date of input and the name of every person who generated the entry into the database or changed during later QC (the editor) is documented.

Specifically for MEET, all crucial samples and related subsamples collected and investigated within WP5 are labelled after the naming convention shown in Figure 4 as it was agreed at the 2nd WP5-meeting in Göttingen early November 2018 (MEET Deliverable 5.2, 2019). All names start with the project identification MEET. Each demonstration site is represented by the two letters under "Demo site ID". The abbreviation "PB" as an ID for the Paris Basin and "AB" as an ID for the Aquitaine Basin was defined after the meeting in line with CYU (formerly UCP). The "Location ID" refers to surface and subsurface outcrops as well as to drill sites. Sample and subsample ID refer to a sequential numbering of the specimen.

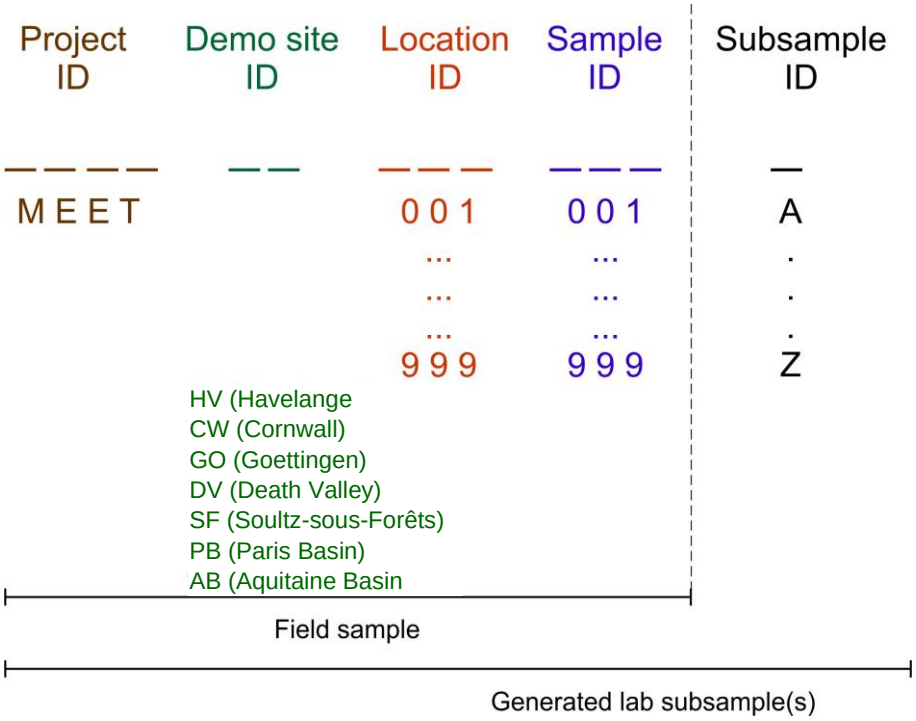

Figure 4: Scheme of the sample naming convention within MEET

All lab and experimental data generated within WP5 are stored in the P³ Database. TUDa provided tailored Excel sheets on Aymingsphere for data entry, which will be carried out by the respective person/partner, who primarily created the data. Each partner has to take care of the data quality control. The final quality check will be conducted by TUDa during the data migration process into the database.

The setup or adaption of parameter-specific input tables and masks that are not available by now, has to be clarified by each partner with TUDa.

2.1.3.2 Sampling Location

The sub-section 'sampling location' contains all relevant information on the location where a sample was obtained. Generally, rock samples can be sampled in an outcrop, a quarry or a well.

In case neither the sampling location is given as outcrop, quarry or well, nor any exact coordinates are given in the corresponding publication, the location type “area” is selected. Furthermore, for every location type, a name, a country and state is given (e.g. location type: outcrop, location name: Fontainebleau, location country: France, location state/department: Seine-et-Marne).

2.1.3.3 Location Coordinates

The location coordinates describe the latitude and longitude with the reference system WGS84 of the sampling point at the surface in decimal degrees. Another category of entry is the elevation given in metres above sea level (m.a.s.l.). In the case of a core sample taken from a well, the latitude and longitude of the wellhead is given. In case of an area with undefined sampling point, e.g. “sample from the Rhenish Massif”, a midpoint from this geological province has been assessed and a radius of uncertainty (in km) for the sampling location is estimated. For elongated areas (e.g. the Red Sea, the Upper Rhine Graben etc.) the choice of a circular radius of uncertainty artificially increases the uncertainty. The introduction of polygons for the definition of an area is discussed to be included in future releases of the database. If no information is given for the location, the longitude and latitude are noted as 999 to avoid wrong map displays and half the circumference of the earth is used as uncertainty.

For a conversion of the sample coordinates retrieved from the literature we used either Google Earth (Web Mercator Projection) or ArcGIS to allocate a latitude/longitude value in decimal degrees and a rough estimation of the associated uncertainty to each data point. We are aware that this 'Google maps method' is not accurate but exact geographic information is quite often not provided in the literature used for this compilation. Most common are the provision of location names or maps only. For all literature data points where both the exact coordinates and the reference system was given, or where the location was given on a georeferenced map with the required information on the coordinate system used, we used ArcGIS for transformation. Therein, we used the same geographic projection as given in the original literature and either included the points as tabular values or we georeferenced the given maps accordingly and picked the points on the maps. Afterwards, the resulting coordinates were transferred to decimal degrees in the WGS84 reference with the transformation method for the specific projected coordination system as suggested by ArcGIS. We have not documented the exact coordinate transformation used in each case since a rough location is in by far most cases of database use sufficient.

2.1.3.4 Original Sample ID

To allow for reviewing original publications, the primarily given sample identification numbers or names are documented in addition to the P³ sample ID. This makes it easier to search for a specific sample in a publication, which might have been used for further measurements or more detailed descriptions by other authors subsequently or individual users of the database.

2.1.3.5 International Geo Sample Number

The International Geo Sample Number (IGSN, cf. Devaraju *et al.*, 2016, Lehnert *et al.*, 2006) is a unique identifier for samples and specimens collected from the natural environment (http://www.igsn.org/). In order to enable locating, identifying, and citing physical samples, the

IGSN number was listed if available. Furthermore, entries allow for cross-linking both, the P³ as well as the IGSN database in order to ensure access to more meta-information like sampling methods, project related information, etc., currently not implemented in P³. As described by Strong *et al.* (2016) the adoption of IGSNs will ensure compatibility and interoperability with other international databases, including the promotion of standard methods to locate, identify and cite physical samples.

2.1.3.6 Sample Type

Samples can have different shapes that are particularly relevant for the measurement technique. Core samples do have different characteristics than rock blocks or drill cuttings, etc. so that P³ reserves a separate column for the sample type.

2.1.3.7 Sample Dimensions

Together with the documentation of the sample type, if available, information about its length, height, width and for cores, diameter, all given in meters, are documented. If the rock property "density" is measured for any sample where the dimensions are given, sample volume and weight might be calculated as well. This additional information together with its petrography was essential to evaluate whether a sample reaches a Representative Elementary Volume (REV) or not.

2.1.3.8 Sample Coordinates

For several samples taken at a single sampling location (e.g. a large outcrop or quarry), eventually individual sample coordinates are given (longitude, latitude and elevation). For samples from a cored well, additionally, the depth of the sample is given in measured depth (MD) and, if available, in true vertical depth (TVD) referenced to the ground level (i.e. meters below ground level, m b.g.l.). If data on the geometry of deviated wells are available, it is optional to either enter the sample location relative to the wellhead or with its exact location and elevation (with respect to the sea level).

2.1.3.9 Petrography or Rock Type

The petrography or rock type classification scheme is defined in a complementary database (Bär *et al.*, 2019: P³ - Petrography, http://dx.doi.org/10.5880/GFZ.4.8.2019.P3.p) directly published together with P³. Its internal structure is based on a hierarchical subdivision of rock types, where the rock description generally becomes more detailed with increasing rank of petrographic classification (based on the well database of the Geological Survey of Hessen, Germany: Hessisches Landesamt für Umwelt, Naturschutz, Umwelt und Geologie (HLNUG)). This hierarchical subdivision is based on international conventions (e.g. Bates and Jackson, 1987, Gillespie and Styles, 1999, Robertson, 1999, Hallsworth and Knox, 1999, Bas and Streckeisen, 1991, Schmid, 1981, Fisher and Smith, 1991). Furthermore, the classification corresponds to the subdivision provided by existing property data compilations such as e.g. Hantschel and Kauerauf (2009), Schön (2011), Rybach (1984) and Clauser and Huenges (1995).

Petrographic classifications from rank 1 to rank 4 can usually be identified from macroscopic descriptions of well logs, cores and geological mapping (Figure 5). The petrographic classifications from rank 5 to rank 9 require additional information on the texture or grain size, the modal

composition or the geochemistry etc., which can usually only be acquired by microscopic or comparable special investigations. Overall, there are nine ranks covering a total of 1494 petrographies. The petrographic classification of a sample in P³ is based on the sample description within the original literature reference. A petrographic ID and a corresponding petrographic parental ID directly correlate the different classifications and their ranks (Table 1). This allows for example, to integrate all petrographies with higher ranks to a corresponding general term of lower rank and statistically analyse the associated physical rock property values across petrographic definition boundaries (Figure 5).

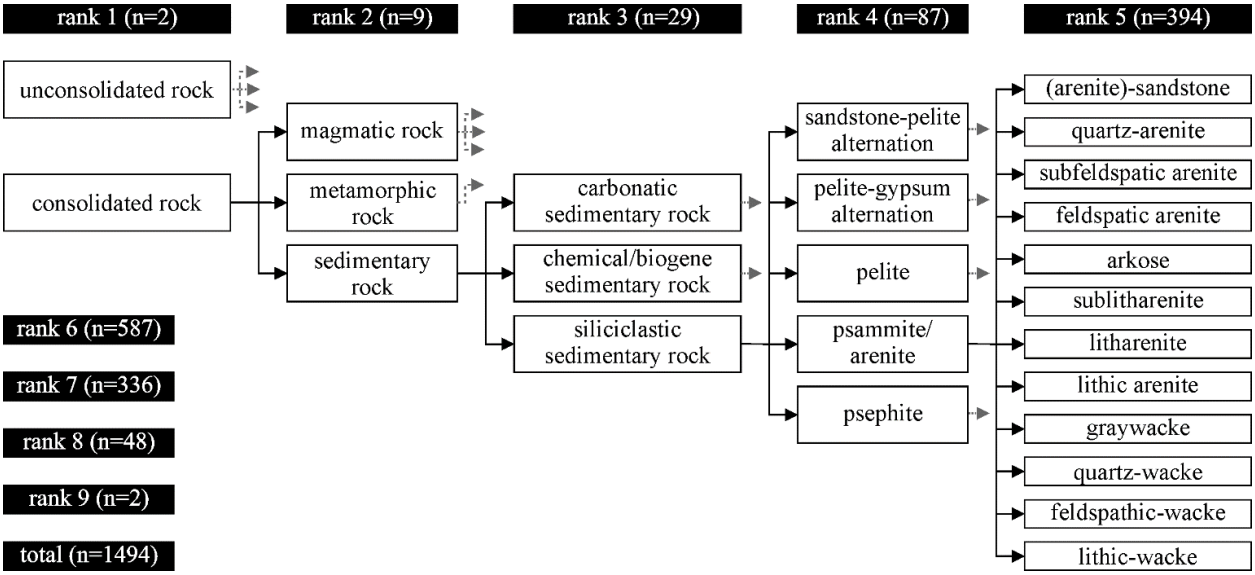

Figure 5: Hierarchical system of standardised petrographic terms used for the database. White boxes are an exemplarily chosen extract to illustrate the structure of the petrography classification. Black boxes document the number of rock type categories per rank for the entire classification scheme. These interconnected standardised terms allow for the connection of certain lithologies/petrographies to specific petrophysical properties and are thus the basis for statistical analysis. Black arrows show direct connections, while grey arrows indicate that there are additional terms not displayed here.

In P³, the petrographic ID, the petrographic parent ID and the simplified petrographic term are documented. Additionally, for each sample original petrographic descriptions of the primary references can be presented if available. Details on the texture, homogeneity, layering, consolidation state of the sample and the direction of measurement with regard to internal structural features (such as bedding etc.) as well as degree of alteration or weathering can be documented together with specific remarks.

Table 1: Excerpt from the rock classification table used for P³. Different ranks and their interconnection by petrographic ID and petrographic parent ID as well as their connection to international definitions as indicated. QAPF = Quartz-Alkali feldspar-Plagioclase-Foids (Le Maitre and Streckeisen, 2003).

Petro-graphic ID	Petro-graphic parent ID	Rank	Petrographic term	Definition
10102		1	Consolidated rock	
10104	10102	2	Magmatic rock	Rock formed from magma
10105	10104	3	Plutonic rock	Igneous rock with phaneritic texture
52349	10105	4	Plutonic rock, modal (QAPF)	Intrusive igneous rock, nomenclature by QAPF-classification for plutonic rocks
10107	52349	5	Quartzolite (QAPF)	QAPF-classification for plutonic rocks, field 1a, Qz > 90 vol%
10110	52349	5	Granite (QAPF)	QAPF-classification for plutonic rocks, field 2, 3a, 3b, colour index < 90 %
10111	10110	6	Alkali-Feldspar-Granite	QAPF- classification for plutonic rocks field 2
10112	10110	6	Syenogranite	QAPF- classification for plutonic rocks field 3a
10113	10110	6	Monzogranite	QAPF- classification for plutonic rocks field 3b
10114	52349	5	Granodiorite (QAPF)	QAPF-classification for plutonic rocks, field 4, colour index < 90 %
10115	52349	5	Tonalite (QAPF)	QAPF-classification for plutonic rocks, field 5, colour index < 90 %
10127	52349	5	Syenite (QAPF)	QAPF-classification for plutonic rocks, field 7, colour index < 90 %
10128	52349	5	Monzonite (QAPF)	QAPF-classification for plutonic rocks, field 8, colour index < 90 %
10129	52349	5	Monzodiorite (QAPF)	QAPF-classification for plutonic rocks, field 9, An (PL) < 50 mol%, colour index < 90 %
10130	52349	5	Monzogabbro (QAPF)	QAPF-classification for plutonic rocks, field 9, An (PL) > 50 mol%, colour index < 90 %
10131	52349	5	Diorite (QAPF)	QAPF-classification for plutonic rocks, field 10, An (PL) < 50 mol%, 10 % < colour index < 90 %
10132	52349	5	Gabbro (QAPF)	QAPF-classification for plutonic rocks, field 10, An (PL) > 50 mol%, 10 % < colour index < 90 %

2.1.3.10 Stratigraphy

The stratigraphy of each sample was inserted into the database in two complementary ways. The first way is to use the definitions of the international chronostratigraphic chart of the IUGS v2016/04 (Cohen *et al.*, 2013, updated) according to international standardisation. These chronostratigraphic units are also compiled in a complementary database (Bär *et al.*, 2019: P³ - Stratigraphy, http://dx.doi.org/10.5880/GFZ.4.8.2019.P3.s) to ensure that formations of a certain age are connected to the corresponding stratigraphic epoch, period or erathem. Thus, the chronostratigraphic units are directly correlated to each other by their stratigraphic ID and stratigraphic parent ID, allowing for statistical analysis of the properties of certain stratigraphic units (Table 2). In contrast (second way), a more detailed description of the local stratigraphic unit can also be documented if provided in the primary reference.

Table 2: Excerpt from the stratigraphic classification table used for P³ (based on Cohen *et al.*, 2013, updated). Different ranks and their interconnection by stratigraphic ID and stratigraphic parental ID are indicated. Num. = numerical; SD = standard deviation; Phan. = Phanerozoic.

Strati-graphic ID	Strati-graphic parent ID	Eon	Era	Period	Series / Epoch	Stage / Age	Num. Age [Ma]	SD num. Age [Ma]	Chronostrati-graphical unit
129	102	Phan.	Mesozoic	Cretaceous			145		Cretaceous
130	129	Phan.	Mesozoic	Cretaceous	Lower		145		Lower Cretaceous
131	130	Phan.	Mesozoic	Cretaceous	Lower	Berriasian	145		Berriasian
132	130	Phan.	Mesozoic	Cretaceous	Lower	Valanginian	139.8		Valanginian
133	130	Phan.	Mesozoic	Cretaceous	Lower	Hauterivian	132.8		Hauterivian
134	130	Phan.	Mesozoic	Cretaceous	Lower	Barremian	129.4		Barremian
135	130	Phan.	Mesozoic	Cretaceous	Lower	Aptian	125		Aptian
136	130	Phan.	Mesozoic	Cretaceous	Lower	Albian	113		Albian
137	129	Phan.	Mesozoic	Cretaceous	Upper		100.5		Upper Cretaceous
138	137	Phan.	Mesozoic	Cretaceous	Upper	Cenomanian	100.5		Cenomanian
139	137	Phan.	Mesozoic	Cretaceous	Upper	Turonian	93.9		Turonian
140	137	Phan.	Mesozoic	Cretaceous	Upper	Coniacian	89.8	0.3	Coniacian
141	137	Phan.	Mesozoic	Cretaceous	Upper	Santonian	86.3	0.5	Santonian
142	137	Phan.	Mesozoic	Cretaceous	Upper	Campanian	83.6	0.2	Campanian
143	137	Phan.	Mesozoic	Cretaceous	Upper	Maastrichtian	72.1	0.2	Maastrichtian

2.1.4 PetroPhysical Properties

The properties included in P³ can be grouped into 'classical' petrophysical properties, thermo-physical properties, mechanical properties as well as electrical and magnetic properties (Figure 6). Overall, 28 different rock properties are included so far and documented in separate sub-tables of the database following a similar internal structure. Based on the original reference, the measurement is given as a value, which if available is complemented by a standard deviation, a minimum and maximum value and the number of measurements. Thus, it is possible to either include single measurements or mean values while still offering the opportunity of statistical evaluation by incorporating the number of measurements corresponding to a mean value. Furthermore, the measurement method for each property value is presented by means of a common nomenclature documented in the supplementary report (Bär *et al.*, 2019: P³ - Data Description, http://dx.doi.org/10.5880/GFZ.4.8.2019.P3). This is important for statistical analysis and comparability of the results of different methods. Particularly, the type of method might have a large impact on the quality and device-specific error of any measurement. Finally, specific remarks can be made for each value separately.

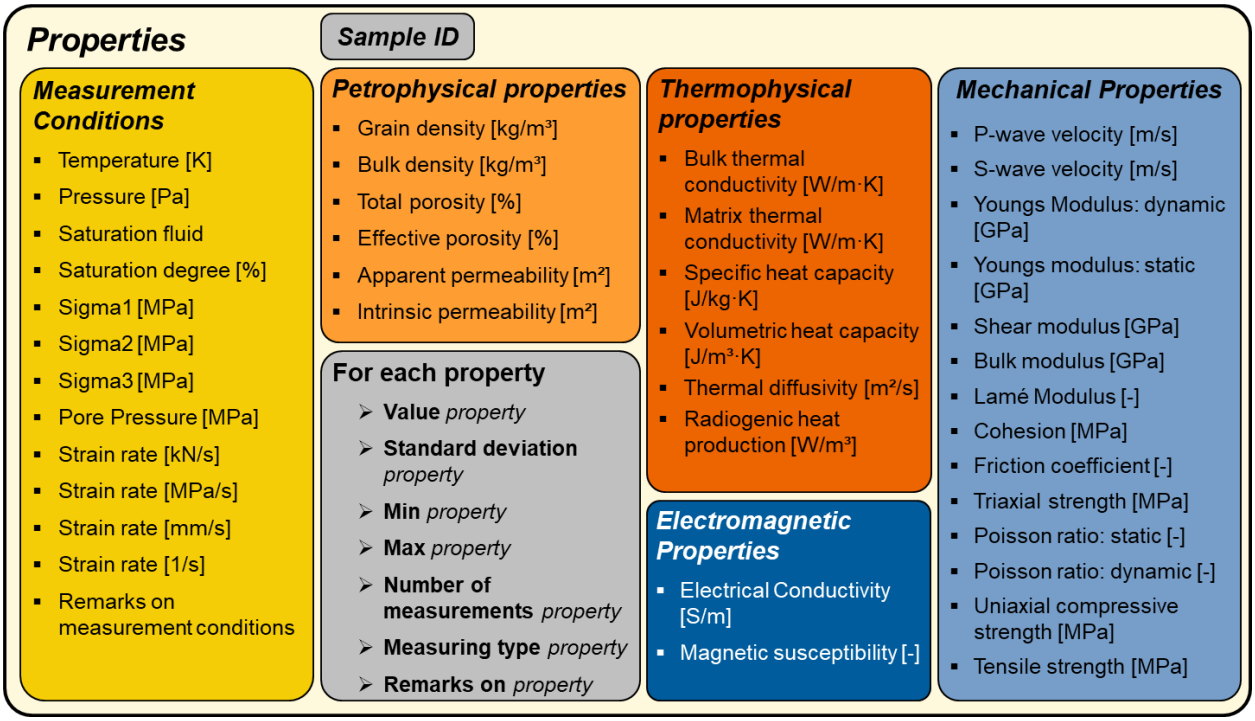

Figure 6: Structure of the properties and measurement conditions sub-tables as listed in P³.

2.1.5 Geochemistry

As addition to the published version of P³ we included for the MEET-specific version 'P³2MEET' a separate table where data on the bulk geochemistry can be included following the structure of the 'Global whole-rock geochemical database compilation' by Gard *et al.* (2019). They have compiled a global whole rock geochemical database, sourced from various existing databases and supplemented with an extensive list of individual publications. Currently this database stands at 1 022 092 samples with varying amounts of associated sample data, including major and trace element concentrations, isotopic ratios, and location information (Figure 7), which depending on their location can be of relevance for the characterization of the variscan basement rocks of Europe within MEET. Spatial and temporal distribution is heterogeneous; however, temporal distributions are enhanced over some previous database compilations, particularly in ages older than 1000 Ma. Also included are a range of geochemical indices, various naming schema, and physical property estimates computed on a major element normalized version of the geochemical data for quick reference. This compilation will be useful for geochemical studies requiring extensive data sets, in particular those wishing to investigate secular temporal trends. The addition of physical properties, estimated from sample chemistry, represents a unique contribution to otherwise similar geochemical databases and thus provides added value for MEET. The data files of Gard *et al.* (2019) are published online and are available at https://doi.org/10.5281/zenodo.2592822 (Gard *et al.*, 2019a).

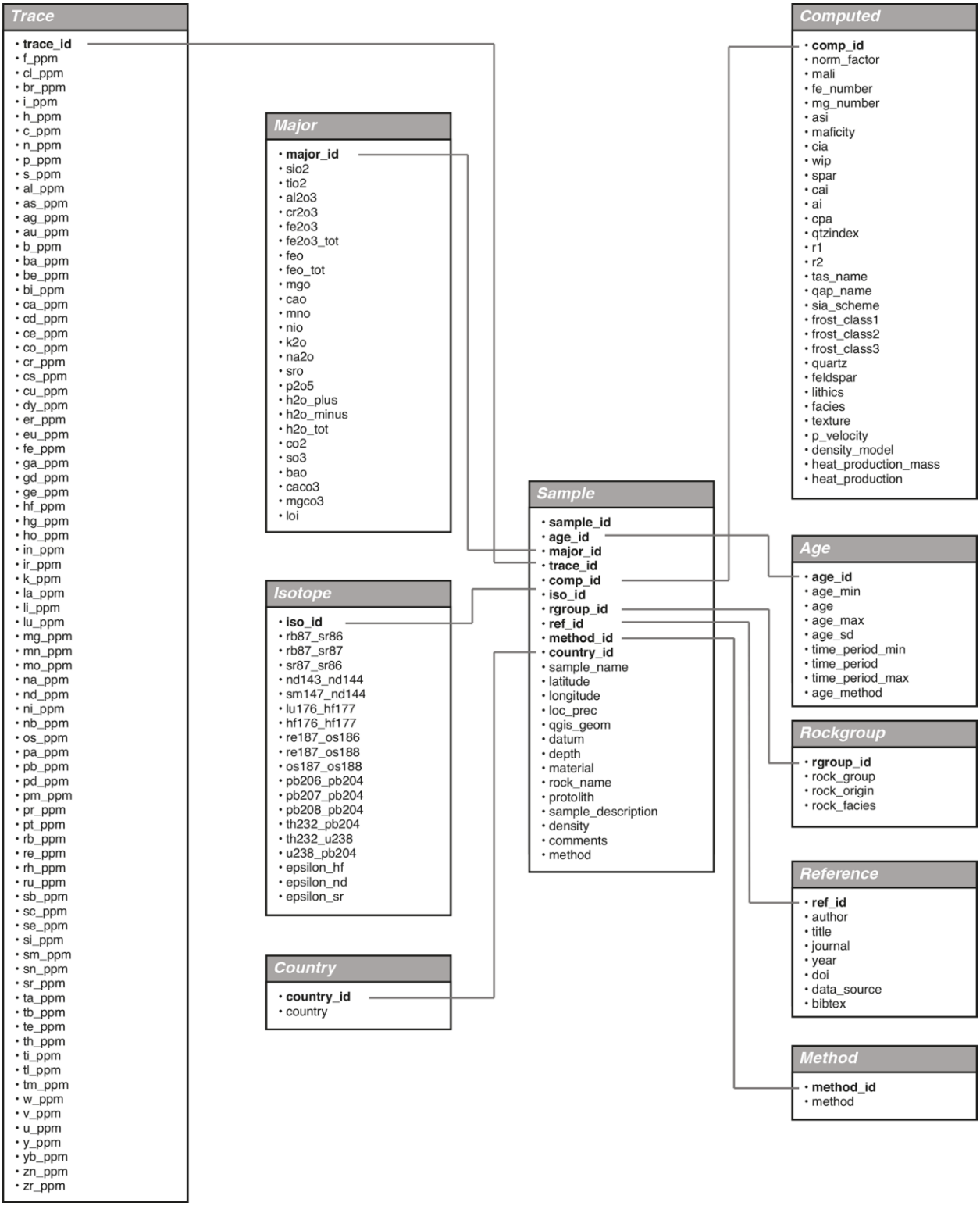

Figure 7: Whole-rock geochemical database relational structure (Gard *et al.* 2019). Sub-tables are linked through foreign id keys and are implemented in P³2MEET.

2.1.6 Hydraulic test data and rock mass permeability

Reservoir scale permeability is among the temperature the key property needed for geothermal reservoir characterization and evaluation. Since it is not a classical petrophysical property, it has not been investigated as part of D5.5. Anyhow, excellent databases of hydraulic test results comprising public data of most deep wells worldwide were published e.g. by Achtziger-Zupančic *et al.* (2017) or Scibek (2020) and can be used within MEET for characterization of basement rock mass and of fault zones in the basement and parametrization of respective models.

It is planned to link these public databases to P³2MEET in the near future.

2.1.7 Quality Control

As addition of the primary option of manual database quality control, which is by providing the information of the original data source, an automatic quality control was implemented in P³. Therefore, minimum requirements for a value to be included in the database were defined.

To provide a quality estimate for each data entry in terms of provided meta-information, a set of key criteria is automatically analysed: (i) uncertainty of the geographic location, (ii) the rank of petrographic classification, (iii) the rank of stratigraphic classification, (iv) the completeness of information on measurement conditions, and (v) the statistical type of a value (e.g. single value, mean value etc.). For each key criterion, four different quality classes (excellent =1, average =2, poor = 3; and minimum) are defined and computed to numerical quality indices (q_i, Table 3). A bulk quality index is calculated according to the arithmetic mean of the quality indices of the different criteria, where values < 1.5 are considered excellent, values ≥ 1.5 < 2.5 are considered average and values ≥ 2.5 are considered poor and values > 3.5 only meet the minimum requirements.

2.1.7.1 Geographic Uncertainty

Concerning the location of the sample, an accuracy of less than 100 m is considered to be of ‘excellent’ quality, which should always be the case for outcrop samples or drill cores. If the information on the location only contains a description of a geological unit in a certain region or area, the related size of this area is considered for the definition of the quality indices. If the location can be constrained to a region with a radius of less than 1 km the quality is considered ‘average’ whereas if the radius of uncertainty is between 1 km and 100 km, it is considered ‘poor’. Larger radius of uncertainty is considered as quality class 4.

2.1.7.2 Petrography or Rock Type

If the original petrographic or lithological description allows for the allocation of a petrographic term with a rank of 6 or higher, the quality is considered ‘excellent’, for a rank of 5 it is considered ‘average’ because these petrographic terms usually allow for a distinction of petrographies as used for reservoir- or site-scale geological models. For a rank of ≤ 4 the quality is considered ‘poor’ (compare Figure 5 and Table 1). To enter the database at all, the petrographic description of a sample has to allow for an allocation of a petrographic term of rank ≥2. This classification at least allows for a distinction of petrographies on a level used for continental-scale geological models.

2.1.7.3 Stratigraphy

Concerning the stratigraphy of the sample, (i) information on the chronostratigraphic Stage or Age is considered to be 'excellent', (ii) information on the stratigraphic Series or Epoch is defined as 'average' and (iii) if only the chronostratigraphic System or Period is given, it is considered 'poor'. To enter the database, there is no minimum requirement for the information on the stratigraphic age, since (i) stratigraphy does not directly control physical properties and (ii) scientific users might retrospectively derive stratigraphic information from the sampling location in combination with the petrography of the sample and additional information such as geological maps.

2.1.7.4 Measurement Conditions

For every data point, the measurement conditions can be entered. These are the temperature (K), pressure (Pa), saturating fluid and the degree of saturation (%) as well as for the mechanical properties additional information about the ambient stress field, σ_1, σ_2, σ_3 (MPa), and the pore pressure of the sample (MPa). For the sonic velocities (v_p and v_s) the frequency of the sonic pulse and, for the uniaxial compressive strength and related mechanical properties, the strain rate can be given as additional measurement conditions.

The quality assessment of the measurement conditions is based on both the measurement conditions and the measurement device, which is needed to be able to quantify the specific measurement error typical for a certain method. Excellent quality is only provided if information is available on all these points. If only the measurement device and the temperature and pressure conditions or the degree of saturation is available, the data quality is defined as 'average'. If only the device, or the temperature and pressure conditions, or the degree of saturation is described in the original reference the quality is considered to be 'poor'.

Table 3: Quality indices defined by the input data available. (n = numbers of measurements, NA = not available).

Parameter	*1 = excellent*	*2 = average*	*3 = poor*	*4 = minimum requirement*
Geographic uncertainty	≤ 100 m	> 100m ≤ 1 km	> 1 km ≤ 100 km	*> 100 km*
Petrography	Rank ≥ 6	Rank = 5	Rank = 4	*Rank ≥ 2*
Stratigraphy	Stage / Age or lower or numerical age (Rank ≥ 5)	Series / Epoch (Rank = 4)	System / Period or higher (Rank ≤ 3)	*NA*
Measurement conditions	Measurement device AND temperature and pressure AND degree of saturation available	Measurement device AND temperature and pressure OR degree of saturation available	Measurement device OR temperature and pressure OR degree of saturation available	*NA*
Parameter value	Single measurement	Mean value and number n of measurements AND standard deviation or Minimum and Maximum	Mean value and number n of measurements	*(Value), NA*

2.1.7.5 Measurement Parameter

The last criterion for the quality control is the type of value representing the property. In general, single measurement values for a sample are ranked higher in quality than mean values of various measurements applied to a sample. Accordingly, single measurements are considered as ‘excellent’ and mean values as ‘average’ or ‘poor’. If the mean value is not only accompanied by the number of measurements to calculate the mean value, but also by the minimum and maximum as well as the standard deviation from this set of measurements, the quality is defined as ‘average’. In contrast, a mean value accompanied only by a number of measurements is defined as ‘poor’. Values resulting from an unspecified number of measurements are not considered for quality control but still included into the database with NA (“not available”) in the respective column for number of measurements to enable the user to exclude these values in statistical analyses.

2.2 GEOTHERMAL CHARACTERIZATION OF THE FOUR VARISCAN RESERVOIR TYPES

In this chapter, a short introduction to the local geology, the origin and short description of the sample material and a detailed description of the investigation method and measurement procedures is given for each demosite and its outcrop analogue of the four variscan reservoir types as defined in the MEET grant agreement (cf. Figure 8, MEET grant agreement and D5.1 and D5.2) and for the labs of the different partners, respectively.

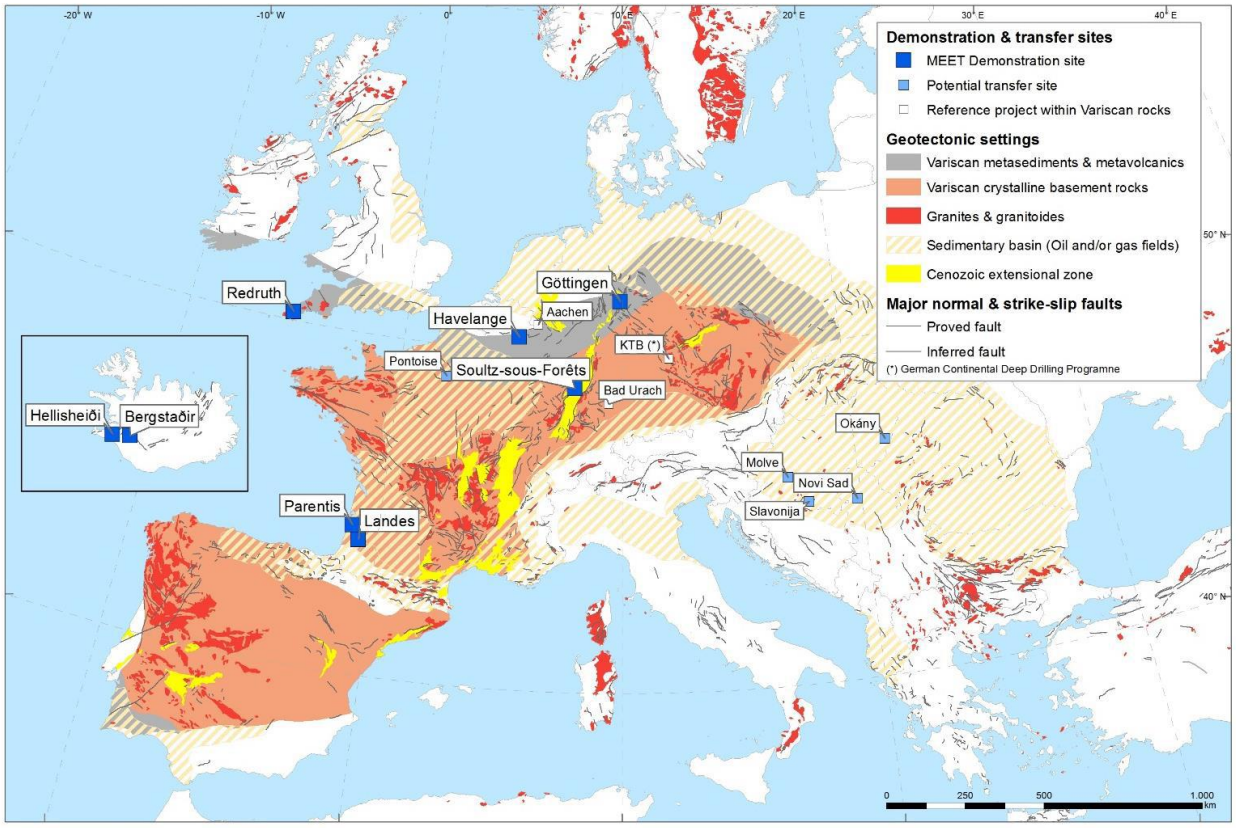

Sources of geological datasets:
Asch, K. (2005): IGME 5000: 1 : 5 Million International Geological Map of Europe and Adjacent Areas. BGR (Hannover).
U.S. Geological Survey World Petroleum Assessment 2000: U.S. Geological Survey Digital Data Series DDS60: http://greenwood.cr. usgs.gov/energy/WorldEnergy/DDS-60

Figure 8: MEET demonstration sites and potential transfer sites during project duration next to EU geotectonic settings. Variscan environment, granite/granitoides and sedimentary basin illustrate the new terrains where MEET concept will enable the production of heat and/or power.

2.2.1 Short geological overview and sample material

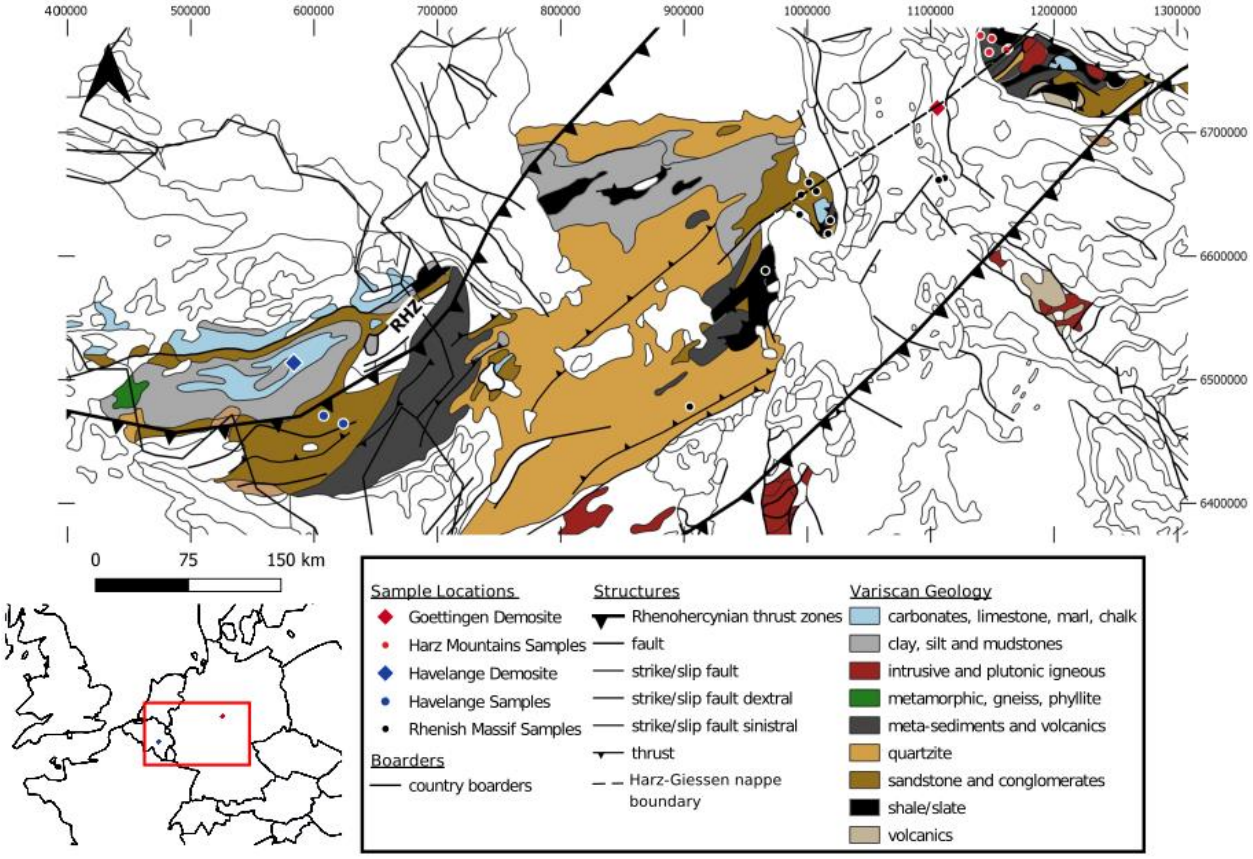

Figure 9: Overview map of the Rhenohercynian belt with sampling positions including both Demosites: Havelange in Belgium and Göttingen in Germany together with the associated outcrop analogue sites.

2.2.1.1 Sample material – origin and short description: Göttingen demosite and Harz mountains outcrop analogue site

For the demo site "Göttingen University Campus" the Variscan target horizons for deep geothermal energy are expected to be found below a sedimentary cover of 1,500 m thickness. Since there is no well in or around Göttingen from which Variscan sample material is available, we could collect representative samples only from appropriate analogue areas. The demo site "Göttingen University Campus" is situated along the Variscan strike between two analogue areas namely the exhumed Rhenish massif (far-field) in the SW and the Harz Mountains (near-field) in the NE (for more details see D5.1 and D5.2). The main lithologies are represented by meta-greywackes, slates, intercalations of slate/meta-greywackes, cherts, and meta-limestone layers all deformed by Variscan tectonics, which is characterized by NW-SE trending fold and thrust structures that are developed at all scales.

Meta-greywackes, slates and the meta-greywacke/slate intercalations are the most important rocks in view of the volumetric portion as target horizon in a first approach to develop a reservoir model for the demo site of the Göttingen University Campus. Since the Rhenish massif physical property data are already existing in the "P³ - Database", in this project we focused on sample campaigns in the Western Harz Mountains. Sample campaigns were carried out in the field and

in the well core archive of the Geozentrum Hannover in Grubenhagen (Brinckmann & Brüning 1986).

Slate samples, however, only come from the well core samples. The unloading relaxation near the surface related to the uplift of the Harz Mountains and the surface weathering processes lead to the mechanical opening of cleavage planes of the slates, which leads to the decomposition already during sample collecting or during sample preparation. Fortunately, most of the slate samples from the well cores are still robust enough for sample preparation and, of course, are therefore more representative for the physical properties to be expected for the reservoir in about 4,000 m depth below Göttingen. The meta-greywackes sampled in the field were taken by drilling directly at the outcrop wall

Samples were collected in view of covering the different Devonian and Carboniferous stratigraphies, different sampling depths of the wells as well as different locations. For the greywackes we additionally focused on a differentiation of more fine- and coarse grained samples.

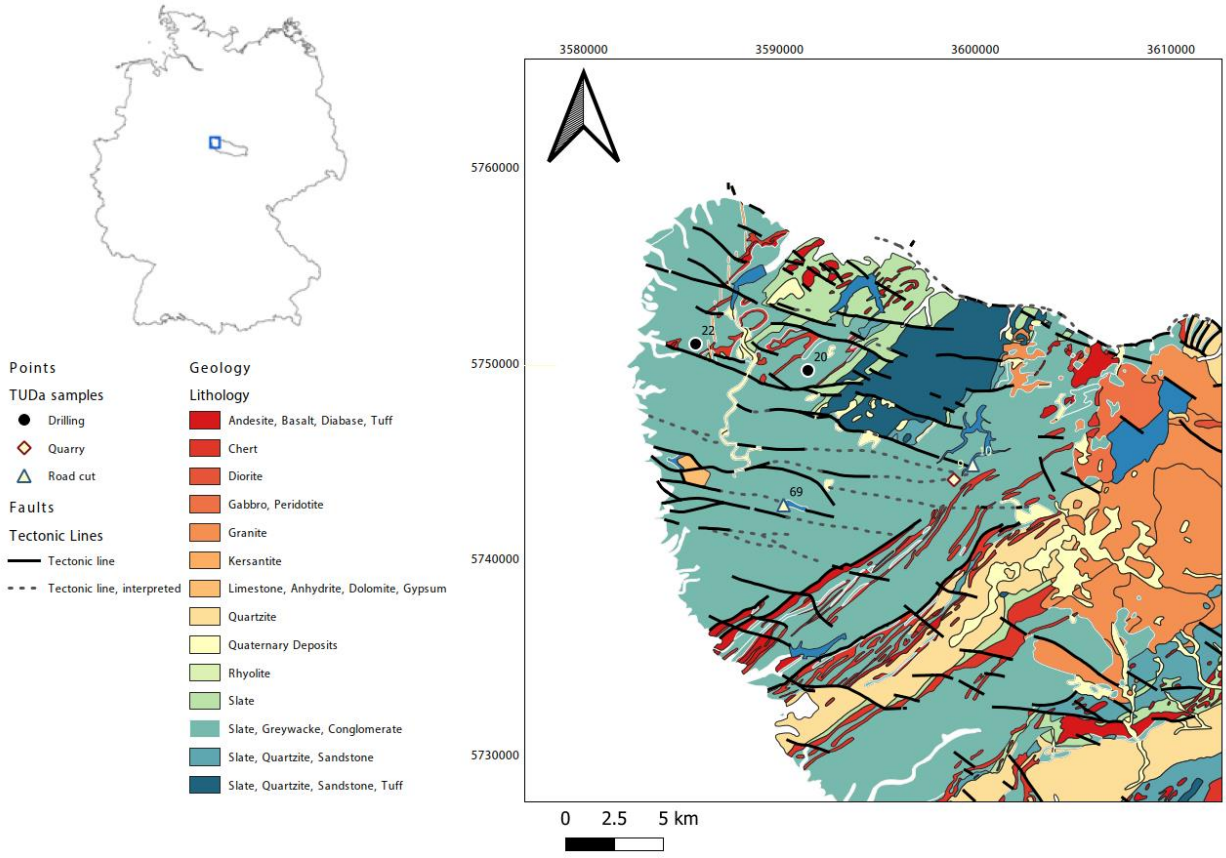

Figure 10: Main rock types and sample locations of the North-Western Harz Mountains (Germany) serving as analogue for the Göttingen demo site (see Figure 9 for the geological relation by the boundary of the Harz-Gießen-Nappe).

2.2.1.2 Sample material investigated by GFZ

The investigated Variscan slate samples for long-term fluid-rock interaction experiments were recovered from the 'Hahnenklee' well (sample depth z ≈ 1,150 m) drilled into the Devonian Wissenbach (WBS) shale formation (GER) in the early 1980's (Brinckmann & Brüning 1986).

2.2.1.3 Sample material – origin and short description: Havelange demosite and respective outcrop analogues

In the framework of the Havelange demo-site study and its near-field analogue outcrops in the Ardenne, three types of samples are studied. Cores and cutting samples were selected from the Havelange borehole collection. In the analogue outcrop zones the samples are based from hand-specimens collected during the field campaigns (cf. deliverable 5.2 and 5.4). Following their nature, the samples represents different sources of information, hence they follow different analysis workflow described below.

Core samples from demo-site

The available core samples from the Havelange borehole collection were selected and cut according to the requirements for the mechanical and petrophysical investigations of the partner laboratories. As already described in deliverable 5.2, the off-cut pieces were kept for additional mineralogical and petrological laboratory analyses at the Geological Survey of Belgium. The cores were the object of non-destructive imagery (core-scan and micro-CT) before shipment towards the TUDa partner.

The core samples from the Havelange borehole cover two main stratigraphic horizons, namely the lower Famennian shale formations encountered at shallow depth and the lower Devonian meta-sedimentary rocks drilled in the deepest part of the borehole. The stratigraphic intervals between those horizons were not core-drilled and therefore these intermediate units can only be studied through the analysis of cuttings or from analogue outcrops.

The lower Famennian shale units consist of low-grade green shales frequently associated with carbonate nodules, sometimes interlayered with siltstones and fine-grained sandstone beds. The detailed lithostratigraphy of these units is well-documented. The lower Devonian meta-sediments consist mainly from low-grade schists and meta-sandstone or quartzite units. The current knowledge regarding the lithostratigraphy of these units is more difficult due to the monotonous characters of these units, their high thickness (sometimes several km) and the importance of the structural and metamorphism overprints. Nevertheless, some constraints are possible for the samples from the Havelange borehole thanks to micropaleontological investigations.

Cuttings from demo-site

The nature of the cuttings limits their field of applications to common mineralogical analyses described below. The samples were selected according to a multiple-criterion approach:

1- a full cover of the entire Havelange borehole length;

2- a specific focus to arenaceous horizons, since they represent potential target geothermal reservoirs;

The cuttings were intensely washed to remove potential residues of drilling mud before grinded for powder production required for X-Ray Diffraction (XRD) mineralogical analyses and calcimetry measurements of the carbonate content.

The interpretation of the XRD spectra must be carried out with caution, since the cuttings commonly correspond to a mix of different lithologies encountered during the drilling operation. In addition, the cuttings are frequently subject of contamination by other cuttings from shallower depth units.

Hand-specimens from the analogue outcrops

The hand-specimens were collected in a series of outcrops and quarries located in the outcropping zones of the different geological formations observed in the Havelange borehole. These samples were accurately located by GPS. All these analogue samples were drilled to produce cores equivalent to those collected from the Havelange borehole collection.

The hand-specimens collected in the analogue outcrop zone focus mainly on lower Devonian formations observed at ground surface in the Eastern and Southern part of the Dinant Synclinorium. A specific attention was given to Lower Devonian metasedimentary formations representing the lateral equivalent to those observed within the deepest parts of the Havelange borehole. The main difference between the samples collected in the analogue zone and those from the study-site is the weathering texture and mineralogy of samples collected in the analogue zone.

Material for petrophysical and mechanical investigation:

A total of 221 core samples from the MEET project sampling and supported with Hessen 3D (Bär, 2012) and Hessen 3D 2.0 (Bär *et al.*, 2016) project samples were collected and their petrological classification generalized to three main rock types for comprehensive investigation of petrophysical properties and as the basis of model parametrization of Havelange and Göttingen demo sites. Selected rock types comprise greywacke, quartzite, and slate which originated from various outcrops and boreholes. A complete list of the samples is given in Table 4.

Table 4: List of core samples from Havelange and Göttingen demo sites as well as additional data from all Rhenohercyninan outcrop analogues.

Rock Type	n	Region	Origin	Type	n
Greywacke	92	Harz Mountain	Bullars	Borehole	7
			Wulpke 2	Borehole	1
			Eselsberg	Borehole	6
			Schwarzes Wasser	Outcrop	9
			Predam	Outcrop	7
			Silbernaal	Outcrop	9
		RHZ	Berkatal	Borehole	8
			Waldeck	Outcrop	3
			Marburg	Outcrop	3
			Frankenau	Outcrop	6
			Steinbruch	Outcrop	12
			Bad Sooden	Outcrop	16
			Bad Wildungen	Outcrop	1
			Fürstenberg	Outcrop	1
			Gilserberg	Outcrop	3
Quartzite	34	Harz Mountain	Eselsberg	Borehole	6
		Havelange	Havelange	Borehole	7
			Gives	Outcrop	5
		RHZ	Gilserberg	Outcrop	2
			Armsfeld	Outcrop	2
			Other	Outcrop	12
Slate	86	Harz Mountain	Hahnenklee	Borehole	10
			Bullars	Borehole	6
		Havelange	Havelange	Borehole	6
			Bande	Outcrop	8
		RHZ	Other	Borehole	7
			Kransberg	Outcrop	4
			Steinbruch	Outcrop	15
			Bad Wildungen	Outcrop	3
			Other	Outcrop	27

2.2.1.4 Sample material – origin and short description: Death Valley outcrop analogue site: Soultz demosite and Death Valley outcrop analogues

Noble Hills outcrop analogue site:

The geology and site specific investigations of the Noble Hills, Death Valley outcrop analogue site are described in D3.4 in detail. Samples were taken for the investigation and measurements of petrophysical and mechanical properties at CYU and GFZ, which were not finalized yet to be implemented in D5.5.

CYU plans to perform porosity measurements with ethanol and also porosity measures with mercury. GFZ will characterize the fracture conductivity and will try to determine the roughness, the porosity (He-pycnometry), the permeability, the physical properties, the bulk and grain density and probably the fluid composition of the different samples. Prior to testing, they will prepare the samples by cutting, grinding, drying, weighting and measuring the dimension.

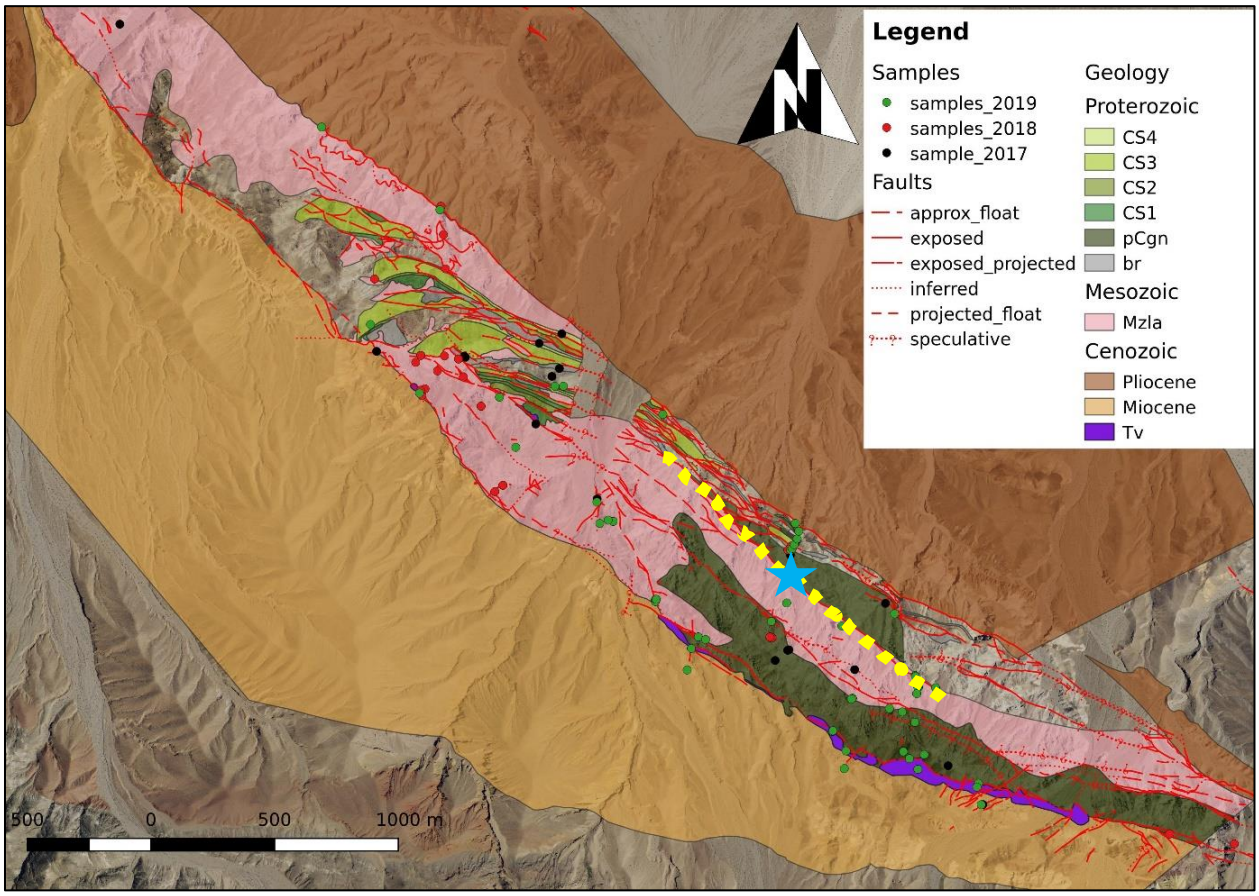

Figure 11: Geological map of the Noble Hills range representing the location of the different samples collected by the dots, the major fault gouge by the yellow line and the major outcrop of the gouge by the blue star.

Hand specimens from the analogue outcrops (Noble Hills):

The hand-specimens were collected during two field campaigns (October 2018 and September-October2019) in the framework of the MEET EU Project and during a preliminary field campaign in 2017, before the beginning of the project. The sampling was organized to follow different

profiles across the range, especially perpendicular to the range and at the same time parallel to the range. The goal is to study the granite evolution in the term of alteration and deformation, to reconstruct the structure and so the story of the range, but also to study the fractured or mineralized areas which can be signs of fluid circulation. All the samples are located by GPS and put in a GIS database which allows to localize all the samples on a geological map of the area. In total 171 samples were collected (Figure 11).

Material for petrophysical and mechanical investigation (Noble Hills):

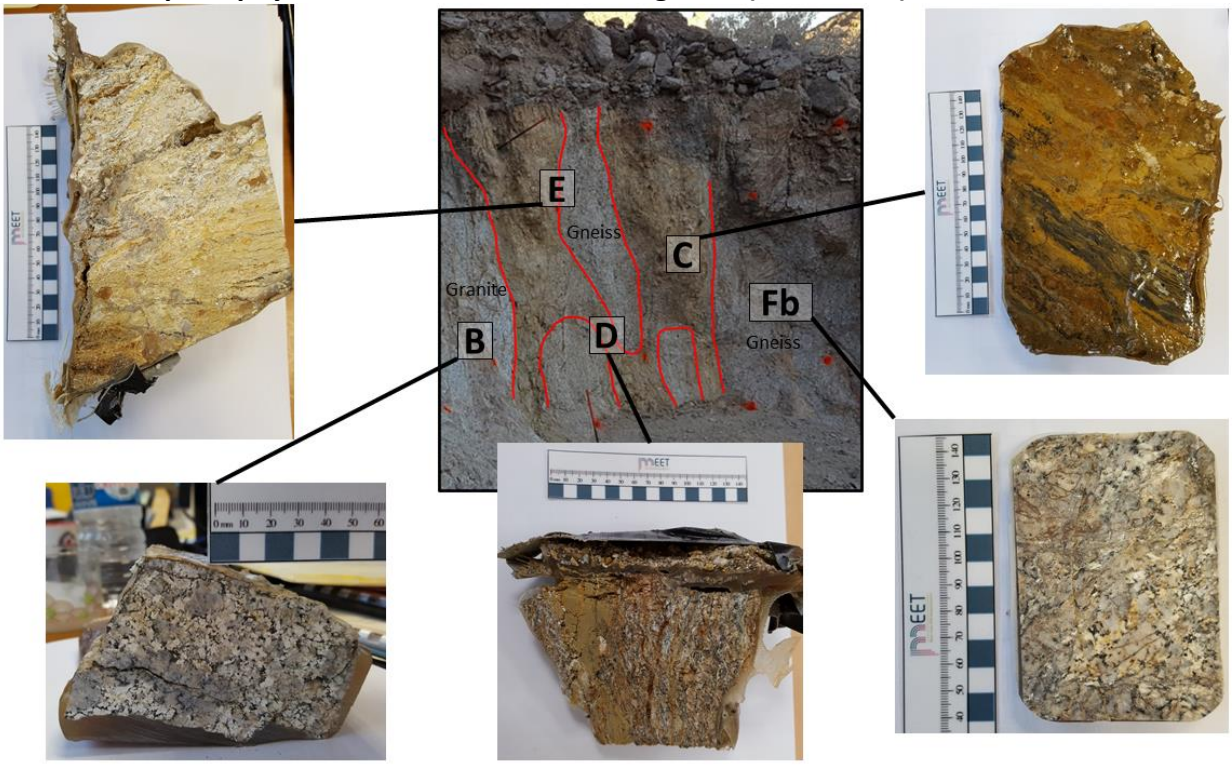

Figure 12: Location of the different sample from the main gouge of the study area.

Of the 171 samples (described in more detail in Appendix 2), 10 samples were selected to do petrophysical analyses. These last 10 samples were shared and given to CYU and the GFZ to measured petrophysical properties such as porosity, sample density (bulk and grain), permeability, mechanical properties and thermophysical properties such as fracture conductivity properties. The selected samples are altered granite, gneiss and some samples from a major gouge rich in illite which is presents in the middle of the range (Figure 11, the yellow line). We mainly decided to focus on this gouge which separates the granitic body from the Proterozoic series at the front, because it represents the zone where the deformation is the most concentrated (Figure 11 and Figure 12). Figure 12 shows different samples taken from the outcrop representing the main gouge with B the granite which is part of the Mesozoic granitic body, D and E a mix between the gouge and what we think is deformed gneiss, C the pure gouge and Fb the gneiss part of the Proterozoic series at the front of the range.

2.2.1.5 Sample material – origin and short description: Cornwall demosite

An outcrop analogue study in Cornwall was conducted to improve the understanding of the petrophysical rock properties of Cornubian Batholith and to enhance the data availability for numerical simulation and geothermal resource assessment studies within the MEET EU project (cf. MEET D5.4).

Fractured or mineralized areas representative of the fracture and fault zones within the United Downs wells were targeted by sampling

- **outcrop analogues** from the
  - Carnmenellis, Carn Brea and Carn Marth plutons as near-field outcrop analogues,
  - Land's End and St. Austell plutons as far-field outcrop analogues,
- Rosemanowes (1980's Hot Dry Rock project site) as described in D5.4 defined as **reservoir analogue**,
- **drill cuttings** from the UD-1 well, whereas sampling
- **sidewall cores** is planned in the open hole section of UD-1 at depths of 4.2 to 5.1 km for July 2020.

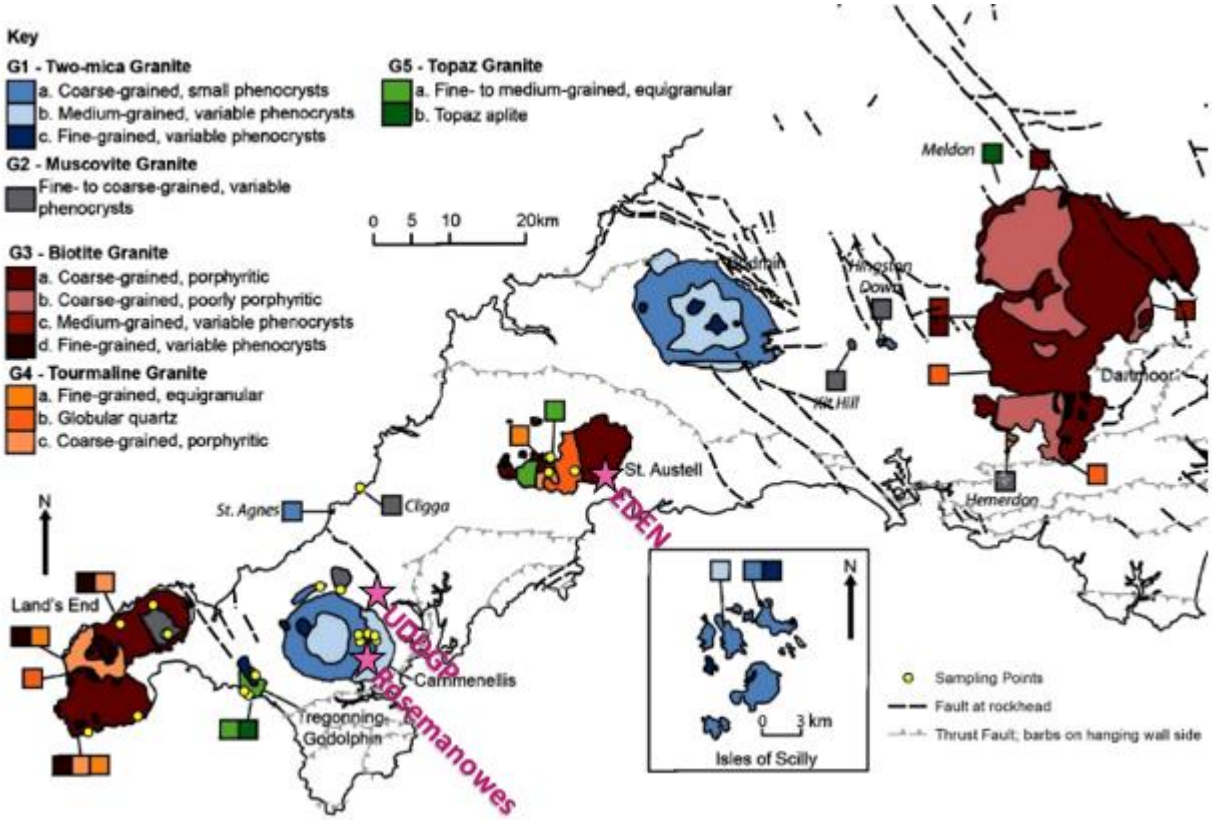

Figure 13: Map of MEET sampling points (shown as yellow dots) with respect to projects' locations (shown as pink stars) (structural data: BGS Onshore Geoindex (2019); granite classification after Simons *et al.*, 2016).

In total 47 outcrop analogue samples, with a total weight of 966 kg, were derived from 23 different sampling locations including 5 active quarries, 4 natural outcrops and 14 abandoned quarries located on the Land's End, St. Austell and Carnmenellis plutons. The sample set includes

five granite types according to the classification of Simons *et al.* (2016): G1 Two-mica granite, G2 Muscovite granite, G3 Biotite granite, G4 Tourmaline granite and G5 Topaz granite. Figure 13 illustrates the sampling points with regard to the corresponding lithology.

Comprehensive petrophysical rock characterization was done through the workflow presented in Figure 16.

Detailed sample description was done on the collected granitic blocks' fresh surfaces. Appendix 2 presents the sampling locations with the corresponding sample numbers and their description with geothermal significance, if applicable.

In the Hydrothermikum Research and Teaching Laboratory of TUDa, 338 cores with different diameters (40 mm, 55 mm and 64 mm) were drilled out of these collected samples. Table 5 and Table 6 provide the number of drillcores and collected samples, respectively.

Table 5: Numbers of different diameter cores

	Diameters		
	40 mm	55 mm	64 mm
Number of Prepared Cores	192	88	58
total	338		

Table 6: Distribution of samples distinguished into outcrop or sample type and analogue sites

		Demo-site	Reservoir Analogue	Near -Field Analogue			Far Field Analogue			
		UDDGP	Rose-manowes	Carn-menellis	Carn Brea	Carn Marth	St. Austell	Land's End	Cligga	Tregonning-Godolphin
OAS	Active quarry	-	-	6	-	-	7	6	-	-
	Aban-doned quarry	-	2	4	-	1	2	-	3	2
	Other	-	-		1	-	-	10	-	3
Cuttings	UD-1 well	44	-	-	-	-	-	-	-	-

Table 7: Distribution of the number of drilled cores at each analogue site

Percentage of Prepared Cores (%)	Total Number of Cores	Percentage (%)
St. Austell	33	10
Land's End	134	40
Carnmenellis	123	36
Tregonning-Godolphin	30	9
Cligga	18	5

Note that 50% of drilled cores are from near-field analogue sites.

Although the petrophysical rock properties were analyzed at laboratory conditions and therefore deviate from in situ properties at reservoir conditions, the presented dataset enhances the knowledge of petrophysical rock properties within the study area for further geothermal applications (see part 2.3.4 for the complete list of measurement results). To estimate the in-situ reservoir conditions, this dataset will be enlarged by considering the increasing pressure, temperature and salinity at reservoir conditions. Therefore, specific samples will be selected for analysis with the TUDa ThermoTriaxial device (Pei *et al.*, 2014) at pressures of up to 60 MPa and temperatures of up to 180°C.

For the petrographical analysis of the samples, material was prepared and shipped for thin sections. Thin section analysis will increase the accuracy of classification of granite samples presented in Appendix 2.

Drill cutting samples, presented in Figure 14 from the reservoir section of the well UD-1 have been sampled by GEL/Geosciences Limited. They represent 44 depth intervals of 10 m length, between 4,050 m TVD and 4,930 m MD, with exception the depth interval from 4,198 to 4,200 m, which is, due to technical issues at the project site, only two meters. All cuttings have been washed with a 63 µm sieve. Thus, the sub 63 µm fraction is lost and cannot be analysed. This includes especially clay minerals, which could have been an indicator for alteration. The cuttings resemble the grainsize range of an intermediate sand, which is not indicative of the rock type but a result from the drilling process. The maximum grain size is 2 mm.

The cuttings have been used for geochemical and mineralogical analysis.

All cutting samples were taken specifically from the zones with intense natural fracturisation, fluid losses during drilling, gas shows during drillings and/or anomalies in the geothermal gradient.

Figure 14: Photo of the drill cuttings taken from United Downs drilling site (Schulz, 2020).

These zones represent the presumably permeable fractures and faults encountered by the well and represent the targets for chemical treatment to enhance permeability (see MEET D5.3).

Additional core samples were initially planned to be obtained from the UD-1 well of UDDGP project, which had its wells finished already in July 2019. The third phase of the program the workover operations, which include downhole logging, the collection of side-wall cores (SWC) and hydraulic testing, was initially planned for end of March 2020. It had to be postponed and the operations are now planned for end of July / beginning of August 2020. Therefore the only available reservoir samples available for D5.5 are the drill cuttings from the well UD-1. Investigation and characterization of the SWCs will therefore only be possible from August onward and will complete the rock property determination for the UDDGP demosite.

2.2.1.6 Variscan basement overlain by sedimentary basins: Paris and Aquitaine basins

CYU (formerly UCP) investigates basement cores from the Variscan belt under the Paris and Aquitaine basins in order to understand in-situ rock properties and petrographical characteristics of deep potential reservoirs.

For this study, CYU explored various lithologies of drill core sections of Paleozoic basement, provided by Vermilion and Total (Figure 15).

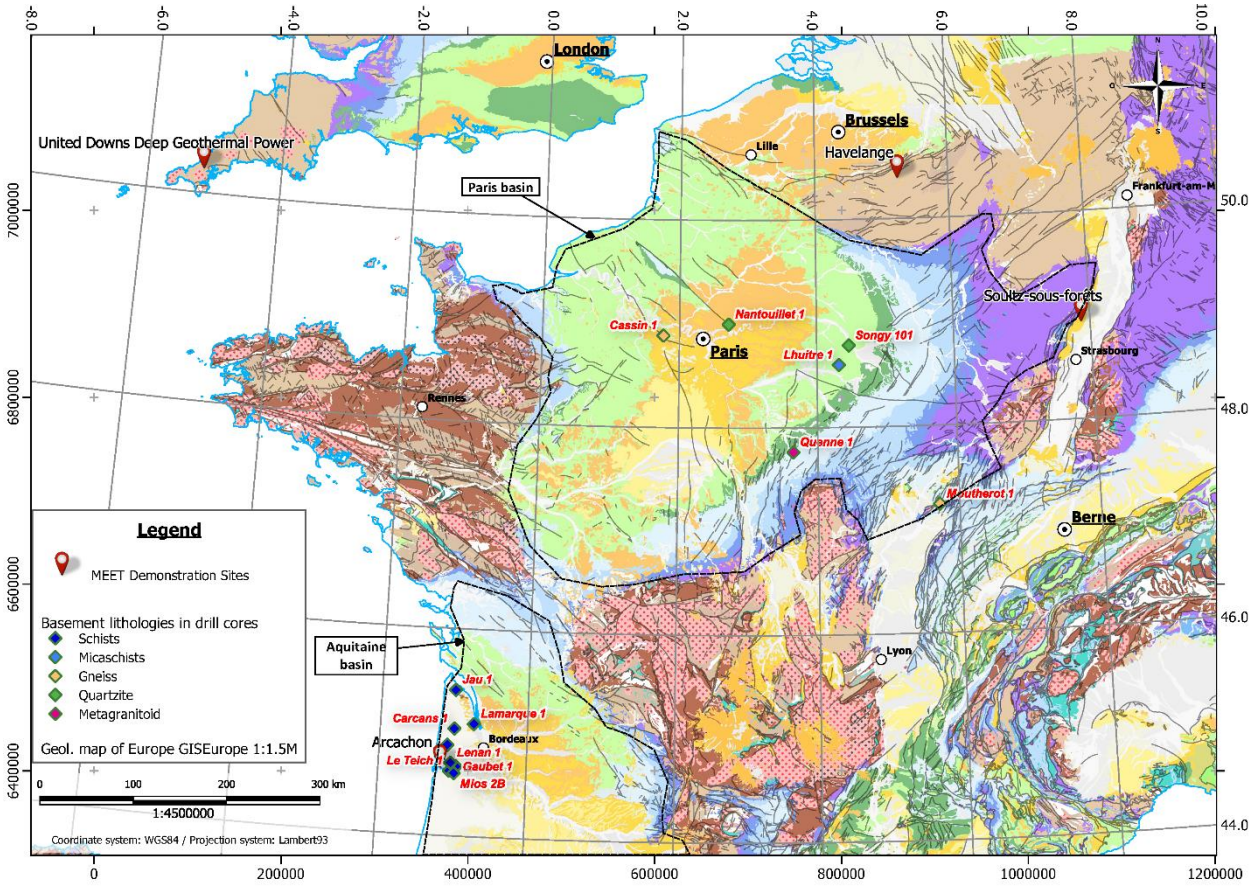

Figure 15: Location of industrial boreholes with access to drill core sections in the basement, were samples were collected for this study.

The structural units of the Paleozoic basement below Paris basin are the relicts of tectonic stacking that occurred during the Variscan orogeny and were later dismantled by post-orogenic extensional and erosional processes. Several domains compose the deformed part underneath the Paris Basin: the Armorican domain to the west, the internal domain of the orogeny to the south and southeast, the Saxo-Thuringian domain to the east and the Rheno-Hercynian zone to the north (Autran *et al.*, 1980; Guillocheau *et al.*, 2000).

Due to a long history of Mesozoic sedimentation under subsidence regime, the Variscan structural features are deeply buried below the subsiding basin and are hardly accessible. The

nature of the basement rocks is very uncertain and has been extrapolated from bottom-hole geology, gravimetry, petrophysics and seismic signature of "Northern France" ECORS profile (Matte & Hirn, 1988; Autran *et al.*, 1994; Baptiste *et al.*, 2016). Few of the deepest boreholes have reached the basement and each well provides only very little information about the basement, since for most of the cases a rather punctual data about the rock type is provided.

The geological context of the Paleozoic basement underneath the Aquitaine basin is also rather unconstrained since the thickness of overlying Meso-Cenozoic sediments is between 1 and 6 km. However, previous studies synthetized deep industrial borehole data from 40 locations as well as deep structures imaged by the "Bay of Biscay" ECORS profile, and assessed the presence of three NW-SE oriented tectonic units, namely the Western, Median and Eastern units, that have distinct stratigraphic, structural, metamorphic and geophysical signatures (Paris & Le Pochat, 1994; Paris *et al.*, 1988). These large-scale units are subdivided into smaller units based on dating, lithological correlations and metamorphic features (Lefort & Agarwal, 1999). These units were probably emplaced on the southern foreland of the Variscan orogeny, most certainly in response to subduction of the South-Armorican ocean (Bourrouilh, 2012; Robardet *et al.*, 1993).

To summarize, there is a poor comprehension of structural and geodynamic evolution as well as reservoir potential of tectonically complex rock units in both Paris and Aquitaine Paleozoic basements. In this regard, the available core materials retrieved from drilling campaigns of the second part of the 20th century represent a unique opportunity to investigate these potential deep reservoirs and to seek for fluid circulation pathways in different rock types at the vicinity of faults or at the paleo-weathering interface with the overlying sediments.

2.2.1.7 Sample material: Paris basin and Aquitaine basin – origin and short description

The drill core samples collected on boreholes from the Paris basin and the Aquitaine basin are organized according to the MEET WP5 naming convention and are presented in the Table 8 and Table 9. A total of 99.66 m was logged, along which 52 samples were collected. 40 thin-sections and 51 plugs taken from these samples were analysed in the laboratory.

Table 8: Basement cores underneath Paris and Aquitaine basins, with sample names, vertical positions and associated lithologies.

Borehole name	ID	Overlaying Basin	Basement Thickness (m)	From (m)	To (m)	Sample names	Measured Depth (m)	Lithology (TS = thin-section)
Cassin 1	CSN1	Paris basin	12	1530	1542	MEETPB001001	1536.5	Gneiss (TS)
						MEETPB001002	1538.8	Gneiss (TS)
						MEETPB001003	1538.9	Quarzitic vein (TS)
						MEETPB001004	1539.9	Gneiss (TS)
						MEETPB001005	1540.4	Quarzitic vein (TS)
						MEETPB001006	1541.2	Gneiss (TS)
Lhuitre 1	LHE1	Paris basin	6	3730	3736	MEETPB002001	3733.5	Micaschists (TS)
						MEETPB002002	3731.5	Micaschists
						MEETPB002003	3732.5	Micaschists
						MEETPB002004	3735.1	Micaschists (TS)
						MEETPB002005	3735.75	Micaschists (TS)
Nantouillet 1	NT1	Paris basin	6.55	2442	2448.55	MEETPB004001	2443.25	Quartzite (TS)
						MEETPB004002	2443.8	Quartzite (TS)
						MEETPB004003	2444.55	Quartzite
Quenne 1	QU1	Paris basin	2.5	949.5	952	MEETPB005001	950.9	Metagranitoid
						MEETPB005002	951.15	Metagranitoid (TS)
Songy 101	SY101	Paris basin	8.4	2070	2078.4	MEETPB006001	2071	Quartzite
						MEETPB006002	2074.1	Quartzite
						MEETPB006003	2074.4	Quartzite (TS)
						MEETPB006004	2075.4	Quartzite (TS)
Carcans 1	CS1	Aquitaine basin	5.89	1851.65	1854.65	MEETAB001001	1852.65	Schists
				1926.71	1929.6	MEETAB001002	1926.7	Schists
						MEETAB001003	1927.7	Schists
						MEETAB001004	1928.1	Schists
Gaubet 1	GAT1	Aquitaine basin	7.7	3869.5	3877.2	MEETAB002001	3872.9	Schists
						MEETAB002002	3873	Schists
						MEETAB002003	3874.7	Schists
						MEETAB002004	3875.2	Schists
Jau 1	JAU1	Aquitaine basin	7.2	1442.3	1449.5	MEETAB003001	1443.3	Schists
						MEETAB003002	1446.8	Schists
						MEETAB003003	1449	Schists
Lamarque 1	LE1	Aquitaine basin	9.98	1852.46	1857.55	MEETAB004001	1852.86	Schists
						MEETAB004002	1854	Schists
				1877.55	1882.44	MEETAB004003	1878.25	Schists
						MEETAB004004	1879.25	Schists
						MEETAB004005	1880.06	Schists
						MEETAB004006	1881.86	Schists
Le Porge 1	PG1	Aquitaine basin	6	2679.1	2685.1	MEETAB005001	2681.5	Schists
						MEETAB005002	2682.25	Schists
						MEETAB005003	2683.3	Schists
Le Teich 1	LTH1	Aquitaine basin	10.24	3587.2	3592.59	MEETAB006001	3587.7	Schists
						MEETAB006002	3588.2	Schists
						MEETAB006003	3588.4	Schists
						MEETAB006004	3588.5	Schists
				3673.3	3678.15	MEETAB006005	3675.5	Schists
						MEETAB006006	3674.7	Schists
Lenan 1	LEN1	Aquitaine basin	17.2	4046	4054.2	MEETAB007001	4046.5	Schists
						MEETAB007002	4048.25	Schists
						MEETAB007003	4050.25	Schists
				4144	4153	MEETAB007004	4145.85	Schists
						MEETAB007005	4147.5	Schists
						MEETAB007006	4149.4	Schists
			99.66 m			**52 samples**		

Table 9: Number of samples, thin-sections and plugs analysed at CYU for each of the target zone in Paleozoic basement rock underneath Paris basin and Aquitaine basin.

	Paris basin	Aquitaine basin	Total
Samples	20	32	52
Thin-sections	14	26	40
Plugs	21	30	51

2.2.2 Investigation methods

2.2.2.1 Workflow at HydroThermikum laboratory facilities of TU Darmstadt

The investigation and measurements of petrophysical and mechanical properties were performed in the HydroThermikum laboratory facility in TU Darmstadt. The laboratory tests were divided into the three stages 1) general petrophysical characterization including all non-destructive measurements, 2) rock mechanical characterization (destructive) and 3) chemical and mineralogical characterization. The non-destructive tests included grain density, bulk density, porosity, intrinsic matrix and in few cases fracture permeability, thermal conductivity and thermal diffusivity at dry conditions, P-wave velocity and S-wave velocity at dry conditions, and specific heat capacity at dry conditions. Afterwards the destructive uniaxial and triaxial rock mechanical tests were performed to determine uniaxial compressive strength, Young's modulus, Poisson ratio, tensile strength, friction angle and cohesion. Samples that were identified as suitable for destructive tests were grinded plane parallel prior to analysis. Quantitative and qualitative chemical analyses like X-ray fluorescence (XRF) and X-ray diffraction (XRD) as well as thin section analyses are planned to be performed for the petrological and geochemical characterization. The comprehensive laboratory workflow is depicted in Figure 16.

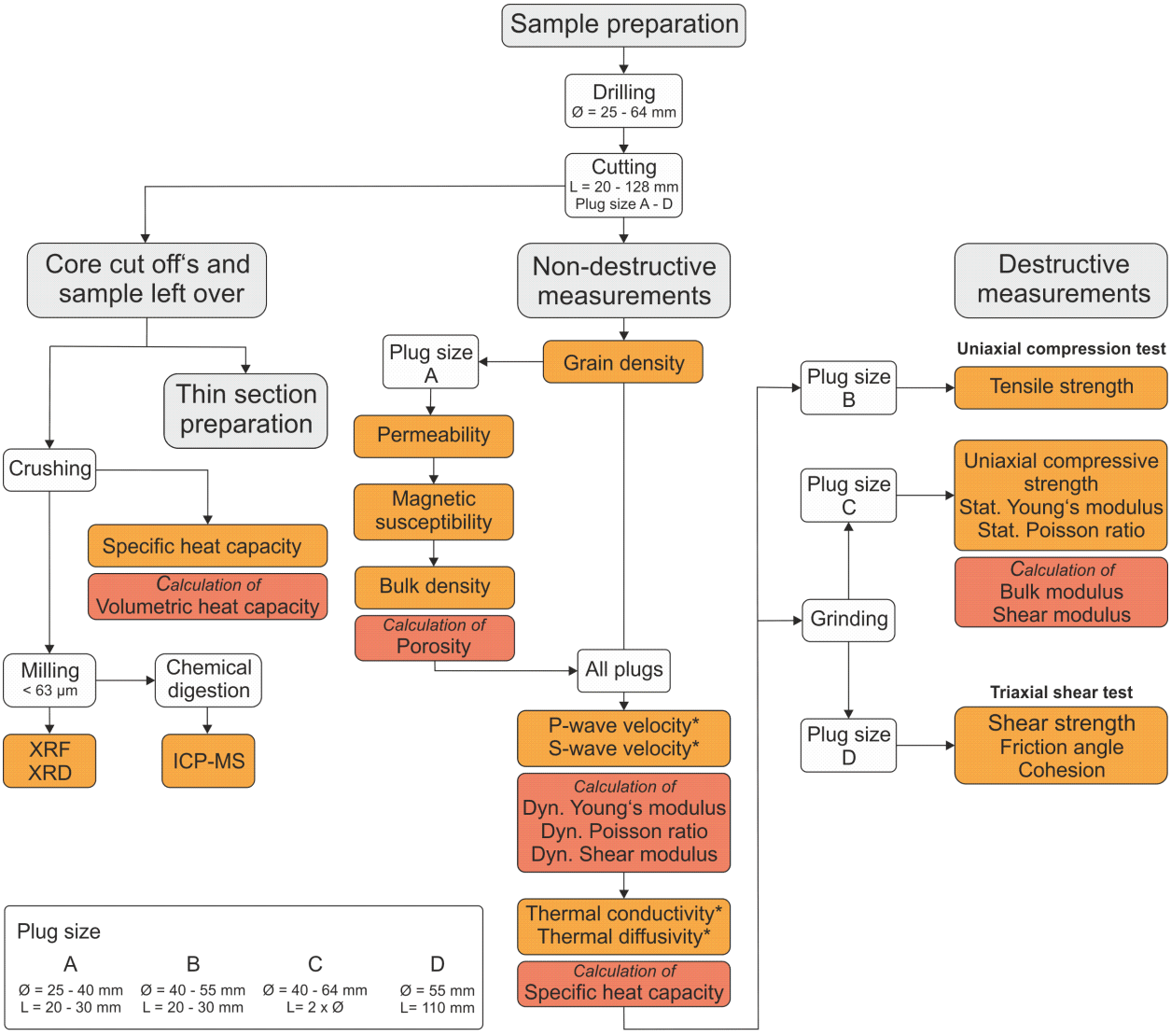

Figure 16: Schematic workflow of the comprehensive petrophysical and mechanical rock sample characterization at TU Darmstadt. The properties displayed in orange are determined on sample material and used to calculate those shown in red. Parameters marked with * are analysed at dry and saturated conditions (Weydt *et al.* 2020, subm.).

Sample Preparation:

All the available samples were initially drilled as cylindrical cores with diameters ranging from 40 to 65 mm and subsequently cut according to the standards (ASTM D4543-19, 2019) for the required sample length whereby the irregular and rough core ends were cut to be parallel. The outcrop samples can be drilled directly either on-site or in the drilling laboratory. However, reservoir samples must be cemented to provide integrity during the drilling process. As a result, the average processing time to drill reservoir samples ranges from one up to two weeks including the drying time for the cement.

Once drilling is completed, the samples are put in the parallel grinding machine to ensure smooth and parallel surface on both ends of the core samples. The final preparation stage involves drying the samples at 105°C for 24 hours to mass-constancy to ensure that no water remains inside the pores. Due to the existence of alteration minerals, Cornwall samples were dried at max 65°C for 48 hours.

The short plugs (diameter: 40 mm, length: 25 to ~30 mm) were predominantly used for the non-destructive petrophysical measurements like bulk density, porosity and permeability due to the specific sample size requirements of the measurement devices. The remaining plugs were prepared to meet the requirements for the different destructive rock mechanical tests, which were conducted after the petrophysical characterization. For most of the rock mechanical tests a length to diameter ratio of 2:1 (uniaxial and triaxial tests) or 1:2 (Brazilian test) is required. Furthermore, the plane surfaces of the plugs had to be plane-parallel with a maximum angular misalignment of 0.05°.

Density, Porosity and Permeability Measurement:

At TU Darmstadt, density measurements were performed in a multi-step procedure using an AccuPyc helium pycnometer (ASTM D5550) and a GeoPyc powder pycnometer (Micromeritics GmbH, Germany, 1997, 1998, 2014), analyzing particle and bulk volume five times for each plug, respectively (cf. Weydt *et al.*, 2020).

Following Boyle's law, the AccuPyc consists of two chambers with specified volume and pressure as presented in Figure 17. Core sample with known mass and dimension was put into the first chamber where helium gas was then introduced. The valve connecting both chambers was then opened allowing helium to flow from the first into the second chamber.

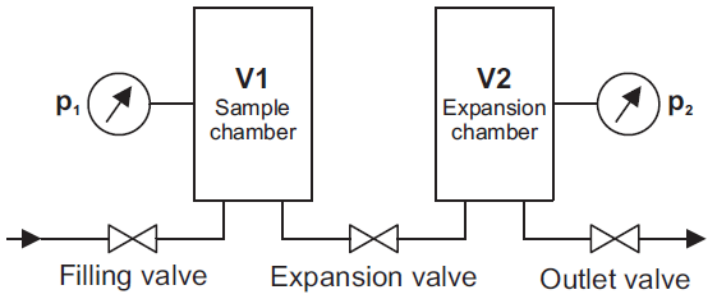

Figure 17: Schematic diagram of CorePyc for density measurement.

The following formula to calculate bulk density and porosities were calculated from the resulting differences in volume and represent the gas-effective porosity:

$$P_1(V_1 - V_g) = P_2(V_1 - V_g + V_2)$$

$$V_g = \frac{P_2 V_1 + P_2 V_2 - P_1 V_1}{P_2 - P_1}$$

$$\phi = \left(1 - \frac{V_g}{V_b}\right) \times 100$$

The accuracy of the method is 1.1% (Micromeritics, 1998).

Intrinsic matrix permeability was determined on cylindrical plugs (diameter 40 mm) with a column gas permeameter constructed according to ASTM D4525 (2013) and ASTM D6539 (2013) standard. The plugs were analyzed in a Hassler cell at constant differential pressure under steady state gas flow using at least five pore pressure levels (Tanikawa and Shimamoto, 2008). The corresponding gas flow rates were measured with different flowmeters that allow for the detection of flow rates in the range between 10 to 10,000 cm^3 min^{-1}. The method is based on Darcy's law enhanced by factors for the compressibility and viscosity of gases in order to calculate the gas permeability (Scheidegger, 1974; Jaritz, 1999). The water equivalent permeability was derived from the gas permeability after Klinkenberg correction (Klinkenberg, 1941). The samples were analyzed with dried compressed air at five pressure levels ranging from 1 to 3 bar and 1 MPa confining pressure (Hornung and Aigner, 2004; Filomena *et al.*, 2014).

Ultrasonic Waves Velocity Measurement:
Ultra-sonic wave velocity was measured with pulse generators (TU Darmstadt: USG-40 from Geotron-Elektronik, 2011) comprising point-source transmitter-receiver transducers. Transmitter emits polarized pulse at high voltage in high frequency range from 20 kHz to 1 MHz. The pulse travels through the core sample with known length and is received in the receiver on the other end of the sample as shown in Figure 18. The transmitted signals were recorded using digital oscilloscopes and the arrival times of the P-waves and S-waves were picked manually and corrected for the dead time, which arises from the recording device (transducer, function generator, oscilloscope).

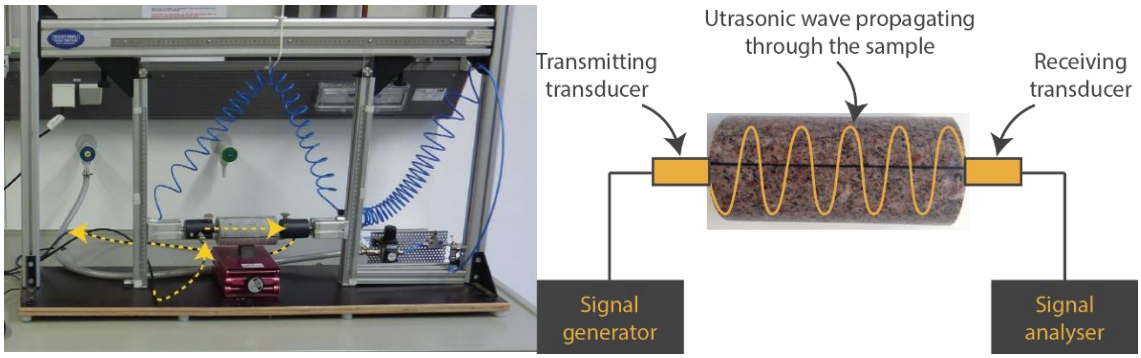

Figure 18: Defining ultrasonic velocities by measuring the time to travel from transmitter to receiver.

The measurement of P and S wave velocity enables estimation of mechanical properties (Mielke *et al.*, 2017). Bulk density, P and S wave velocities were used to determine dynamic elastic mechanical parameters, such as dynamic shear modulus, G_{dyn}, dynamic Young's modulus, E_{dyn}, and dynamic Poisson ratio, μ_{dyn} after Zoback (2011):

$$G_{dyn} = \frac{v_s^2}{\rho}$$

$$E_{dyn} = \frac{\rho v_s^2 (3v_p^2 - 4v_s^2)}{v_p^2 - v_s^2}$$

$$\mu_{dyn} = \frac{v_p^2 - v_s^2}{2(v_p^2 - v_s^2)}$$

, where ρ is bulk density [kg m^{-3}], v_p is compressional wave velocity [m s^{-1}] and v_s is shear wave velocity [m s^{-1}].

Thermophysical Properties Measurement:

Thermophysical properties comprises thermal conductivity and thermal diffusivity. Thermal conductivity is defined as the ability of a material to transfer heat along its body. While thermal diffusivity is defined as the rate of heat transfer along a material. In the HydroThermikum laboratory facility in TU Darmstadt, both properties are measured simultaneously using Thermal Conductivity Scanner after Popov et al (1999, 2016).

Thermal Conductivity Scanner is equipped by heat source and three optical temperature scan systems mounted in a motion box which heats the sample and measures the temperature of the sample before and after heating as shown in Figure 19. Prior to measurement, the samples have to be painted in black to maximize heat absorption. According to Lippman and Rauen (2009), the measurement accuracy for thermal conductivity and thermal diffusivity is 3% and 5% respectively.

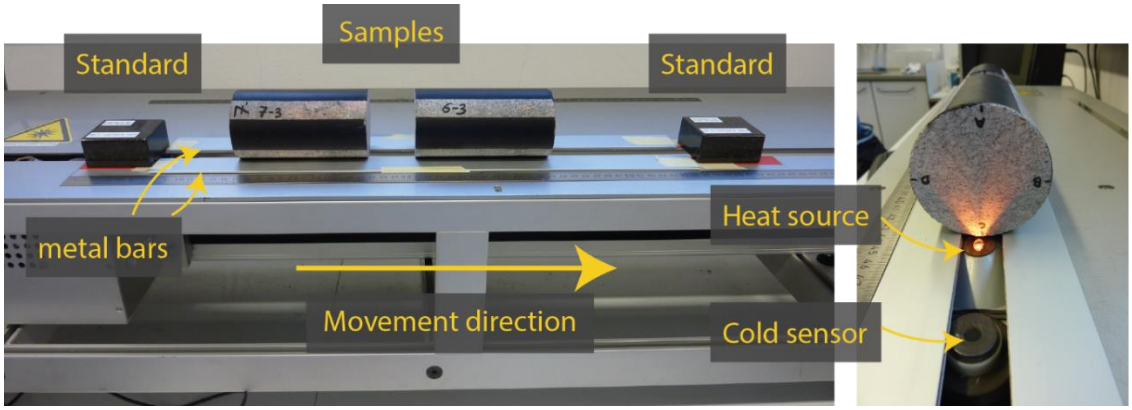

Figure 19: Thermophysical properties measurement using Thermal Conductivity Scanner (TCS).

Specific heat capacity at TU Darmstadt will be only determined in the upcoming months using a heat-flux differential scanning calorimeter (C80, Setaram Instrumentation, 2009). Therein crushed sample material will be heated at a steady rate from 20 up to 200°C within a period of 24 h. Specific heat capacities will be derived from the resulting temperature curves through heat

flow differences. The accuracy is 1% (Setaram Instrumentation, 2009). Volumetric heat capacity will be calculated by multiplying the specific heat capacity with the associated bulk density of each sample.
Additionally, specific heat capacity will be calculated for each plug by dividing thermal conductivity by the product of bulk density and thermal diffusivity (Buntebarth, 1980).

Uniaxial Test:
The primary outputs of uniaxial press device are unconfined compressive strength (UCS), Young's modulus, and tensile strength. At HydroThermikum laboratory in TU Darmstadt, the common sizes of the samples for this measurement are 55 or 64 mm in diameter with the length of twice of its diameter, except for tensile strength measurement where the diameter is four times of the length as shown in Figure 20. Note that the parallel grinding at preparation stage is necessary to minimize the shear stress resulting from rough or unparalleled surfaces.

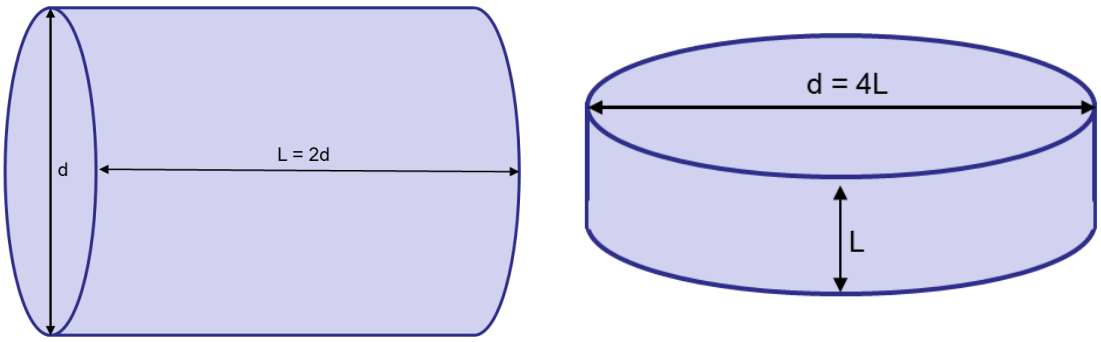

Figure 20: Sample requirement for UCS and Young's modulus measurement (left) and tensile strength measurement (right).

Unconfined Compressive Strength (UCS) is measured as the first stage of mechanical properties determination. Therefore, the measurement of UCS is of importance to the continuation of comprehensive mechanical properties measurement.

For the determination of the unconfined compressive strength (UCS) at TU Darmstadt, cylindrical plugs with a diameter of 40 mm and a length of 80 mm were introduced into a hydraulic uniaxial press (Formtest Prüfsysteme, Germany) with a capacity of 1,000 kN and a maximum loading rate of 0.5 kN/s until sample failure. The stress at this particular point represents the UCS, which was calculated according to ASTM D7012 (2014) and DIN 18141-1:2014-05:

$$UCS = \frac{F}{A})$$

, where F is load [N] and A = area [mm²]. Whenever the plugs were shorter than 80 mm and did not fulfil the required 2:1 length/diameter ratio, a correction function was applied as proposed by DIN 18141-1:2014-05:

$$\sigma_{U(2)} = \frac{8 \cdot \sigma_U}{7 + 2\frac{d}{l}}$$

, where $\sigma_{U(2)}$ is corrected UCS [MPa] and σ_U measured UCS [MPa] respectively and d is sample diameter [mm], while l denotes its length [mm]. At TU Darmstadt all destructive tests using the hydraulic uniaxial press were performed based on 'force controlled' method with a maximum loading rate of 0.5 kN/s.

Young's modulus is the next step of mechanical properties determination. For the determination of the static Young's modulus and Poisson's ratio cyclic uniaxial tests were performed on 3 plugs (same dimension as described above) for each sample according to DIN 18141-1:2014-05 and Mutschler (2004). During loading phase, the sample is pressed up to 25% of UCS and followed by unloading phase where the sample is relaxed. Displacement sensors are set around the cylindrical samples with 120° spacing to measure lateral deformation. Whilst axial displacement is measured by the hydraulic press. The loading-unloading sequence continues to higher loading phase for instance, 50% and 75% for the determination of the deformation moduli (Figure 21).

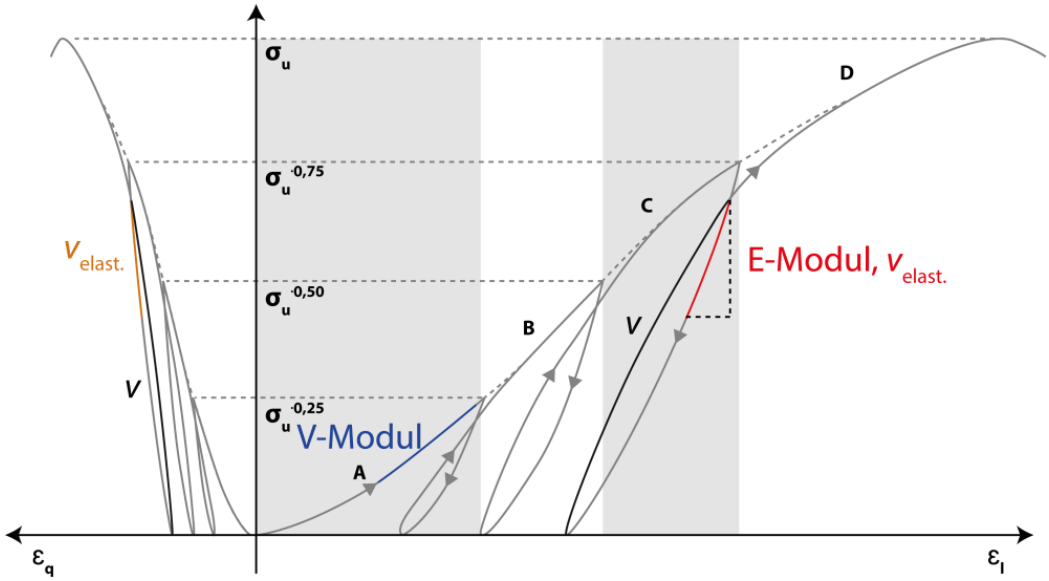

Figure 21: Sequence of loading and unloading phase for Young's modulus measurement.

According to Mutschler (2004), a holding time of five minutes was set at the maximum value of each cycle. After the end of the holding time of the second cycle, the sensors were removed, and the sample was loaded until failure point to obtain the UCS. Using the results of the first unloading cycle, the static Young's modulus (average modulus) of each plug was calculated as the difference in stress divided by the difference in the vertical deformation according to ASTM D 3148 (2002). Likewise, the static Poisson's ratio was calculated as the ratio of lateral deformation to original diameter divided by the ratio of vertical deformation to original plug length. Subsequently, G-modulus, G, and Bulk modulus, K, were calculated after ASTM D7012 (2014):

$$G = \frac{E}{2(1+\mu)}$$

$$K = \frac{E}{3(1-2\mu)}$$

, where E is Young's modulus [N mm^{-2} or MPa] and μ the Poisson's ratio [-].

The last measurement that is determined by uniaxial device is tensile strength. Note that direct measurement of tensile strength is not possible due to the difficulty to resemble tension stress in real sample and thus it is rather hypothetical. The most popular test is the Brazilian Test, according to ASTM 3967 (2016) and Lepique (2008). Despite the identical procedure to UCS determination, the sample size requirement for tensile strength measurement is rather circular disc shape where the diameter is twice of its length. The sample is constantly pressed until it reaches failure point. Afterwards the tensile strength of the plug was calculated using the following equation:

$$\sigma_t = \frac{2 \cdot F}{\pi \cdot d \cdot l}$$

, where σ_t is the tensile strength [N mm^{-2} or MPa], F the load at failure [N], d the diameter [mm] and l the sample length [mm].

Friction Angle and Cohesion:

Friction angle (φ) and cohesion (C) are measured using a hydraulic triaxial press (Wille Geotechnik, Germany) with a capacity of 500 kN as shown in Figure 22 (left). Besides axial stress from the top and bottom of the sample (σ_1), the sample is subject to lateral stress ($\sigma_2 = \sigma_3$), which is transmitted from the pressurized hydraulic oil. Note that special jacket is used, and the sample size is strictly limited to 55 mm in diameter and 110 mm in length.

The idea of using triaxial device is to simulate failure criterion due to the stress from three principal direction as depicted in Mohr-Coulomb diagram in Figure 22 (right). Note that a minimum of three samples per rock type are required to construct the Mohr-Coulomb diagram by varying confining pressure. The resulting tangent line of the circles is then used to approximate the Mohr-Coulomb failure criterion. Whereas cohesion is determined by the intersection with y-axis or shear stress.

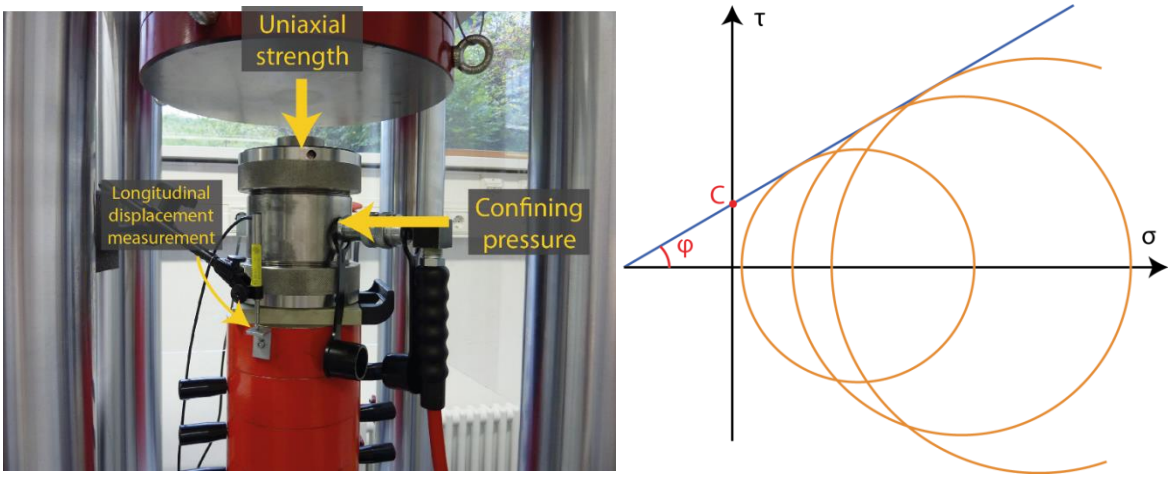

Figure 22: Hydraulic triaxial press device (left) and example of Mohr-Coulomb diagram to derive friction angle (φ) and cohesion (C) (right).

Depending on the availability, three plugs (diameter of 55 mm, length of 110 mm) for each sample were tested using different confining pressures (σ_3) of 10, 20 and 30 MPa, respectively. According to ASTM 2664 (2004), the confining pressures and resulting vertical stresses (σ_1) were transferred into a shear stress diagram to construct the Mohr-Coulomb criterion of failure to derive cohesion (intersection with the vertical axis) and friction angle (the angle between the line and the horizontal axis). Whenever needed, the vertical stresses from UCS tests (with $\sigma_3 = 0$) were considered to construct an additional circle in the shear stress diagram, thus enhancing the data evaluation.

Lab investigation of chemical stimulation effectiveness:
For the United Downs demosite specific investigations were performed to quantify the impact of chemical rock treatment on the permeability and to understand the governing processes. This work is explained in more detail in MEET deliverable 5.3 and in the associated Masterthesis of Katja Schulz, student at TU Darmstadt. Figure 23 represents the specific workflow for these investigations on drill cuttings and selected outcrop analogue samples to identify how chemical sample treatment at reservoir conditions increases the permeability (cf. Schulz, 2020).

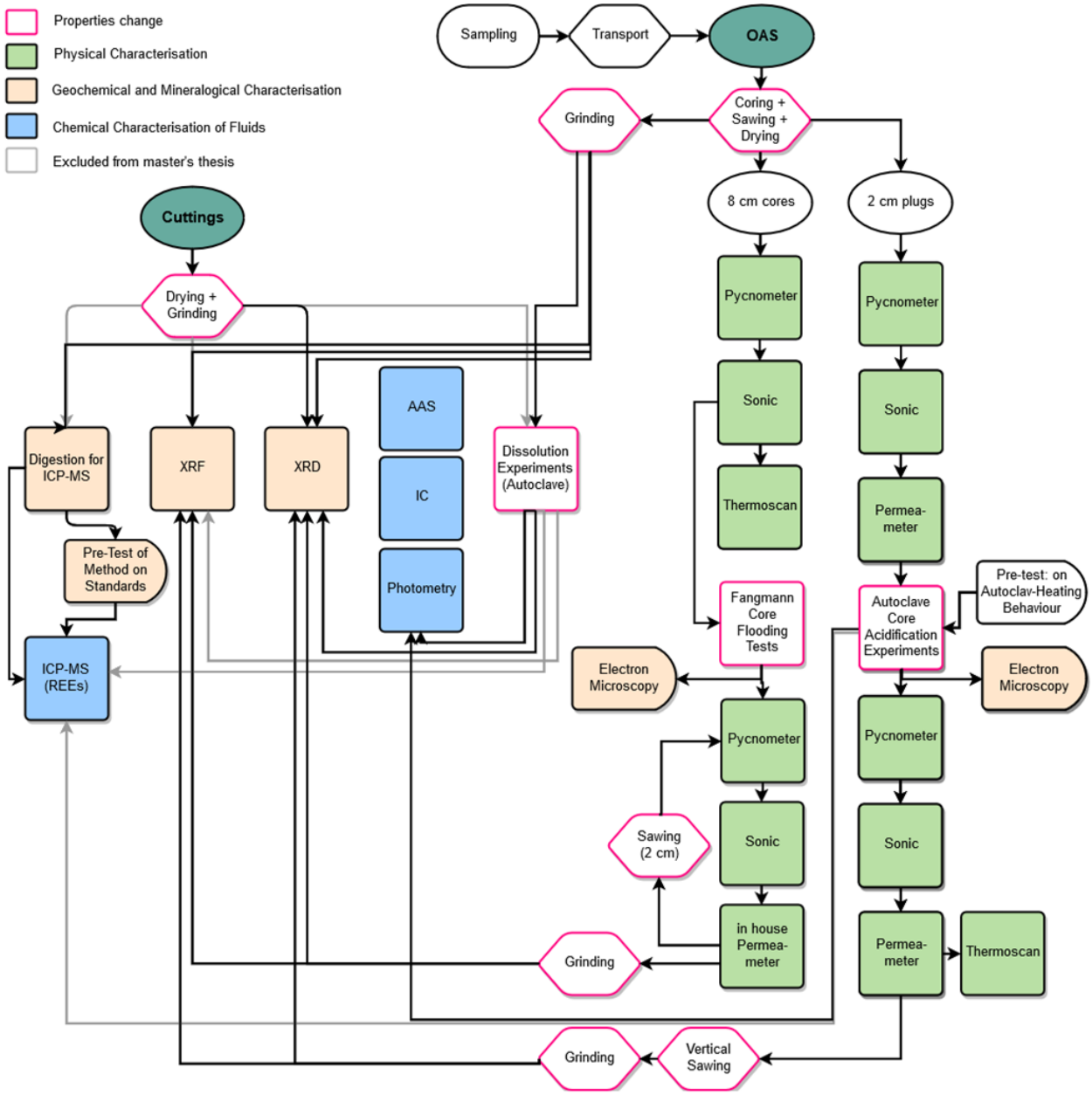

Figure 23: Lab work has been done on drill cuttings and on outcrop analogue samples, with the numbers 4, 21, 24, 27, 35 and 45, selected for chemical analysis (Schulz, 2020).

2.2.2.2 Workflow at laboratory facilities of Cergy University

In the scope of this study, CYU followed an analytical approach that integrates three main aspects:

- Logging cores in order to reveal an evolution in the rock type, which gives clues about the emplacement of metamorphic units. To complement these observations, emphasis is put on the description of main structures, fractures, veins or cleavages, as they provide potential pathways for fluid circulation.
- The collection of thin-sections for the analysis of detailed mineralogical characteristics under optical microscopy and Raman spectroscopy. These investigations give indications about the processes leading to precipitation of newly formed secondary minerals. This classical approach is coupled with calcimetry in order to quantify the calcite content, to estimate the potential impact of calcite formation and to evaluate the chemical stimulation potential.
- The collection of plug samples of the drill cores in order to perform petrophysical measurements for understanding the distribution of porosity/permeability and their anisotropy in the different kinds of basement rock types. In this way, the investigation also covers the link between permeability, magnetic susceptibility and structural patterns at micro- and meso-scales in the metamorphic rocks.

To achieve these objectives, CYU team logged nearly 100 m of rock cores in the core boxes and sampled pieces of representative facies.

Hand specimens were collected for thin-section making, used for standard petrography analysis as well as Raman Spectroscopy, and further analysis. In addition, representative pieces of samples were ground up in order to prepare powders that were analysed for magnetic properties and calcimetry. These powders are planned to be used later within MEET for X-ray diffraction (XRD), especially for the identification and quantification of clay minerals. Plug sampling followed a protocol with a specific sense convention operative in anisotropy of physical properties (Louis *et al.*, 2003), X and Y being perpendicular to the main core, and Z being parallel to the main core.

CYU performed various in-situ analysis as described in the analytical workflow (Figure 24).

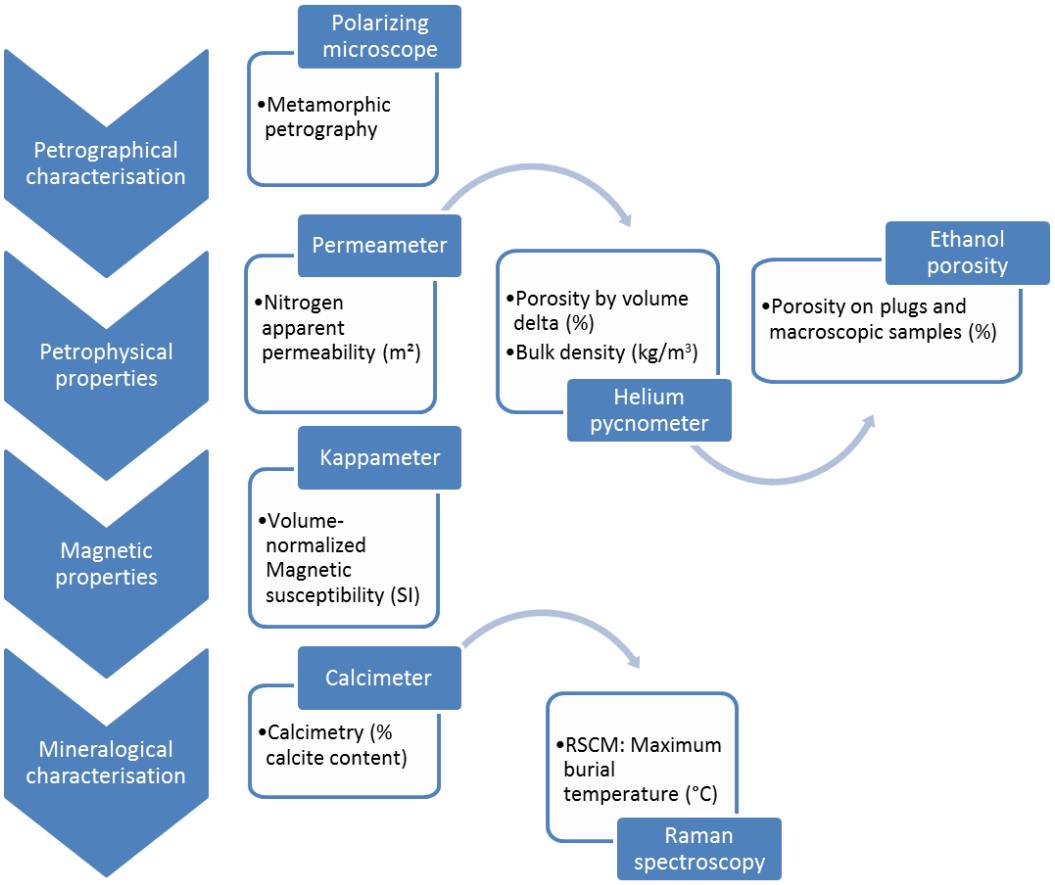

Figure 24: Analytical workflow for data acquisition on samples from the Variscan basement, underneath Paris and Aquitaine basins.

Permeability

The measurement device for permeability is a steady-state gas permeameter (VINCI Poroperm - Figure 25). Acquisition is performed using forward method that does not need to keep ΔP or flow constant and that is more suitable for low-permeability rocks, such as those sampled in the project. The fluid used in this experiment is nitrogen for its small molecular size in order to access pore throats The obtained permeability is apparent since the apparatus measures the flowing response to an increase in gas pressure, taking into account the Klinkenberg effect (gas slippage effect on pore walls causing an increase in permeability) and a simplification of Darcy's law for an ideal gas (nitrogen) at ambient conditions. For material with very low permeability, the necessary conditions to satisfy Darcy's law cannot be maintained as the flow is non-laminar and ΔP between top and bottom of the plug is not high enough to measure a significant flow rate.

Figure 25: VINCI Poroperm.

Porosity-Density

In terms of petrophysical characterization, porosity data were acquired using two methods in order to evaluate the sensitivity of the technique for this key parameter.

The first employed method is a helium gas displacement pycnometry system (Micromeritics AccuPyc II 1345 pycnometer - Figure 26) and consists of high precision volume acquisition and volume difference between gas volume and cylindrical volume of the plug. This allows calculating the pore volume. However, the outer volumetric envelope is obtained from measurements of length and diameters that are subject to slight dimensional changes along the plug. The associated uncertainty is difficult to predict and would be overcome with a 100 µm accuracy 3D scanner that would allow to calculate a very precise volumetric external envelope. Without such a scanning device, this method provides inconsistent results due the low accuracy of the external volume compared to highly precise volume calculation in the pycnometer.

The bulk density of the plugs is also measured by the pycnometer.

Both volume and density are provided after 10 measurements with minimum value, maximum value, average value and standard deviation.

Figure 26: Micromeritics AccuPyc II 1345 pycnometer.

The second employed method to determine porosity is based on hydrostatic weighing protocol – i) dry mass; ii) wet mass under fluid saturation; iii) immerged mass under Archimedes force – applied using ethanol fluid (Figure 27). Ethanol has been chosen instead of water, as used in classical methods, in order to avoid possible clay swelling, which could lead to the destruction of the sample. Even though ethanol (0,469 nm) is a larger molecule than water (0,343 nm), the pore volume is not estimated to be underevaluated. The technique is robust and the results are preferred to helium pycnometer data when compared to other petrophysical parameters on graphical plots.

The applied formula for calculating ethanol porosity is:

$$\emptyset_{ethanol}\,(\%) = \frac{m_{sat} - m_{dry}}{m_{sat} - m_{im}}$$

Figure 27: Facilities used for ethanol imbibition under vacuum (left) and for weighing the dry, wet and immerged masses (right).

Magnetic susceptibility

The acquisition of magnetic susceptibility data is carried out from a high precision kappameter (KLY4/CS3 AGICO Kappabridge - Figure 28) that allows to measure bulk magnetic susceptibility from a sample powder. The data presented in this document are normalized to standard volume.

Figure 28: KLY4/CS3 AGICO Kappabridge.

Calcimetry

Calcite is a frequently observed mineral in geothermal systems and its precipitation can contribute to hinder fluid flow. Calcimetry is now performed as a routine in many geothermal prospects. Depending on calcite content and connectivity through the rock media, calcite could be mobilised by chemical stimulation. It is therefore important to quantify the amount of calcite and to confront it to the petrographic results in order to characterize the geometry and continuity.

The protocol for measuring calcite content consists in hydrochloric acid attack of dried sample powder, approximately 1 to 1.4 grams, in two calcimeters (Figure 29) for ensuring data replicability. Both calcium carbonate and magnesium carbonate are reacted with 10 percent hydrochloric acid in a sealed reaction cell to form CO_2. As the CO_2 is released, the pressure build up is measured using a pressure gauge during 45 minutes-long dissolution process. During the calibration process, a calibration curve is created by reacting HCl with pure, reagent-grade $CaCO_3$. By using a known weight of $CaCO_3$ reagent, you can determine the relationship between the amount of pressure released and the weight of $CaCO_3$ in the sample. Since all reaction cells are slightly different, this relationship will be different for each cell. Therefore, a calibration curve is required to obtain accurate results.

The following formula allows determining the percentage of $CaCO_3$:

$$\% \, CaCO_3 = \frac{\text{Pressure reading (PSI)} * 100}{\text{Sample weight (g)} * \text{Average calibration slope}}$$

The average calibration slopes for the two calcimeters used on each sample are:

Calcimeter #1 coefficient = 18.85

Calcimeter #2 coefficient = 19.36

Figure 29: Calcimeter and detail of the pressure gauge on the top.

Petrography

Petrological analysis is performed on standard 30 µm-thick uncovered thin-sections with a classical polarizing microscope (OLYMPUS BX51). Every sample is investigated in order to depict mineralogical content, characteristic mineral assemblages indicating the degree of metamorphism, chronology of paragenesis as well as miscrostructures resulting from deformation processes.

Raman Spectroscopy on Carbonaceous Material (RSCM)

Raman spectroscopy is a non-destructive method for observing the external structure and molecular characterization of materials. This method allows measuring the evolution of organic matter, which is a good indicator of the degree of transformation of the rock (mainly temperature).

The observations/characterizations are made with the Raman confocal microscope associated to a spectrometer (WITEC Rise) under ambient atmosphere (standalone mode) or under vacuum (SEM coupling mode). It is equipped with a Nd laser of 532 nm and 75 mW, with 1-2 s accumulation time during application of laser beam, repeated 25-50 times. Raman spectrometer is installed on the "i-Mat Plateforme Microscopies et Analyses" of CY Cergy Paris Université (Figure 30).

In standalone mode that was used for the observations, the horizontal resolution is comprised between 0.36 and 0.81 µm, whereas the vertical resolution is rather between 0.92 and 4.85 µm.

Raman spectra of each data point were compiled in PeakSpectroscopy® software for smoothing, de-noising, baseline correction, peak picking and identification of minerals through RRUFF Raman spectra library, and finally peak measurements. The deconvolution of Raman spectra is necessary to quantify the height, full-width at half-maximum (FWHM) and area of the D1, G and D2 peaks. It must be realized on a baseline-curve in order to allow addition of Gaussian-type functions to mimic the Raman spectrum.

These quantitative data were then used to determine characteristics of the D1, G and D2 bands of carbonaceous materials that are needed in Raman Spectroscopy on Carbonaceous Material (RSCM) by calculating the maximum burial temperature, with a 50°C uncertainty on the method (Beyssac *et al.*, 2002), based on R1 and R2 ratios:

$$R1 = \frac{D1}{G} \qquad \text{(intensity ratio)}$$

$$R2 = \frac{D1}{(\mathrm{G} + \mathrm{D1} + \mathrm{D2})} \qquad \text{(area ratio)}$$

$$T\ (°C) = -445 * R2 + 641$$

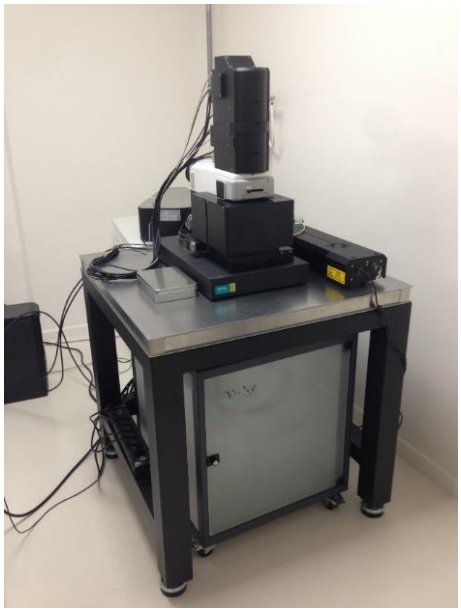

Figure 30: WITEC Rise Raman spectrometer, connected to optical microscope (standalone) or SEM (coupled).

In addition to the calculation of maximum burial temperature, Raman spectroscopy also allows to identify specific unknown minerals by comparing the spectra to the RRUFF database or any other mineralogical spectral databank.

2.2.2.3 Experimental analyses at GFZ

Prior to deformation experiments, sample composition as well as porosity were determined by X-Ray Diffraction (XRD) on powdered sample material and He-pycnometry, respectively Figure 31). Brazilian Disk at ambient and const. strain rate experiments performed at elevated confining pressure and temperature have been conducted to generally characterize the sample material with respect to its mechanical properties (e.g., tensile strength, σ_t, triaxial compressive strength, σ_{TCS}, static Young's modulus, E).

Constant strain rate experiments were performed on cylindrical samples with a diameter of d=10 mm and a length of l=20 mm at an axial strain rate of $\dot{\varepsilon}=5\times10^{-4}s^{-1}$, p_c=50 MPa and T=100°C, representing in situ deformation conditions. Here, two experiments were performed: 1) loading direction perpendicular to bedding orientation and 2) loading direction at angle of $\theta\approx30°$ with respect to bedding. Three Brazilian disk tests have been performed on cylindrical disks (d=30 mm, thickness, t=15 mm) at ambient pressure and temperature and axial strain rates of $\dot{\varepsilon}=6.67\times10^{-5}s^{-}$

[1], following the ISRM suggested methods (ISRM, 1978). Comparable to conducted const. strain rate experiments, BD were also performed at varying bedding orientations.

A general overview of the whole procedure including sample preparation and experimental in terms of a flow chart is given in Figure 31.

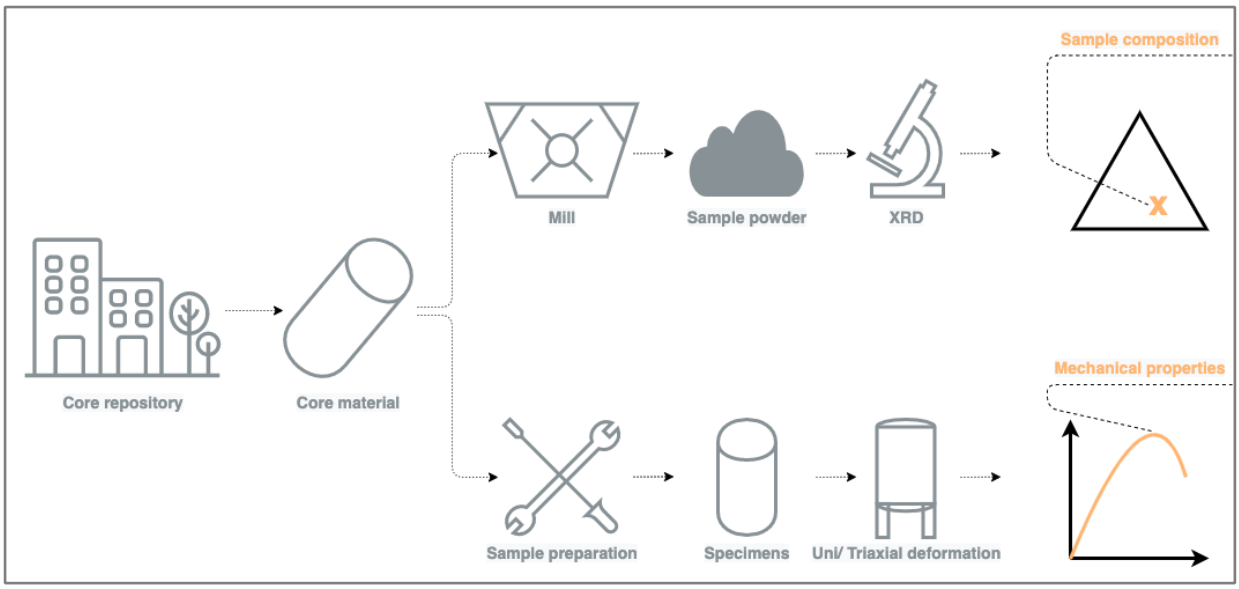

Figure 31: Sample preparation and experimental procedure at GFZ.

Specimens made of the same slate material as used for the previously mentioned experiments will be used to conduct flow tests with the aim to characterize fracture permeability (D5.8). Here, we will investigate the influence of specific in situ reservoir conditions such as confining pressure, temperature and differential stress as well as time on the long-term conductivity of fractures within this rock type. Additionally, fluid-rock interactions will be characterized to ultimately estimate the feasibility and economy of an EGS utilizing slate rocks. Results of these investigations will be reported in Deliverable D5.8.

2.2.2.4 Experimental analyses at ULS

Petrographical investigations (Death Valley, Noble Hills):

For the petrographical analysis of the samples, more than 94 thin sections were made. This analysis allows to determine the type of granite and to understand the alteration and deformation processes that occurred.

XRD analyses on 54 samples were performed by separating the different clay fraction (<2 µm and 2-6 µm) to study the evolution of clay composition and to determine the thermal gradient thanks to the illite crystallinity index.

2.2.3 Results

2.2.3.1 Outcrop analogue sample results: Havelange and Göttingen outcrop analogues

Petrophysical and thermophysical properties were analysed on about 221 core samples. Note that, not all measurements were conducted in all 221 core samples. The data shows heterogeneity of each rock type as shown in Figure 32.

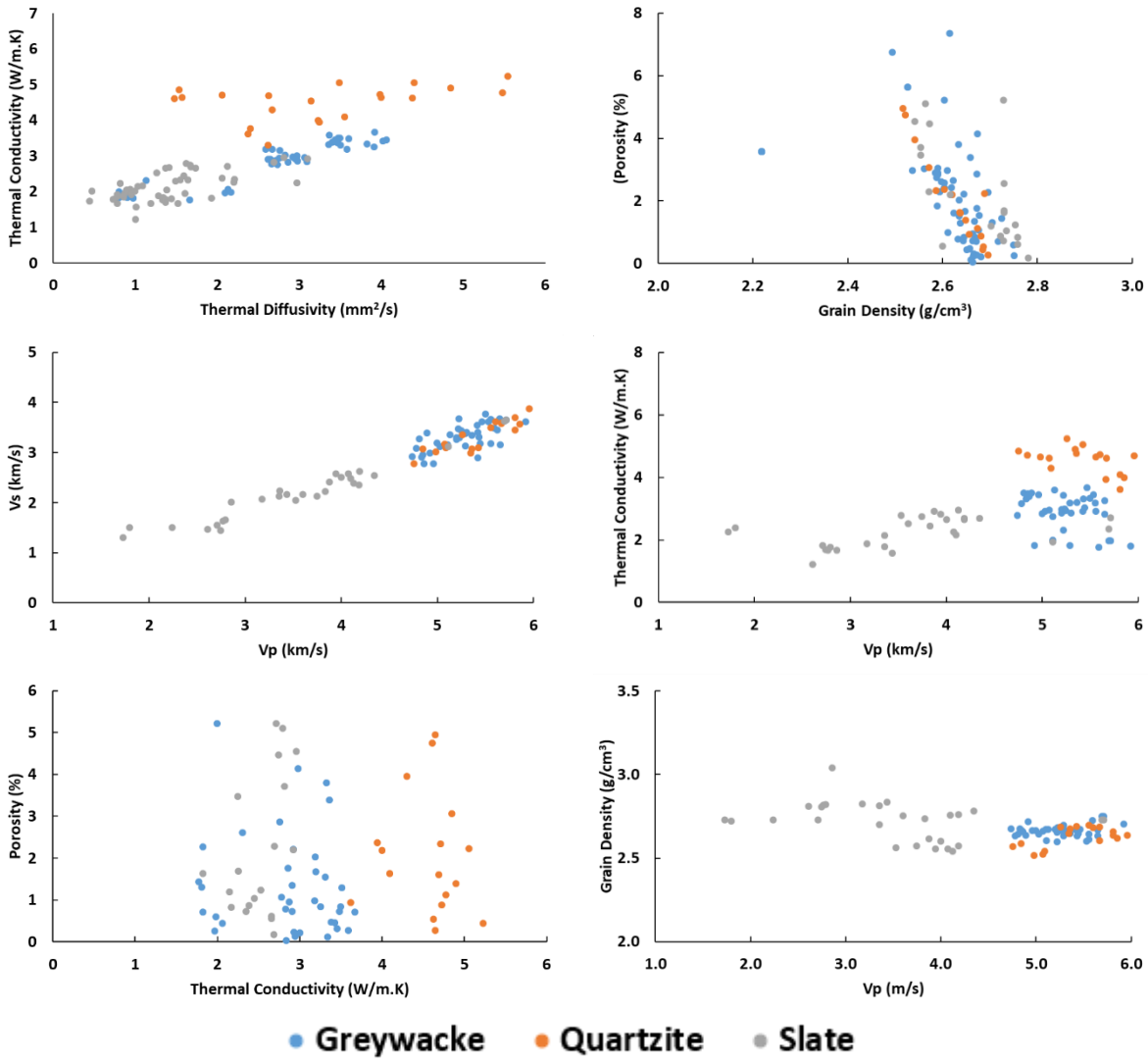

Figure 32: cross plot of petrophysical properties measured on the greywacke, quartzite, and slate samples at dry conditions.

Thermal diffusivity correlates linearly with thermal conductivity. Quartzite has the highest thermal conductivity among other rock types with relatively wider range of thermal diffusivity. This has to be supported by thin section to identify the mineral content which exhibits high thermal conductivity. Thermal diffusivity and thermal conductivity of slate and greywacke are rather low to moderate.

Density and porosity show linear correlation, despite the presence of scattered data. Note that porosity was calculated volumetrically assuming perfectly cylindrical core sample. Therefore, negative porosity and large porosity might be observed and thus are treated as error data. All rock types generally show low porosity with range of density between 2 600 to 2 800 kg/m^3.

P-wave velocity increases proportionally with the increase of S-wave velocity. Low porosity leads to relatively homogeneous rock in terms of the ability to transmit ultrasonic velocity which is shown by clustered data for each rock type. Furthermore, P-wave velocity is independent of the rock density and thermal conductivity.

Figure 33 shows the cross plot of thermophysical and petrophysical properties clustered according to the origins.

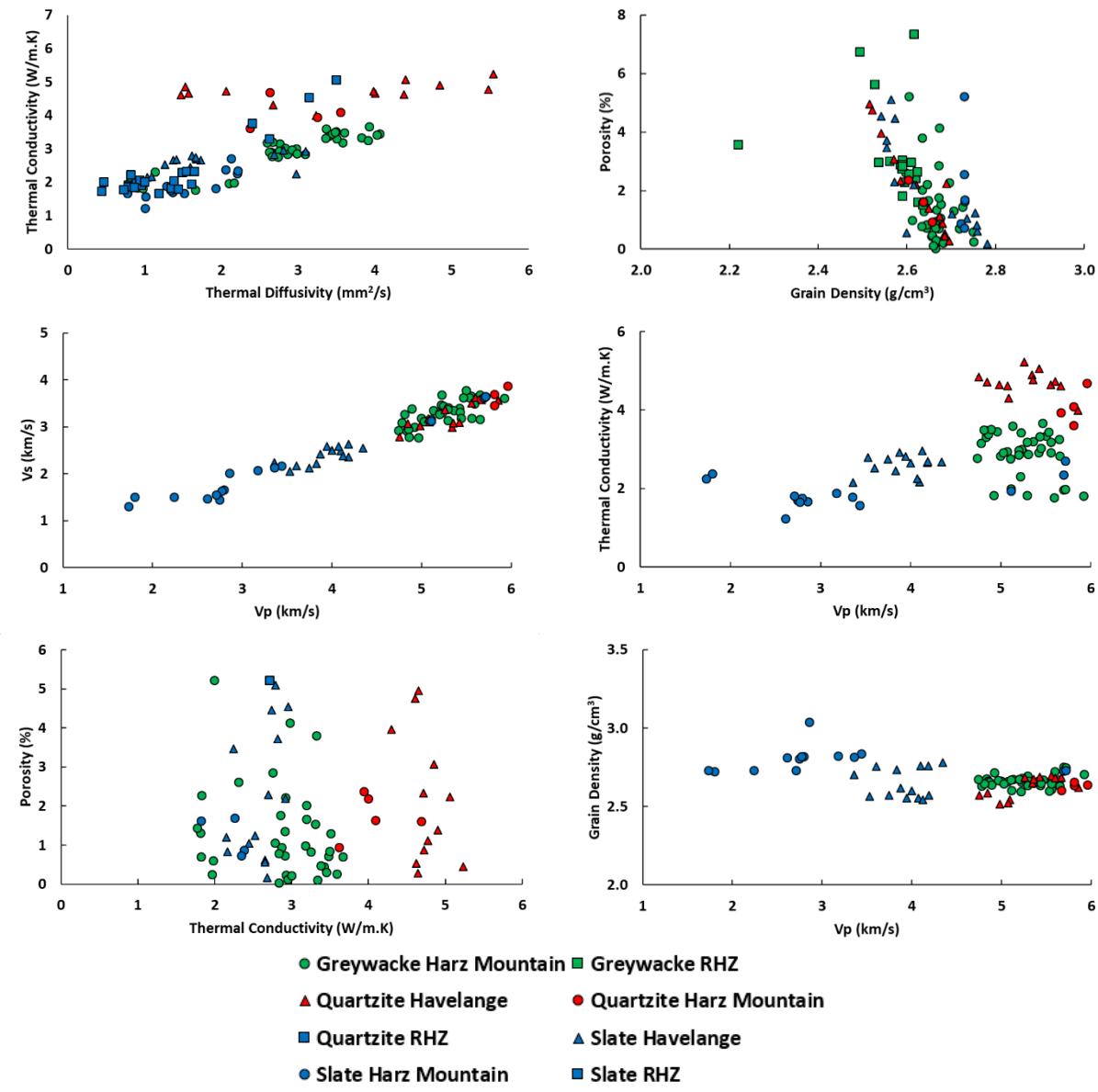

Figure 33: cross plot of petrophysical properties measured on the greywacke, quartzite, and slate samples at dry conditions sorted based on their origins.

2.2.3.2 Results obtained at GFZ

XRD analyses reveal a slate matrix mainly made of Clays + Mica (50 wt%), Carbonates (25 wt%) and Quartz + Feldspar (25 wt%).

He-pycnometry yielded relatively low porosity values of ϕHe=1-2%. (Tab. 1)

Table 10: Petrophysical properties determined by GFZ.

Material	Clay+Mica [wt%]	Carbonate minerals [wt%]	Quartz+Feldpar [wt%]	ϕ_{He} [%]
Wissenbach Slate	50	25	25	1 – 2

ϕ_{He} = porosity measured by Helium pycnometry

Table 11: Mechanical properties determined by GFZ.

sample	E [GPa]	σ_{TCS} [MPa]	σ_t [MPa]	Annotation
MEET_01	51	315		$\alpha \approx 30°$
MEET_11	69	498		$\alpha \approx 90°$ (perpendicular)
MEETBD_01	/	/	26.65	Divider config.
MEETBD_04	/	/	20.19	Arrester config.
MEETBD_05	/	/	7.85	Short-transvers config.

E = static Young's modulus, σ_{TCS} = Triaxial compressive strength, σ_t = Tensile strength, α = loading direction with respect to bedding orientation

2.2.3.3 Reservoir sample results: Göttingen demosite

At the Göttingen University Campus demo site, no reservoir samples are available since no well down to the Variscan basement suitable for sample collecting exist yet.

2.2.3.4 Reservoir sample results: Havelange demosite

All the results from the mineralogical analyses (XRD and Calcimetry) from the Havelange borehole cuttings are both integrated into an in-house viewing platform allowing to compare the lab results with other source of information such as the borehole logging (dipmeter, Gamma-ray) as well as P³. An extract of this platform is presented in Figure 34.

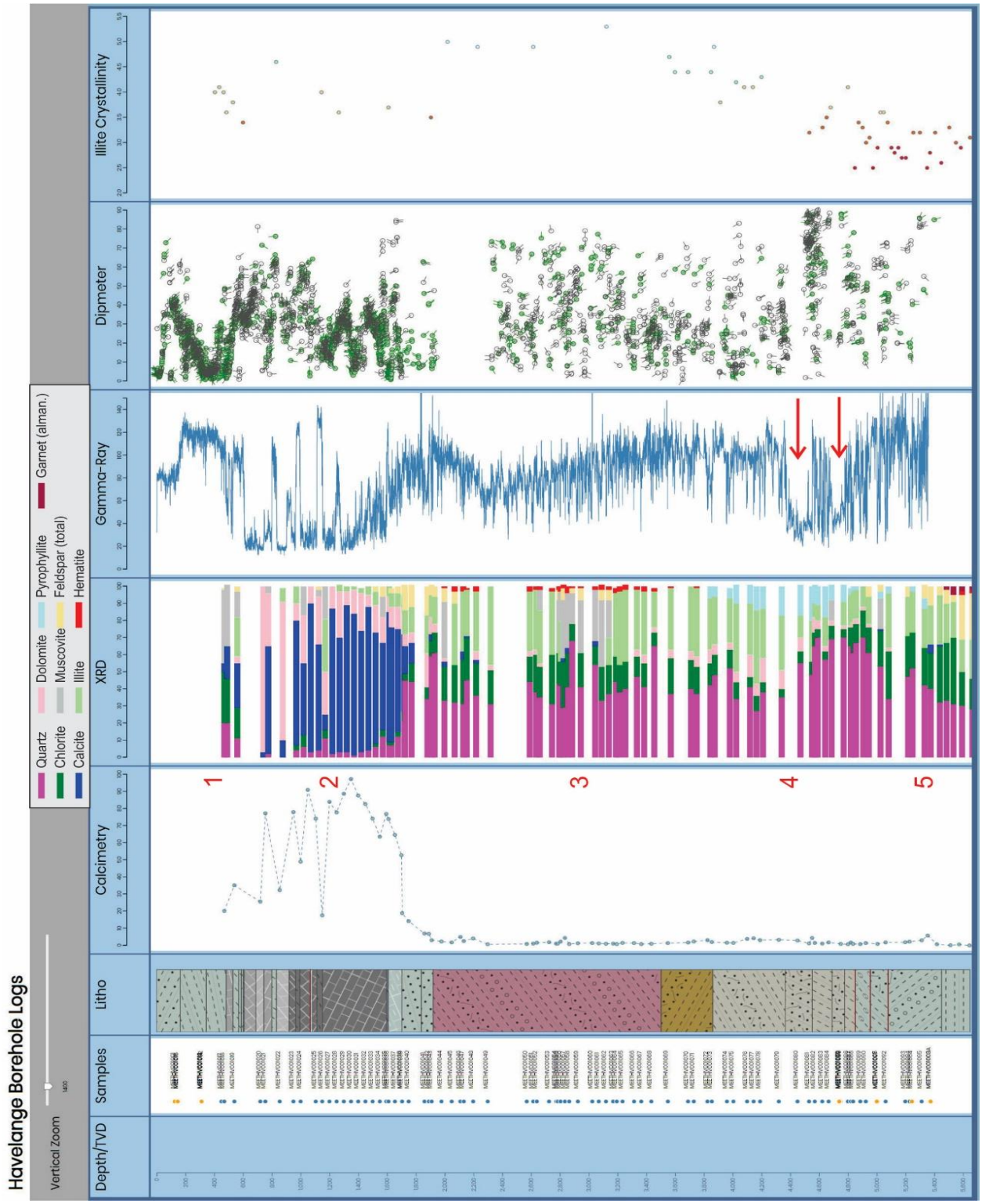

Figure 34: Extract from the Havelange logging viewing platform presenting from left to right: borehole depth, sample, lithologies, calcimetry results, XRD result, Gamma-ray log, dipmetry and illite crystallinity. For explanation of red numbers and arrows, please refer to the following text.

The comparison of the various sources of information indicates that the subsurface of the Havelange borehole can be divided into 5 units, namely:

1- A shale-dominant unit of the Lower Famennian composed of quartz, chlorite (probably clinochlore), muscovite and a small amount of calcite and/or dolomite;
2- A limestone and dolostone unit of Frasnian/Givetian age associate with small amount of quartz and illite;
3- A detrital unit (Emsian-Eifelian) rich in quartz, chlorite, illite and muscovite. It is also frequently associated with small amounts of feldspar and hematite;
4- A composite unit (Lower Devonian) very rich in quartz and illite associated with the presence of pyrophyllite. The remaining mineralogical phases are chlorite and dolomite.
5- A Lower Devonian unit with the higher degree of metamorphism as shown by the illite crystallinity index and by the presence of garnet (probably almandine). The significant amount of chlorite and feldspar is another characteristic of this unit. Pyrophyllite observed in unit 4 seems to disappear in this unit.

The main target horizons for the development of a geothermal reservoir in the Havelange borehole correspond to the quartzite members of unit 4. They are indicated by 2 red arrows corresponding to two local minima of the low Gamma-ray signal.

2.2.3.5 Fluid sample results: Havelange demosite and outcrop analogues

In the framework of the Havelange demosite a spring water sampling campaign was conducted by the Geological Survey of Belgium (GSB) during winter 2019-2020. The aim of this task is threefold: 1) to evaluate the geochemical water composition in different geological formations encountered in the demo-site local stratigraphy; 2) to detect potential deep fluid circulation both in the near- and far-field of the study zone; 3) to assess the hydrogeological behaviour of the geological formations and the existence/absence of fluid flow between different units. All these actions are part of an exploration strategy to detect potential target for the development of geothermal reservoir in meta-sedimentary formations.

Campaign development

- An initial step (summer-fall 2019) consisted of identifying the key chemical elements and ions that are suitable for the exploration campaign. This activity included a literature review combined with interactions with other MEET partners in order to strengthen the requirements;
- A map analysis work was realised during summer and fall 2019 to identify the different sources in the study zone and to classify them into a set of priorities for sampling. This work was conducted by our sub-contractor VS-GEOFORMA.
- A public procurement tender was launched during fall 2019 towards analytical laboratories specialized in geochemical water analysis. Three offers were received, and we have selected the “Société Wallonne des Eaux” (SWDE) to conduct the analyses.
- A preliminary work of land-owner identification and sampling methodology was set-up before the actual start of the sampling campaign, which took place in November 2019

until the beginning of March 2020. For each sampling site an extensive list of information and parameters were collected including the GPS-site location, a description of the environment conditions, some pictures, the eventual infrastructures, the weather conditions during the sampling and the spring water physicochemical parameters (pH, EC and temperature).

- All water samples collected during the campaign were referred according same sample annotation convention decided during the MEET project (see D5.2.). We paste the letter 'W' at the end of the annotation to stamp the specimen as the 'water'.
- Small accurate temperature loggers, called SpringNiph and derived from the existing Niphargus logger (Burlet *et al.*, 2015) were installed to record the spring temperature during a long period. The installed loggers are currently recording the temperature with a timestep of 1h and this monitoring will last until the end of the project. We are planning to download the recorded values on the few month-basis periods.
- A total of 50 samples were collected at the end of the campaign and all the field observations, location combined by the result of the geochemical analyses were integrated into a database. Figure 35 shows the location of the 50 samples in the near and far fields presenting a preliminary result with the Lithium concentration.
- All results will be analysed during the second half of year 2020 and will be possibly combined with complementary analyses or observations to reinforce the study.

The preparation works, the parameters and information collected during campaign has quickly required the development of a dedicated database, called MEET-WATER. Its architecture has constantly evolved during the sampling campaign to cope with the field reality and it has reached now a mature stage presented in Figure 36. The MEET-WATER database includes 15 tables with the "site" table representing the backbone of the architecture. This table includes all information regarding the sampling site position, naming along with other information such as different categories of site, a description of eventual infrastructures, etc.

The "visitlog" table gathers all information and activities during a visit of a site, such as the date and time, the weather conditions, the collection or not of the water sample, the installation or downloading of temperature records of a SpringNiph, the measurements of the physicochemical parameters, etc.. Finally, the "geochemistry" and "geochemistryfiltered" tables include all the geochemical analyses for both unfiltered and filtered water samples, respectively.

The MEET-WATER database is a relation database based on the open-source systems: PostgreSQL and PostGIS. These systems allow a rapid and easy integration of the results into GIS software, but also the potential data interfacing within web applications.

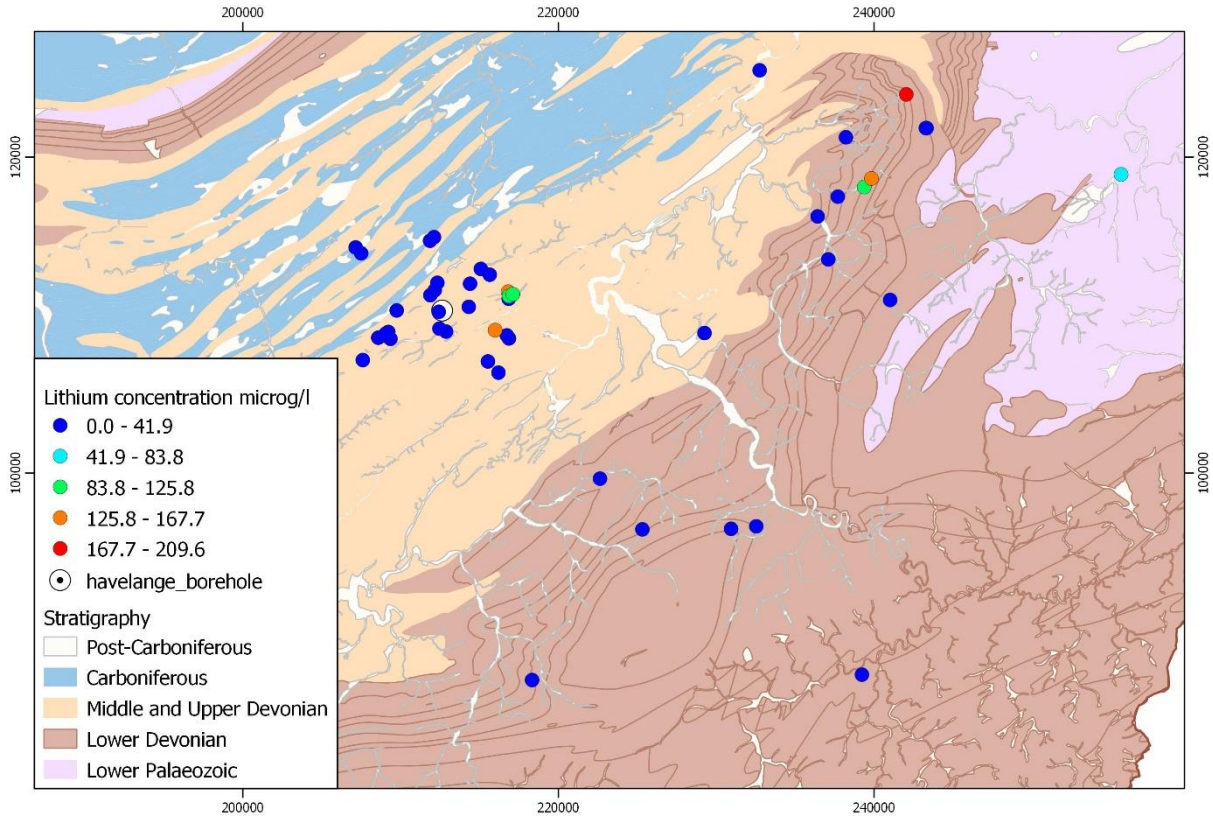

Figure 35: Location map of the spring water samples collected in the framework of the MEET-WATER database.

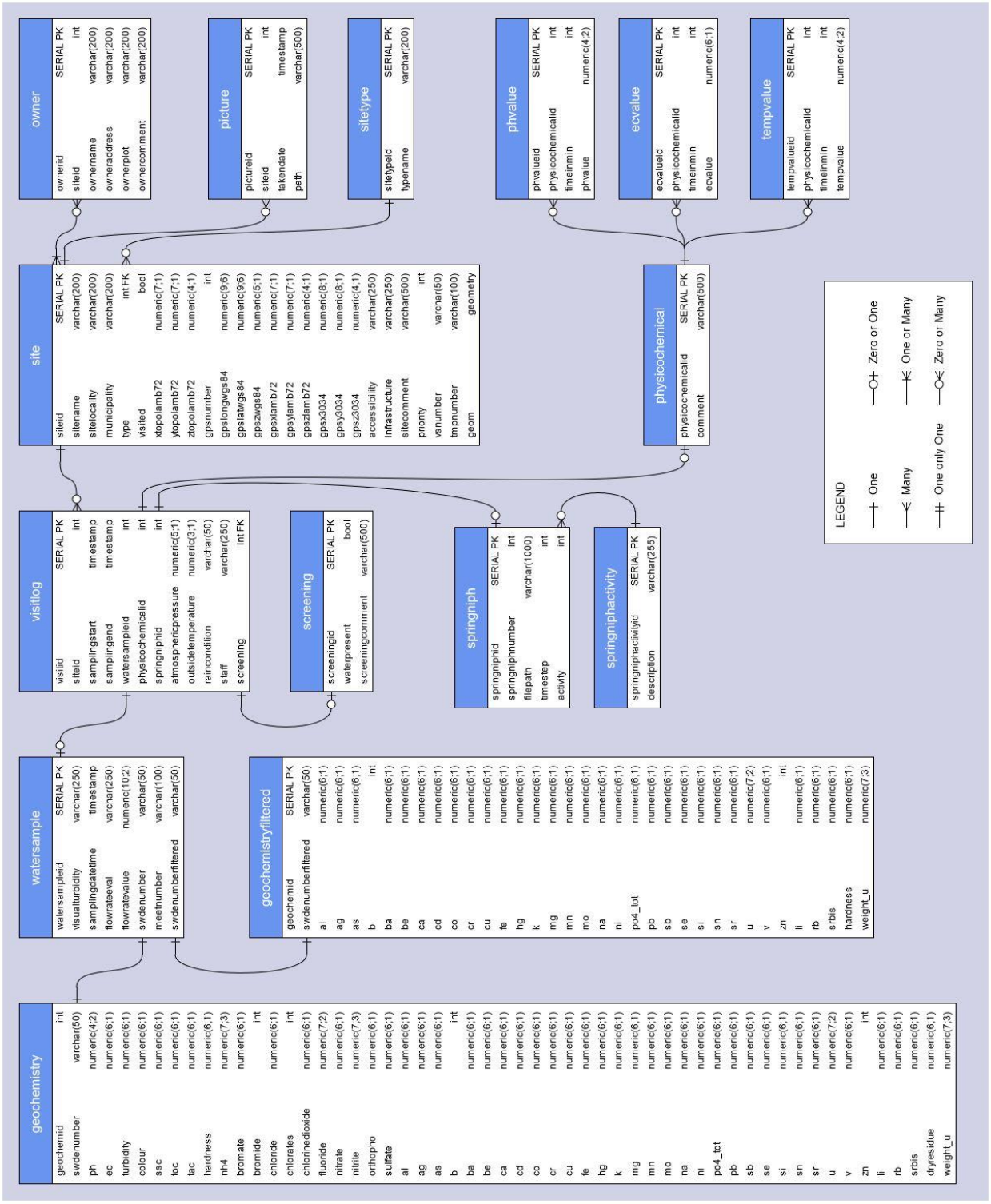

Figure 36: Logical data model of the MEET-WATER relation database.

2.2.3.6 Fluid sample results: Göttingen demosite

At the Göttingen University Campus demo site and for Harz outcrop analogues no fluid samples were available, neither from the demo site nor from the analogue sites.

2.2.3.7 Outcrop analogue sample results: Death Valley, Noble hills

Since a numerical simulation of the DV outcrop analogue site is not planned within MEET petrophysical analysis was not prioritized and thus no results are available to be presented as part of D5.5 yet. However, investigations are planned in the next months and will be presented in deliverable D5.9.

The Noble Hills samples were investigated mineralogically by thin section analysis and presents as one granitic body composing by quartz, plagioclase, K-feldspars, biotite and more rarely muscovite as primary minerals. During alteration processes, we observed that the quartz and the K-feldspars are unaffected. However, the plagioclase following by the biotite are the first minerals affected. Indeed, plagioclase are transformed mainly into illite, which can have different appearance (patches, needles, fans and honeycombs shape) meaning that we have different generation of fluid or plagioclases with different chemical composition, and/or into kaolinite. Different fracture fillings were identified and a preliminary chronology is suggested with a first generation composed by illite veins, following by carbonates veins (dolomite) mixed probably with oxides and following by calcite veins. This last event can be found as a matrix around angular clasts of quartz or K-feldspar that may reflect a hydraulic fracturing event.

XRD analyses on 54 samples were performed by separating the different clay fraction (<2 µm and 2-6 µm) to study the evolution of clay composition and to determine the thermal gradient thanks to the illite crystallinity index. The obtained results allowed us to defined a temperature gradient increasing from the NW towards the SE (Figure 37a). Indeed, the degree of metamorphism is higher in the SE than in the NW. We saw on the field that the topography is higher in the southern part of the range than in the northern part, with a tilting of around 30° of the quaternary series. We deduced that the temperature gradient is linked to the tectonic and not to the fluid circulation. Another temperature gradient was identified, based on the distribution of clay minerals and especially the mix-layers which are characteristic for the lower grade of metamorphism. These mix-layers are more present in the NE, meaning that the temperature gradient increase towards the SW (Figure 37b).

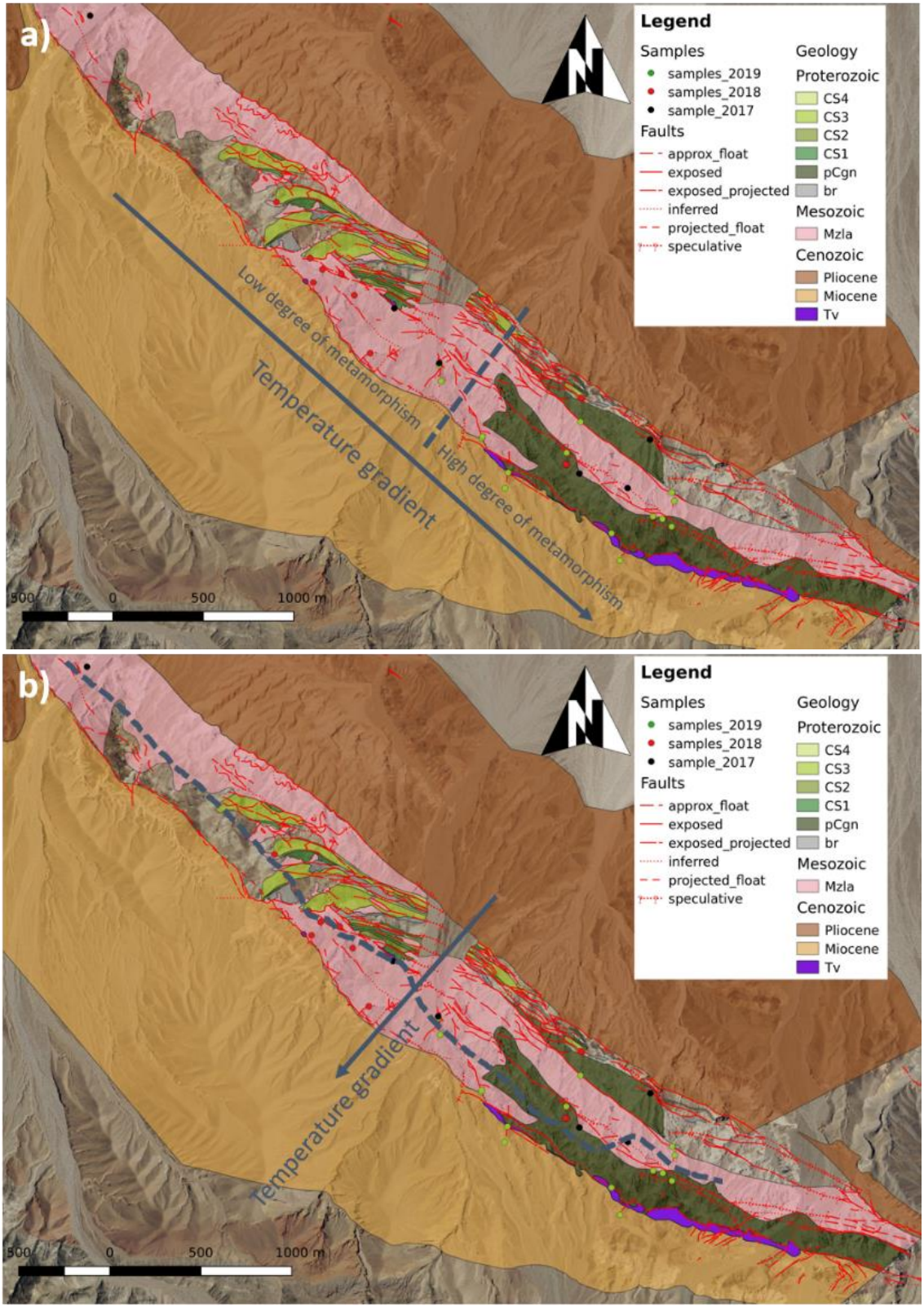

Figure 37: Maps showing the temperature gradients based on a) the illite crystallinity index and b) the presence and amount of mix-layers.

2.2.3.8 Reservoir sample results: Soultz sous Forêts

Comprehensive petrophysical and rock mechanical characterisations are already available for the Soultz-sous-Forêts altered and fractured granite and its analogue of the Graben shoulder of the Upper Rhine Graben (Rummel *et al.*, 1991, 1992, Ledesert *et al.*, 1993, Vernoux *et al.*, 1993, 1995, Sizun *et al.*, 1995, Greksch *et al.*, 2003, Surma and Geraud, 2003, Rosener and Géraud, 2007, Haffen *et al.*, 2012, Maire, 2014, Welsch *et al.*, 2014, Hoffmann, 2015, Kushnir *et al.*, 2018, Villeneuve *et al.*, 2018). The recorded permeability is between $1.57 \cdot 10^{-15}$ and $1.56 \cdot 10^{-20}$ m² and the porosity between 0.13 and 10 %. For the numerical models of Soultz performed and ongoing in Task 3.2 of the MEET project these values are sufficient. The future results of the DV analogues petrophysical characterization will be compared to the values for the Soultz demo sites.

2.2.3.9 Fluid samples results: Soultz and Upper Rhine Graben

Fluid hydrochemistry of the deep geothermal reservoir formations of the Upper Rhine Graben including the Soultz sous Forêts demosite are compiled in Stober & Jodocy (2011), Stober & Bucher (2015) and Sanjuan *et al.*, (2016) and where implemented into the hydrochemical database for MEET.

2.2.3.10 Outcrop analogue sample results: Cornwall

Through the petrophysical characterization workflow presented on Figure 16, following results were obtained on the different plutons of Cornubian Batholite (Figure 38 and Figure 39).

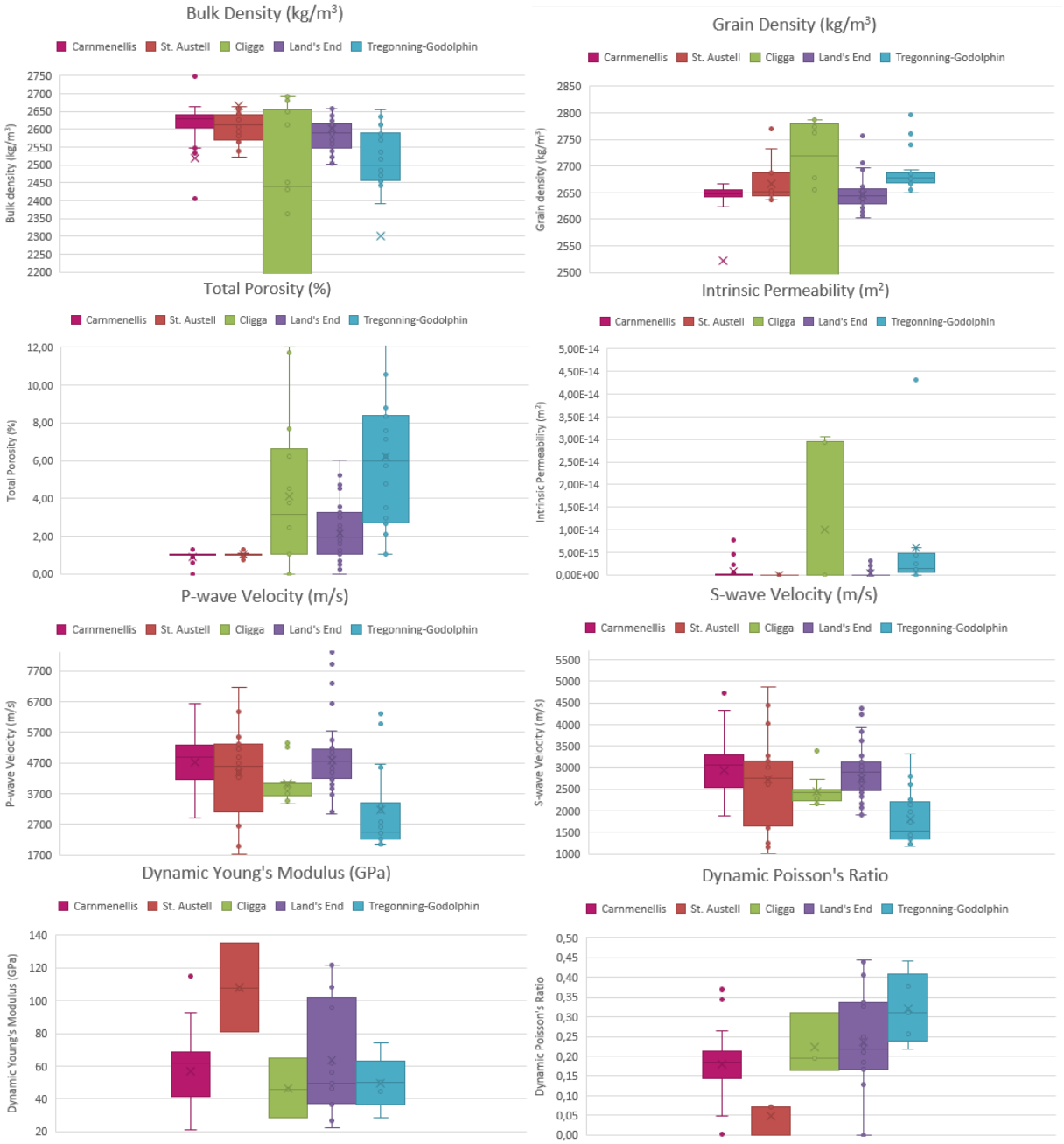

Figure 38: Box-whisker plot of petrophysical and mechanical properties of the different plutons of the Cornubian Batholite.

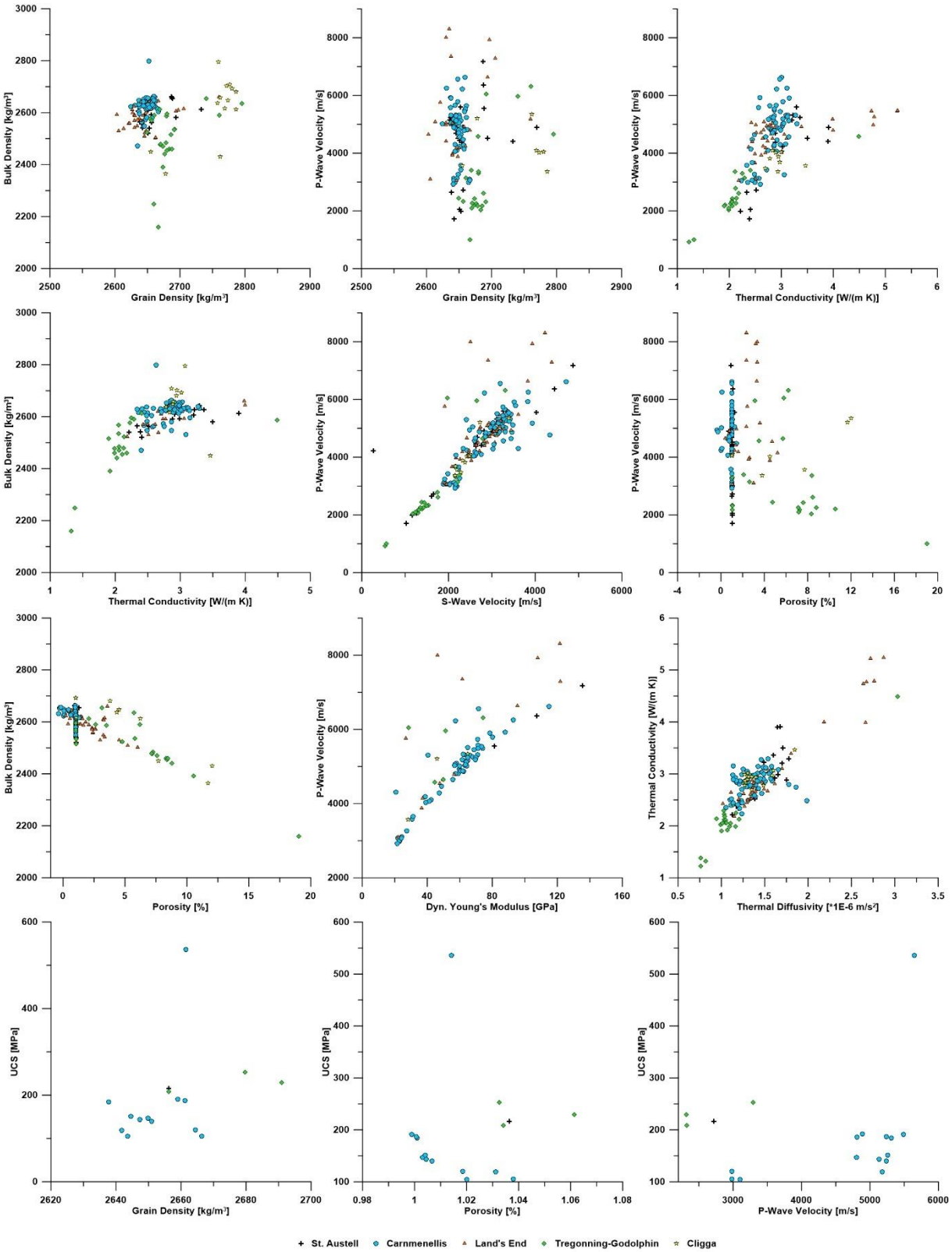

Figure 39: Cross-plots of petrophysical and mechanical properties of the different plutons of the Cornubian Batholite.

Reservoir sample results: Cornwall

The only available reservoir sample available from Cornwall are the drill cuttings from well UD-1 well. Concerning petrophysical properties, only grain density was measured for all 44 cutting samples and found as 2.65 (min), 2.78 (max) and 2.69 g/cm³ (mean) with a standard deviation of 25.9.

The mineralogy of the cuttings was analyzed with XRD. The results are presented in Table 12. The XRD analysis confirms the presence of the following minerals in the samples: Quartz, K-Feldspar, Plagioclase, Muscovite and Biotite, Chlorite, Tourmaline (Schörl) and Hornblende. Ore-minerals are commonly not detected by the method. In every sample, Muscovite is more abundant than Biotite. Chlorite occurs especially in the cuttings and may indicate alteration zones. Tourmaline is mainly present in outcrop analogue samples, but not in cuttings. It is likely, that Tourmaline is generally less abundant in deeper pluton levels than in hydrothermally affected zones around the granite body, which correlate with the thermal convection cell that had been established around the granite body after its emplacement and during cooling. Hornblende occurs only in the UD-1 cuttings. The sub 63 µm fraction is not represented in the cuttings, since these have been washed beforehand. Therefore, further Micas and clay minerals may be present, but also the Quartz content may be underestimated, because fine grained Quartz is the main constituent of the granite matrix.

The following Figure 40 gives an overview on the XRD results, plotted in a QAP diagram. A large part of the individual outcrop analogue sample volumes is represented by the mineralised veins, which indicate, that the samples have been influenced by hydrothermal alteration and which impact the sample composition. Therefore, the samples should ideally not be plotted in a QAP-diagram for plutonic rocks. The figure means to give an overview on the samples and display the main differences between cuttings and outcrop analogue samples.

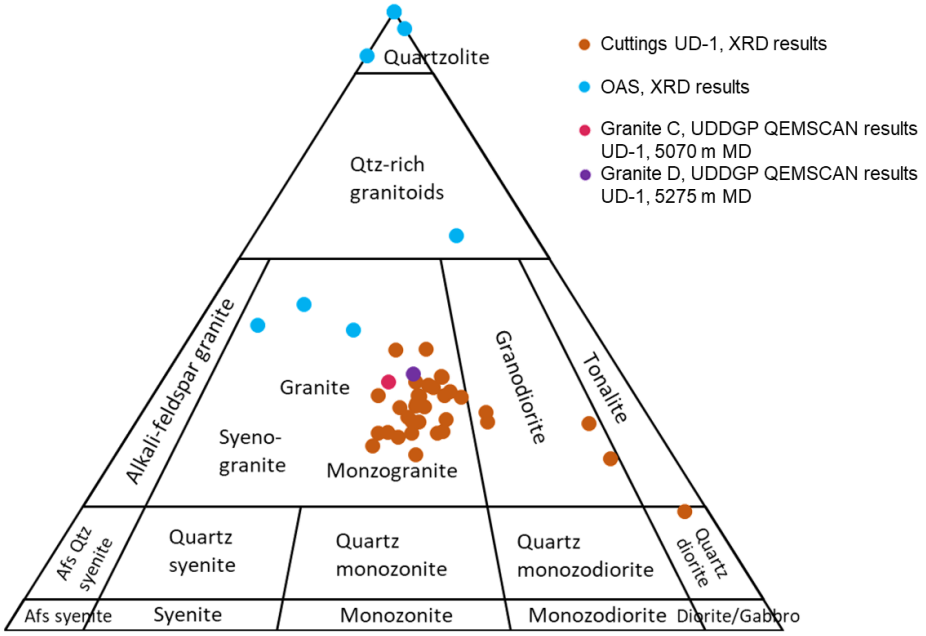

Figure 40: XRD results for cuttings and OAS, displayed in a QAP-diagram (Schulz, 2020).

The cuttings plot relatively close, in the field of Monzogranite. In the analysed depth range below 4 km, Granite C and D are present. Granite C and D are UDDGP internal classifications, their composition is displayed in Figure 40 (Geothermal Energy Limited, 2019). They plot similar to most of the cuttings and confirm the quality of the XRD analysis. Only the cutting intervals 4240 m – 4270 m have a higher Plagioclase content and plot in the area of Granodiorite or even Quartz diorite. Because of the loss of the sub 63 µm fraction, the results from the cuttings may need to be corrected towards higher Quartz contents. This would likely account for both: the project internal classification of Granite C and D and the hereby analysed cuttings. The OAS show a high Quartz content and an elevated K-Feldspar content. The high Quartz content, as well as the presence of Tourmaline in the OAS, is probably related to the veins. Comparing the cuttings and the OAS, the vein filling minerals in the OAS are volumetrically overrepresented, because the veins make up a relatively high percentage of the sample volume. The lower K-Feldspar content in the OAS, compared to the cuttings, may indicate the effect of weathering of the OAS, because the resilience of Plagioclase is commonly lower than of K-Feldspar (assuming similar grainsizes).

Table 12: XRD results for UD-1 cuttings, min. – max. range highlighted per column (Schulz, 2020)

Depth	Quartz	Plagio-clase	K-Feld-spar	Musco-vite	Biotite	Horn-blende	Chlorite	Schörl (Tourmaline)
m	Rel %							
4050	30.1	22.9	26.2	14.3	3.4	1.9	1.2	0.0
4060	24.2	24.1	27.3	20.0	2.8	0.0	1.5	0.0
4070	24.6	25.5	26.8	16.9	4.1	0.0	2.0	0.0
4100	28.6	27.4	22.3	17.8	2.2	0.0	1.7	0.0
4110	28.4	25.7	24.7	16.9	3.0	0.0	1.4	0.0
4120	22.5	25.0	24.3	21.4	4.8	0.0	2.1	0.0
4180	29.3	26.3	21.5	16.6	4.5	0.0	1.8	0.0
4190	23.2	28.9	19.9	22.2	3.8	0.0	1.9	0.0
4198	24.2	29.9	21.5	18.6	4.4	0.0	1.4	0.0
4210	26.5	25.9	16.2	24.7	5.1	0.0	1.6	0.0
4220	32.1	26.0	21.6	16.3	2.7	0.0	1.3	0.0
4230	24.9	28.3	24.9	17.7	2.7	0.0	1.5	0.0
4240	26.4	45.9	6.5	18.4	2.1	0.0	0.7	0.0
4250	15.6	62.5	2.4	14.7	2.5	0.0	2.3	0.0
4260	22.3	51.2	6.7	15.8	2.9	0.0	1.2	0.0
4270	31.5	31.4	28.2	6.5	1.0	0.0	1.4	0.0
4280	24.5	28.4	18.9	22.6	4.2	0.0	1.6	0.0
4490	30.9	26.8	17.6	19.7	4.2	0.0	0.8	0.0
4500	28.9	25.9	18.6	21.0	4.6	0.0	1.0	0.0
4510	26.4	33.0	15.4	20.4	3.4	0.0	1.4	0.0
4520	28.5	17.3	17.1	31.3	5.3	0.0	0.5	0.0
4530	20.2	27.4	23.5	22.4	4.7	0.0	1.8	0.0
4540	29.4	25.6	19.1	20.1	4.8	0.0	1.0	0.0
4640	25.8	24.5	20.0	23.6	4.8	0.5	0.8	0.0
4650	24.2	26.0	21.4	21.7	5.9	0.0	0.8	0.0
4660	24.5	23.1	19.2	25.4	6.3	0.4	1.0	0.0
4670	25.2	24.8	16.2	26.6	6.2	0.0	1.0	0.0
4680	33.4	22.9	17.0	21.1	4.6	0.0	0.9	0.0
4690	29.1	30.5	17.3	18.2	3.9	0.0	0.9	0.0
4700	28.6	25.9	20.9	20.3	3.3	0.0	0.9	0.0
4710	24.3	32.5	15.2	21.3	5.9	0.0	0.8	0.0
4880	14.7	15.3	13.3	41.9	13.5	0.0	1.2	0.0
4890	13.8	14.9	17.6	41.6	10.2	0.0	1.8	0.0
4900	29.3	25.4	16.7	21.3	6.1	0.0	1.2	0.0
4910	17.0	16.8	13.2	38.0	14.0	0.0	1.0	0.0
4920	23.6	22.4	18.9	21.8	12.9	0.0	0.4	0.0

2.2.3.11 Reservoir sample results: Paris and Aquitaine Basins

For each of the data types acquired at CYU, results are presented according to their geographic location, since it represents two different target zones. Underneath the Aquitaine basin, the basement lithologies are mostly schists at the first order (this must be confirmed via thin-section investigation) and boreholes are very close to each other, whereas underneath the Paris basin, rock types are heterogeneous and boreholes that were sampled are very far from each other. A synthetic table of results for each method provides the number of analyzed samples, as well as the minimum and maximum values (Table 13). The complete set of data is filled in the Petrophysical Properties (P^3) Database developed by MEET partners of TU Darmstadt and attached to this deliverable.

Graphs representing datasets of Paris Paleozoic basement are placed to the left, and Aquitaine Paleozoic basement to the right. The color code in graphs that represents rock type underneath the Aquitaine basin is the same as in the color legend presented for samples underneath Paris basin.

Table 13: Synthesis of data types, number of samples and minimum/maximum values for each method.

	Number of samples	Min. value	Max. value
Helium porosity (%)	46	0.16	12.29
Ethanol porosity (%)	57	0	10.82
Nitrogen permeability (m^2)	45	7.11×10^{-17}	2.12×10^{-14}
Density (kg/m^3)	46	2014.2	3051.5
Magnetic susceptibility (SI)	43	-9.05×10^{-7}	7.48×10^{-5}
Calcimetry (% calcite content)	38	0.08	86.51

Porosity

When comparing the results acquired for the same samples by the ethanol hydrostatic weighing and He-pycnometry method (Figure 41), it appears first that the values of gas volume in pores are systematically higher than the values of ethanol volume in pores. Gas porosities have the same order of magnitude but are 1 to 5 times higher than the ethanol porosities. As explained before, there is certainly a strong effect of the external volume of the plug, which is the product of dimensions measured through calliper, with an associated uncertainty of several tenths of dm^3. It does not have the same level of accuracy than the gas volume measured by gas displacement in the pycnometer, which has a precision of around 10 μm^3. He-porosity is likely to overestimate the pore volume due to this measurement bias.

The data show that rock typing has an effect on the porosity. Schists are the tightest with less than 1.5% porosity whereas gneiss are more variable with 3.5% to 11% porosity; porosity range in quartzite is also very low with values comprised between 0% and 2.5% porosity, always lower than in gneiss.

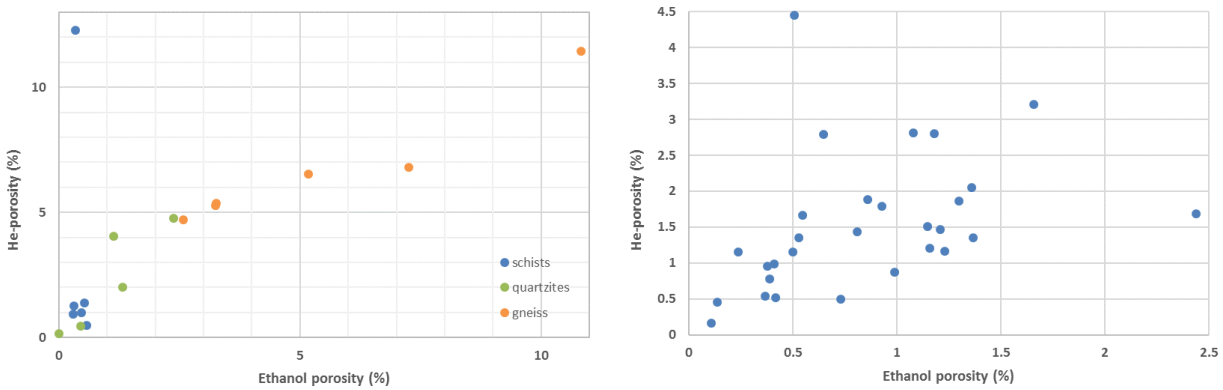

Figure 41: Porosity measurements according to ethanol hydrostatic weighing and He-pycnometry methods for Palaeozoic basement rocks underneath Paris basin (left) and Aquitaine basin (right).

Density

All density values are comprised between 2650 and 2950 kg/m^3 (Figure 42). In general, the rock types are well separated when related to ethanol porosity, especially in the Paris Palaeozoic basement, and respect the standard values commonly observed in nature (gneiss: 2600-2900 kg/m^3; schists: 2700-2800 kg/m^3; quartzite: 2600-2700 kg/m^3). However, some discrepancies are observed in the Aquitaine basin, with values over 2800 kg/m^3. This might be explained by changes in the mineralogy compared to standard schists.

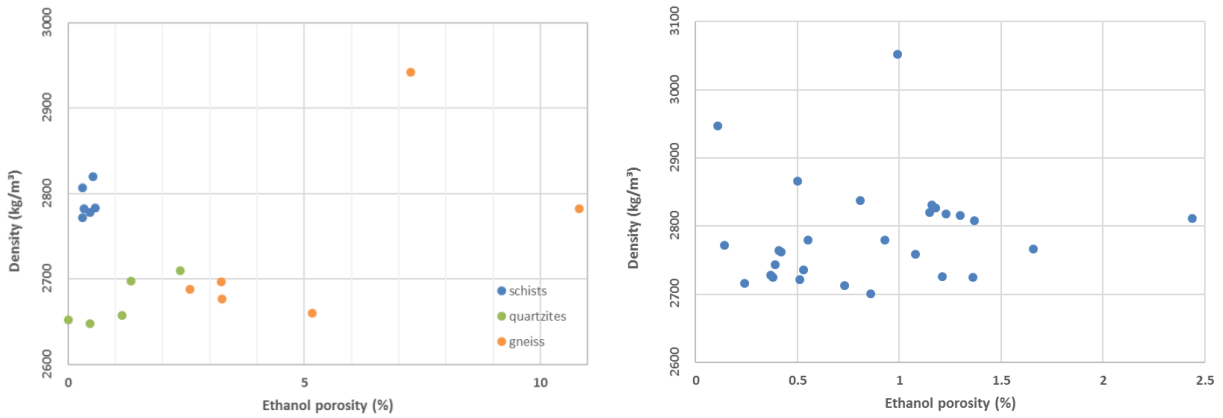

Figure 42: Density values and ethanol porosity of Palaeozoic basement rocks underneath Paris basin (left) and Aquitaine basin (right).

Permeability

The permeability of the different metamorphic rocks sampled in the project are presented below (Figure 43). Most of the plugs have a low to moderate permeability, between 10^{-15} and 10^{-16} m² (~ 0.1-1 mD), whatever the rock type and the geographic location. It appears from this dataset that there is no linear correlation between increase of porosity and consequential increase of permeability. However, certain rock types such as gneiss or schist are characterised by specific range of porosity for a quite constant permeability, 3.5-11% and 0-1%, respectively. Therefore,

reservoir properties are more satisfying in gneiss due to their fair porosity, even though certain high porosity values might be due to alteration processes (see "Petrography" part).

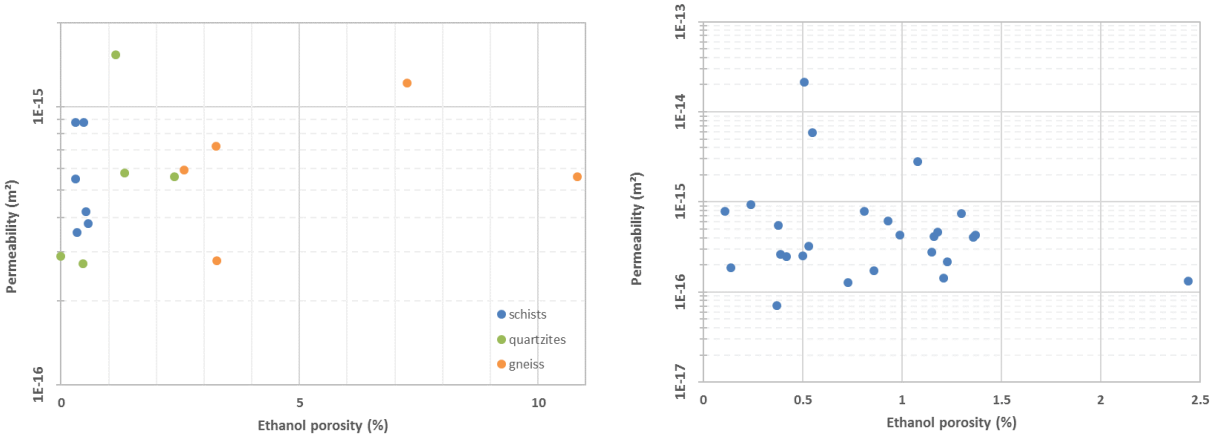

Figure 43: Gas (nitrogen) permeability and porosity of Palaeozoic basement rocks underneath the Paris basin (left) and Aquitaine basin (right).

An attempt to identify if any significant fluid pathways exist in the rock matrix through porosity and permeability anisotropies is also performed (Figure 44). However, these results must be analysed with care since the sampled interval (few centimeters) is not representative of the whole section and the respective data do not express the reservoir anisotropy. At the first sight, it appears from this representation that there is no directional control of either porosity or permeability although this analysis must be pursued with structural data in order to investigate the role of schistosity, cleavage and different sizes of fractures. Furthermore, this structural crossed interpretation needs to reconstruct the original position of the samples in the boreholes, yet this information is most often missing in the well data since the core orientation tool was not deployed at the time of the drilling.

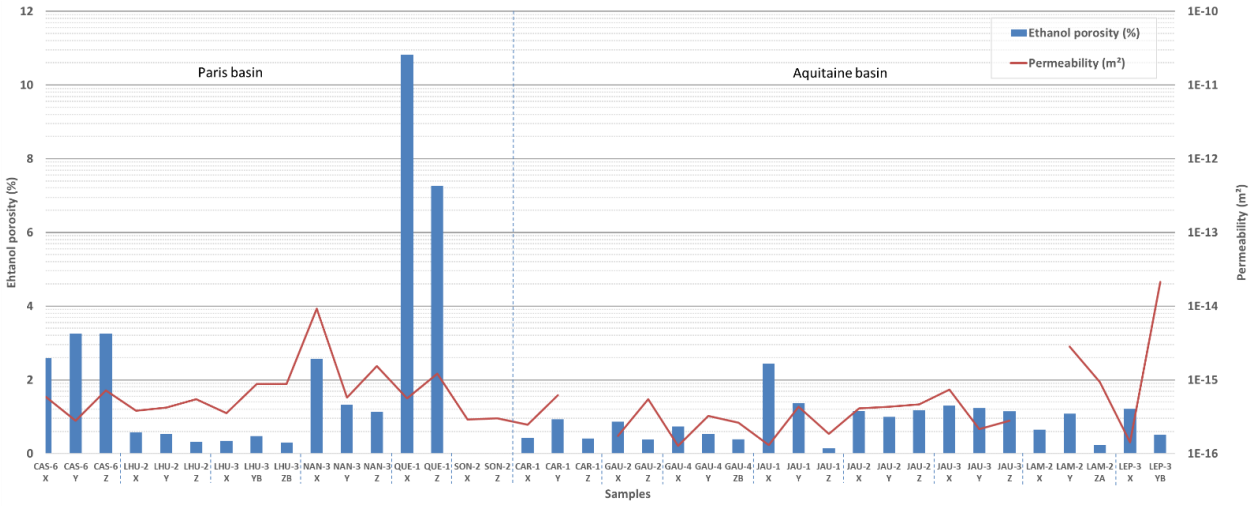

Figure 44: Anisotropies of porosity and permeability of plugs along X, Y and Z axis (convention from Louis *et al.*, 2003 – see part 2.2.5.1) of Palaeozoic basement rocks underneath Paris and Aquitaine basins.

Calcimetry

The calcimetry results provide information about the percentage of calcite (and other carbonates) content in the Paleozoic rocks from Paris and Aquitaine basement (Figure 45).

The proportion of calcite is very low in most of the samples, except boreholes LAMARQUE-1 (up to 47%) and LE TEICH-1 (49-86%). In the Palaeozoic Aquitaine basement, these high values must have some implications since all samples are supposed to be schists. Further petrographic verification must be carried out to correlate these data with mineralogical composition. As for the Palaeozoic Paris basement, the low proportions of calcite fluctuate between 0.5 and 3%, similarly to the values measured on other drill cores of the Aquitaine basement.

It is rather important to keep this data in mind in order to better interpret Magnetic Susceptibility in terms of calcite contribution to magnetic signature, as well as to extrapolate petrographic observations at the macroscopic scale based on the amount of calcite in the bulk rock. When compared to the petrographical observations in the Paris basin in particular, the calcite content measured by calcimetry confirms the presence of veins and cement relicts. Even though the data ranges are low, calcite could be connected through dimensionally acceptable veins or even fault planes, which would have interesting outcomes for chemical stimulations.

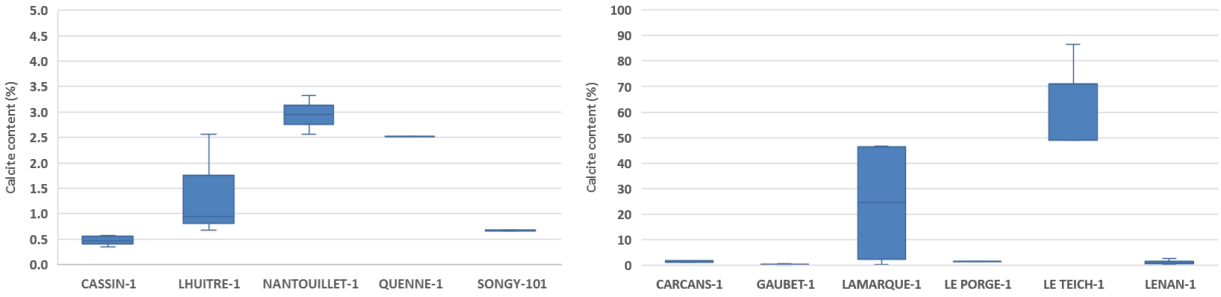

Figure 45: Calcite content (%) of the different rock samples in the boreholes reaching Palaeozoic basement underneath Paris basin (left) and Aquitaine basin (right).

Magnetic Susceptibility

The magnetic susceptibility of Palaeozoic basement samples has been measured in order to identify possible magnetic anomalies and magnetic properties. The results are presented in the following graphs (Figure 46). Almost the entire dataset is paramagnetic ($3.30 \times 10^{-6} < K < 9.28 \times 10^{-5}$), except two samples in CARCANS-1 borehole that have slightly negative value, indicating a diamagnetic character. The values are very low, which means that there is no contribution of ferromagnetic particles. In addition, the signal associated to these very low values is attributed to the matrix, as $K < 30 \times 10^{-5}$ SI and most of the material is phyllosilicate-bearing rocks (Rochette, 1987).

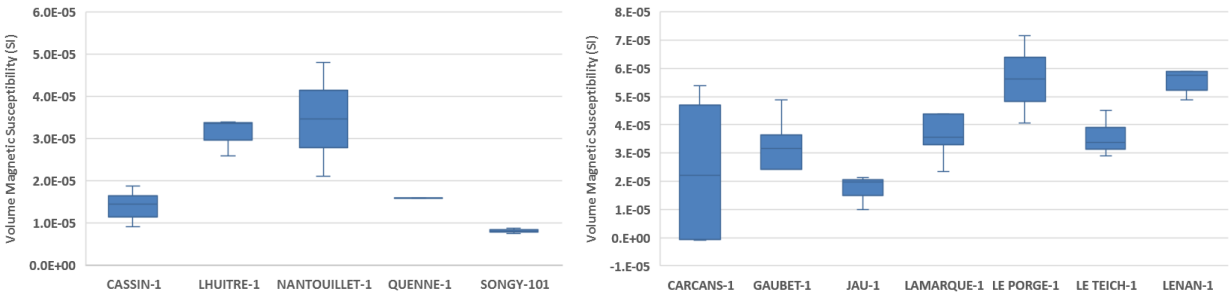

Figure 46: Volume-normalized Magnetic Susceptibility of the Palaeozoic basement rocks underneath Paris basin (left) and Aquitaine basin (right).

Quartz and calcite are known to lower significantly the magnetic susceptibility (diamagnetic). However, in rocks from both study area, quartzite has a moderate to low value range (NANTOUILLET-1 and SONGY-101), whereas some calcite-rich rocks present in LAMARQUE-1 and LE TEICH-1 (see "Calcimetry" part) do not show a drastic drop in magnetic susceptibility. The following graph that combines calcite content and magnetic susceptibility (Figure 47) clearly shows that this is not straightforward to generalize this kind of statement and that the magnetic susceptibility must be analysed in much more details, especially regarding mineral composition, in order to identify which particles influence the signal.

It is also important to bear in mind that magnetic susceptibility is used in routine for continuous recording along boreholes. A sporadic data collection on different boreholes might have introduced a methodological bias and can be an explanation for this lack of correlation with calcite content.

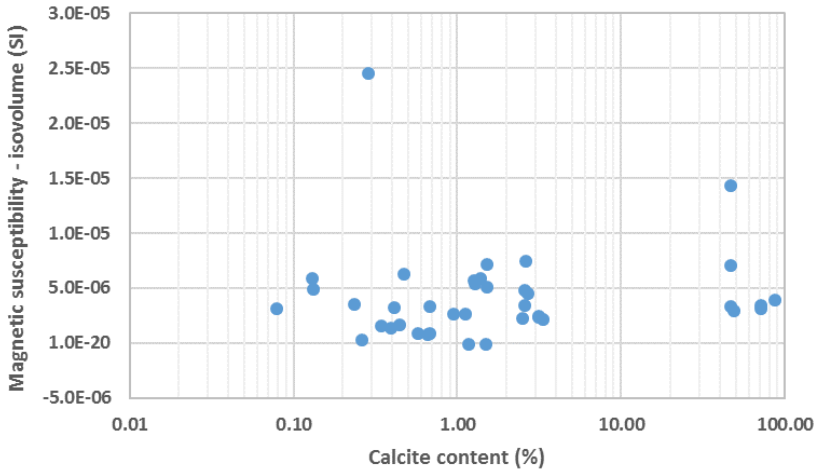

Figure 47: Relationship between calcite content and magnetic susceptibility, showing the absence of correlation between these two parameters.

Petrography

Among the 14 thin-sections observed from five boreholes reaching the Palaeozoic Paris basement, it was possible to classify the different encountered formations into three main lithologies: Schists, Quartzite and Gneiss.

From the mineralogical point of view, quartz/albite/chlorite mineral assemblage, with rare epidote and tourmaline occurrence, characterize a greenschist metamorphic paragenesis. This type of association gives indications about a maximum reached temperature of about 450-470°C. It is also frequent to observe evidences of hydrothermal circulations such as veins (associated with the alteration of the host rock), chlorite aggregates, calcite filling and quartz geodes.

In terms of structural features, an intense shearing is assessed in phyllosilicate-rich rocks, with the presence of various microstructures with many evidences of syn-tectonic metamorphism:

- syn-kinematic albite porphyroblasts;
- strain shadows around quartz or feldspar porphyroclasts, composed of microcrystalline quartz;
- crenulation schistosity showing a polyphasic tectono-metamorphism;
- micro-boudinage, characteristic of intense shearing and vertical strains.

In a late stage, most of the rocks underwent a late structural event with brittle deformation, leading to open microfractures and vertical movement along them.

A synthesis of observations for the different rock types is provided in Figure 48.

The detailed petrographic characterization of each thin-section has been compiled into the P^3 database.

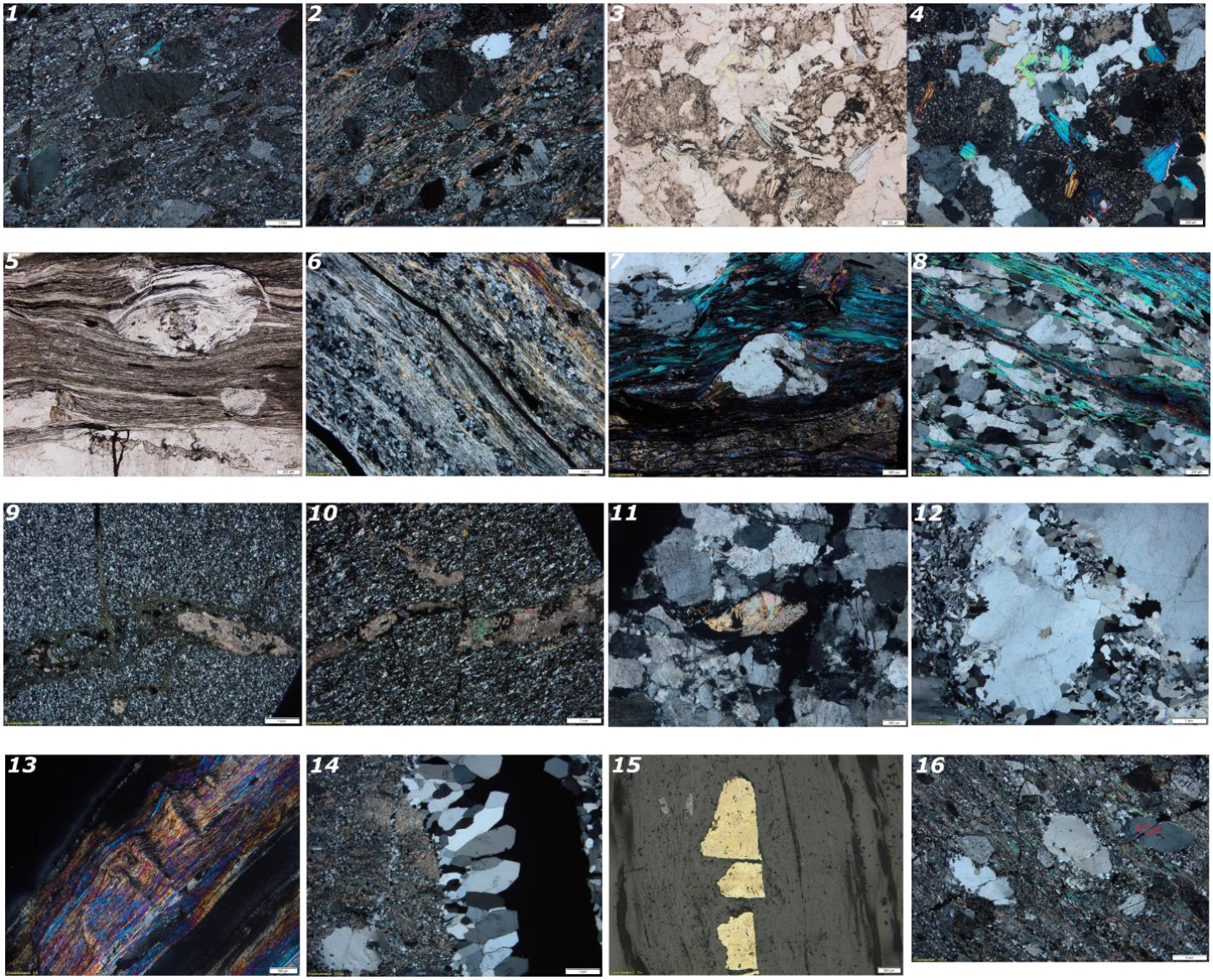

Figure 48: Synthetic petrographic plate.

Rock types: 1-4) gneiss, 5-8) micaschists, 9-12) quartzite;
Microstructural features: 13-16

1) gneiss of sample MEETPB001004, showing porphyroclasts of quartz and K-feldspars associated to strain shadows made of micrometric quartz, microlayers of quartz and phyllosilicates (mostly muscovite). Late stage brittle deformation is expressed by microfractures crosscutting the matrix and the coarser minerals [crossed-polarized light].
2) same type of gneiss in sample MEETPB001006 with variations in the amount of phyllosilicates. Strain shadows are also well-developed [crossed-polarized light].
3 & 4) gneiss of sample MEETPB005002 with association of quartz, feldspars, muscovite and calcite. The alteration of feldspars is intense as shown in picture 3. A detailed observation suggests that the rock type would be an orthogneiss formed out of a leucogranite protolith [3. polarized light - 4. crossed-polarized light].

5) micaschists of sample MEETPB002004 with albite porphyroblast identified by Raman spectroscopy, showing internal schistosity slightly rotated but still aligned with the external schistosity. Black microlayers are composed of disordered carbonaceous material, which is assimilated to graphite in greenschist metamorphic rocks. RSCM on graphite gives peak temperature of 472-500°C. The lower part of the picture is a large quartz veins with calcite aligned crystals close to the wall [polarized light].
6) detail of the composition of micaschists microlayers in sample MEETPB002005, made of quartz, phyllosilicates, feldspars and graphite. Together with frequent albite porphyroblasts associated to phyllosillicates layers as seen in picture 5, and chlorite as well as tourmaline, the paragenesis confirms that the rock reached the greenschist metamorphic facies [crossed-polarized light].
7) micaschists commonly display stretching features in phyllosilicates layers or around coarse grains as in sample MEETPB002005 [crossed-polarized light].
8) common microlayer composition in micaschists, mostly quartz and muscovite, MEETPB002004 [crossed-polarized light].

9 & 10) quartzite with calcite and chlorite in samples MEETPB004001 and MEETPB004002, respectively. In picture 9, chlorite crystallized along microfracture planes, whereas in picture 10, metamorphic calcite precipitated along a former sedimentary plane, which has been displaced by late stage brittle deformation [crossed-polarized light].
11) quartzite of sample MEETPB006003 showing dynamic crystallisation of quartz under strain as well as microfractures on the upper and right-hand parts. Altered calcite and quartz are observed in the center [crossed-polarized light].
12) quartzitic veins in sample MEETPB001003, with at least two episodes of quartz precipitation, a dynamic and a geodic one, later disrupted by brittle deformation [crossed-polarized light].

13) crenulation schistosity crosscutting S1 schistosity in MEETPB002004 [crossed-polarized light].
14) geodic vein with opening mode 1 in MEETPB001002, indicating possible hydrothermal conditions with associated alteration of the host rock [crossed-polarized light].
15) micro-boudinage of titanium oxides in MEETPB002001 [reflected light].
16) late stage microfractures affecting the whole section in a very penetrative way, as observed in many samples like examples 1 & 10 [crossed-polarized light].

Raman Spectroscopy

Raman Spectroscopy on Carbonaceous Material (RSCM) method was performed on six graphitic targets of one thin-section from the MEETPB002004 sample (LHU-1 borehole). The respective Raman spectra were processed (Figure 49) in order to obtain the geometrical characteristics of D1, G and D2 bands. R1 and R2 ratios were calculated and R2 was applied to the temperature relationship explained before (Beyssac *et al.*, 2002).

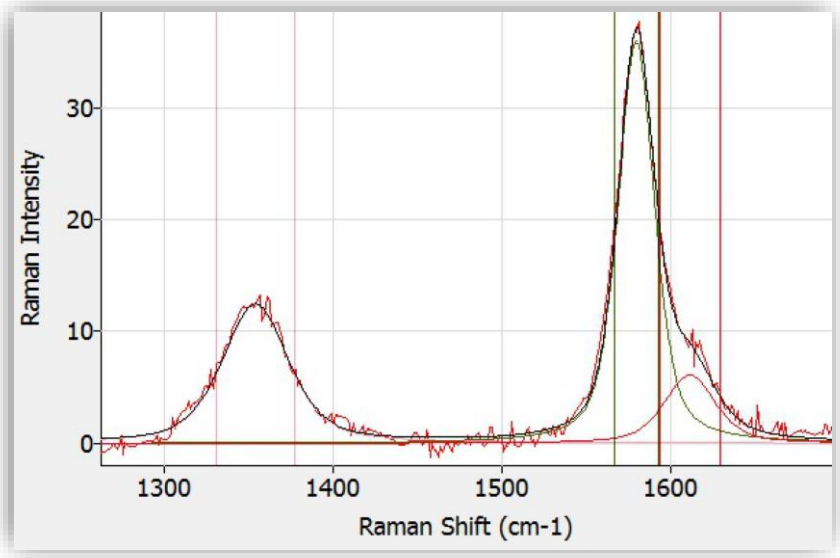

Figure 49: Raman spectra of sample MEETPB002004 (Graphite5) on LHU-1 borehole. Red noisy curve is the raw curve to baseline, black curve is the de-noised curve, which can be deconvoluted into the D1 band (pink curve), G band (green curve) and D2 band (red smooth curve), which allow to calculate the maximum reached temperature, 489.46°C for this sample.

Detailed results are shown in the Table 14. The six spectra show that Raman Shifts are the same for all D1 band (1350 cm^{-1}) and G band (1580 cm^{-1}) at a first order. The data are in good agreement with acceptable ranges for D1 and G bands defined in Beyssac *et al.*, (2003) even though it would certainly be of greater quality if the carbonaceous would be analysed below the polished surface of the thin-section where friction can affect the temperature evaluation.

Table 14: Results of Raman Spectroscopy of Carbonaceous Material (RSCM) analysed on sample MEETPB002004 of LHU-1 borehole, with spectral value of D1, G and D2 bands, as well as Maximum temperature calculated based on R2 ratio (Beyssac *et al.*, 2002).

Bore hole	Sample name	Target on thin-section	D1 band	G band	D2 band	R1	R2	Maximum Temperature (°C)
LHU-1	MEETPB002004	Graphite1	1348.9017	1576.8693	1609.7059	0.3760	0.3792	**472.23**
LHU-1	MEETPB002004	Graphite2-1	1352.609	1580.1204	1612.3426	0.4057	0.3428	**488.44**
LHU-1	MEETPB002004	Graphite2-2	1352.3111	1578.9087	1609.2333	0.4122	0.3166	**500.12**
LHU-1	MEETPB002004	Graphite3	1353.4031	1578.4853	1598.8965	0.4809	0.3338	**492.47**
LHU-1	MEETPB002004	Graphite4	1349.164	1577.0657	1597.5328	0.4674	0.3394	**489.95**
LHU-1	MEETPB002004	Graphite5	1353.7963	1579.1735	1611.9164	0.3494	0.3405	**489.46**

RSCM on graphite shows 470-500°C peak temperature on LHUITRE-1, which is slightly higher than the temperature inferred from petrographic observations in the Palaeozoic Paris basement. This calculated temperature range reflects a local thermal increase, which is a clue that metamorphism certainly reached the highest degree of greenschist facies at certain location in the Paris basin.

The evaluation of pressure conditions in the Variscan belt, nowadays overlaid by the Paris basin, has been reported by Prijac *et al.* (2000) from simulations based on P-T-t paths of surrounding Variscan massifs (Armorican Massif, Massif Central, Vosges). During a retrograde path with temperature between 450 and 500°C, the Paris basin would have experienced a pressure of 0.5-0.6 GPa, that would correspond to around 15-18 km depth. The metamorphic gradient would be 28-30°C/km, which corresponds to a MP-MT Dalradian-type gradient, characteristic of a metamorphism localized in collisional orogenesis. Indeed, with this range of temperature, a subduction-type metamorphic gradient (HP-LT) would generate much higher-pressure mineral phases, whereas rifting or contact metamorphism with LP-HT gradient are very unlikely to occur within this part of the orogeny. This temperature-pressure estimate can also lead us to calculate an exhumation rate prior to Mesozoic subsidence, with the hypothesis of the age of peak metamorphism during the paroxysm of the Variscan orogeny in the Paris basin area (approximately 330 Ma) and an altitude of 1 km at the end of the Permian. This kind of reconstruction gives an exhumation rate of 0.2-0.24 mm/y between the late Carboniferous and the onset of Triassic sedimentation. This value seems quite low compared to conventional erosion rates recorded in mountain belts, which might be due to the localization of the sample in the Variscan fold-and-thrust belt with lower vertical movements than in the core of the chain.

2.3 RECOMMENDATIONS FOR MODEL PARAMETERIZATION

2.3.1 Variscan metasedimentary successions: Havelange and Göttingen Demosites and respective outcrop analogues

Samples from various outcrops and boreholes are collected and their petrophysical properties are measured for model parameterization. The samples were classified according to their rock types. Note that all measurements were performed at dry condition and at ambient conditions (atmospheric pressure and room temperature).

Based on the petrophysical investigation of the three rock types in Variscan basement, statistical evaluation is provided for model parameterization. Note that the statistical investigation was purely addressing the value of each property regardless of its mineral content. Further analysis, for instance, thin section is to be performed in the future to understand the effect of mineral content with respect to the change of rock properties.

Petrophysical Properties:

Petrophysical properties measurement was performed on about 130 core samples. Grain density was the primary output of the petrophysical measurement whereas porosity was calculated volumetrically using known core samples dimension. Note that negative porosity might be observed as a result of volumetric calculation. Consequently, any negative porosity values were simply disregarded in this statistical evaluation.

Table 15: Statistical evaluation of petrophysical properties of greywacke, quartzite, and slate in Variscan basement.

Porosity (%)					
Rock Type	**Mean**	**Min.**	**Max.**	**Std.**	**n**
Greywacke	2.42	0.04	7.35	1.50	88
Quartzite	2.04	0.28	4.95	1.43	17
Slate	2.21	0.17	5.21	1.64	20
Bulk Density (kg/m³)					
Greywacke	2555	2219	2751	163	93
Quartzite	2607	2495	2696	68	21
Slate	2724	2542	3039	114	29

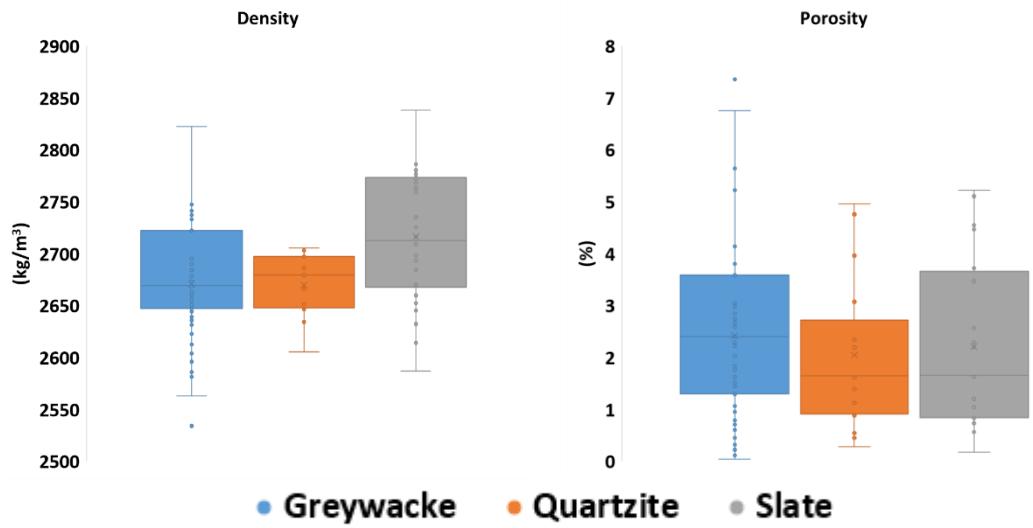

Figure 50: Box-plot of petrophysical properties analysed at dry conditions of greywacke, quartzite, and slate in Variscan basement.

As depicted Figure 50, the three rock types show relatively similar density. Notable here is slate which has higher density due to highly compacted material and exhibits minimum to no microfractures. Meanwhile microfractures are observed in greywacke and quartzite and thus leads to lower bulk density. This observation is supported by the porosity calculation where the three rock types show low porosity (< 5%). Note that some outliers are observed as a result of the difference of porosity calculation based on ideally cylindrical core samples and irregularity of the core samples.

Thermophysical Properties:

Similar to petrophysical properties, thermophysical properties are classified according to rock types.

Among all rock types observed within MEET project, quartzite exhibits the highest thermal conductivity and thermal diffusivity which span between 4.5 to 5.5 W/m·K and 2.5 to 4.0 mm^2/s respectively.

Table 16: Statistical evaluation of thermophysical properties of greywacke, quartzite, and slate in Variscan basement.

Thermal Conductivity (W/m·K)					
Rock Type	**Mean**	**Min.**	**Max.**	**Std.**	**n**
Greywacke	2.91	1.77	3.67	0.56	39
Quartzite	4.96	3.30	6.18	0.79	33
Slate	2.08	0.68	5.05	0.62	85
Thermal Diffusivity (mm^2/s)					
Greywacke	2.23	0.80	4.06	0.82	89
Quartzite	3.27	1.48	5.54	1.22	21
Slate	1.41	0.44	3.10	0.62	49

Lower thermophysical properties were observed in greywacke and correlates to higher porosity compared to quartzite. Thermal conductivity and thermal diffusivity are 3 W/m·K and 1.5 to 2.5 mm^2/s respectively. For slate, thermophysical properties are the lowest with 2 W/m·K and 1 to 2 mm^2/s. The thermophysical properties measurement is provided in Figure 51.

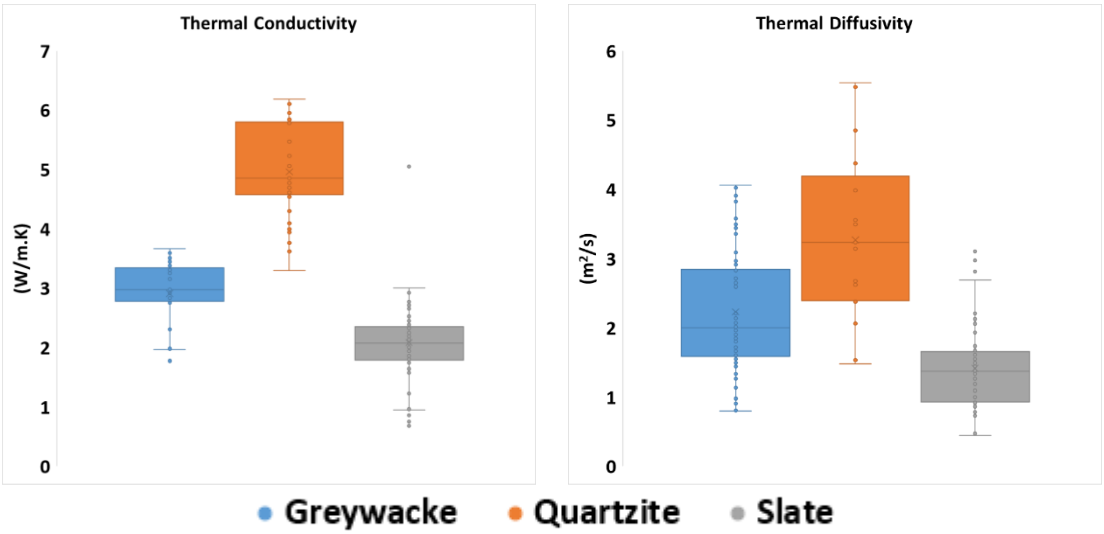

Figure 51: box-plot of thermophysical properties analysed at dry conditions of greywacke, quartzite, and slate in Variscan basement.

Ultrasonic Velocities:

Mechanical properties are derived dynamically by measuring the traveling time of ultrasonic waves reaching the receiver. Ultrasonic velocities are crucial to estimate mechanical properties in case direct measurements of mechanical properties are not feasible.

Greywacke and quartzite show P and S wave velocity around 5000 m/s and 3300 m/s respectively. These velocities are 1.2 to 1.5 times higher than the ones observed in slate. Furthermore, in terms of ultrasonic velocity, slate shows a higher level of heterogeneity. The measurement results of ultrasonic velocities are provided in Figure 52.

Table 17: Statistical evaluation of ultrasonic velocities of greywacke, quartzite, and slate in Variscan basement.

P-wave velocity (m/s)					
Rock Type	**Mean**	**Min.**	**Max.**	**Std.**	**n**
Greywacke	5292	4739	6250	353	41
Quartzite	5496	4753	6336	429	19
Slate	3663	1730	6287	1082	30
S-wave velocity (m/s)					
Greywacke	3303	2776	3771	263	39
Quartzite	3326	2782	3877	309	17
Slate	2210	1300	3650	593	29

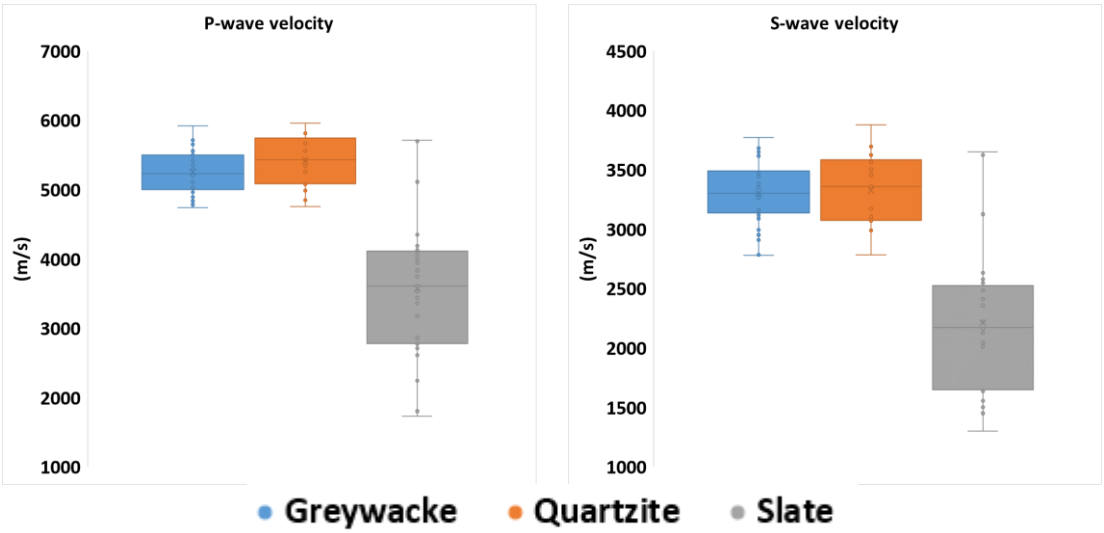

Figure 52: box-plot of ultrasonic velocities analysed at dry conditions of greywacke, quartzite, and slate in Variscan basement.

UCS and Tensile Strength:

Mechanical properties determination involves destructive measurement. Therefore, it is usually performed as the last step of comprehensive investigation. Note that mechanical properties are only available for the samples from Havelange and Harz Mountain sites.

Table 18: Statistical evaluation of UCS and tensile strength performed using uniaxial press device in greywacke, quartzite, and slate in Variscan basement.

Unconfined Compressive Strength (MPa)					
Rock Type	**Mean**	**Min.**	**Max.**	**Std.**	**n**
Greywacke	75.33	20.20	205.00	53.15	12
Quartzite	171.19	113.25	229.12	81.93	2
Slate	75.18	30.77	135.79	44.33	6
Tensile Strength (MPa)					
Greywacke	17.97	10.83	22.15	3.34	14
Quartzite	43.55	22.02	65.08	30.45	2
Slate	15.90	3.18	63.22	23.40	6
Young Modulus (GPa)					
Greywacke	36.20	36.20	36.20		1
Quartzite	36.78	26.90	48.00	7.62	5
Slate	14.10	11.70	22.20	4.57	5

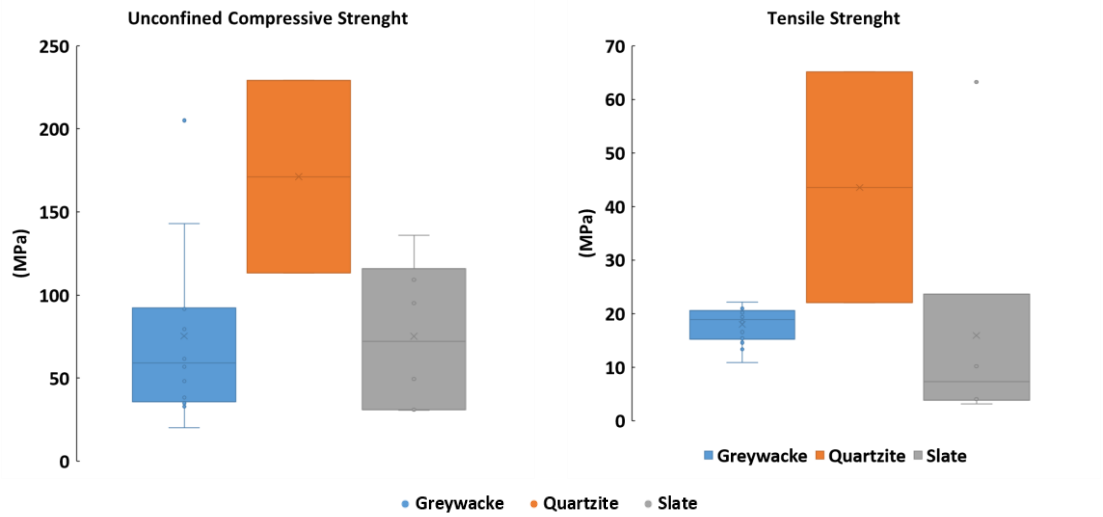

Figure 53: box-plot of mechanical properties analysed at dry conditions of greywacke, quartzite, and slate in Variscan basement.

Figure 53 depicts UCS and tensile strength obtained from the triaxial device. The rock strength strongly depends on the presence of microfractures inside the core samples. The value of UCS for each type is rather wide. This is because of the presence of microfractures influencing the rock strength.

Tensile strength for greywacke is relatively homogeneous with ranges from 15 to 20 MPa compared to quartzite and slate.

Cohesion and Friction Coefficient:

Cohesion and friction coefficients are measured using the triaxial device. Note that two or more core samples are required in order to construct Mohr-Coulomb failure line. Also note that due to limited number of core samples, linear failure curve is typically assumed. The result of UCS measurement can be added to represent free-confining-pressure triaxial experiment.

Triaxial measurements were performed on quartzite and greywacke samples from the Harz Mountain sites and quartzite and slate samples from the Havelange site.

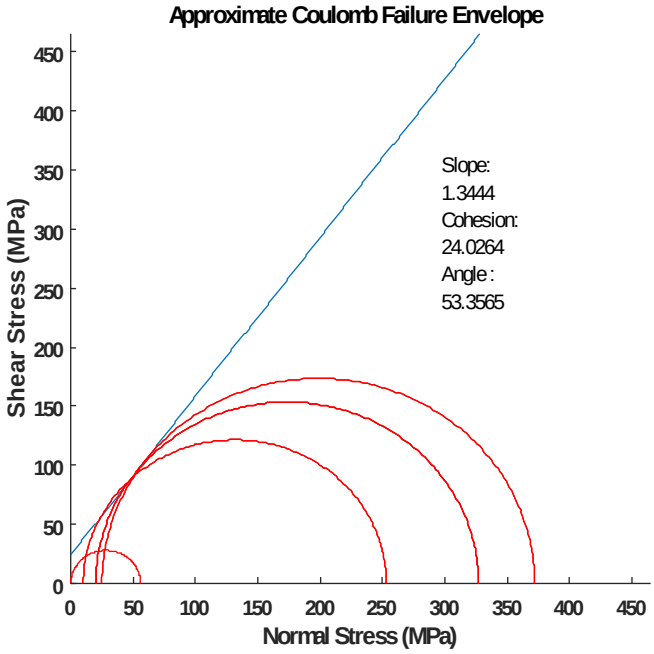

Figure 54: Mohr-Coulomb circle of drillcore fine grain greywacke from Harz Mountain site.

Figure 54 depicts the results of triaxial measurement of greywacke from Harz Mountain. The estimated cohesion is 24 MPa.
With the same procedure, cohesion and friction angle for other samples is shown in Table 19 below.

Table 19: Statistical evaluation of cohesion and friction coefficient performed using uniaxial press device in greywacke, quartzite, and slate in Variscan basement.

Cohesion (MPa)					
Rock Type	**Mean**	**Min.**	**Max.**	**Std.**	**n**
Greywacke	26.57	10.50	45.90	45.90	5
Quartzite	51.93	39.50	83.00	21.23	2
Slate	30.10	30.10	30.10		1
Friction Coefficient (-)					
Greywacke	1.36	0.45	1.85	1.85	5
Quartzite	1.14	0.82	1.27	0.22	2
Slate	0.63	0.63	0.63		1

2.3.2 Variscan crystalline basement: Cornwall, Soultz sous Forêts Demosites and Death-Valley analogue sites

The following tables present the petrophyscial parameters of the different plutons of the Cornubian Batholite we sampled within MEET, with statistical evaluation:

Table 20: Statistical evaluation of the petrophysical properties grain density, bulk density, total porosity and intrinsic permeability of the different granitic plutons of the Cornubian Batholite.

Grain Density (kg/m³)					
Pluton	**min**	**max**	**mean**	**std. dev.**	**n**
Carnmenellis	2624	2667	2649	9	61
St. Austell	2636	2769	2666	35	20
Cligga	2655	2786	2752	50	9
Land's End	2603	2756	2647	29	39
Tregonning-Godolphin	2650	2796	2687	35	22
Bulk Density (kg/m³)					
Pluton	**min**	**max**	**mean**	**std. dev.**	**n**
Carnmenellis	2407	2749	2617	47	78
St. Austell	2521	3872	2666	287	20
Cligga	2365	2693	2576	287	9
Land's End	2502	3331	2602	127	39
Tregonning-Godolphin	2160	2654	2510	105	22
Total Porosity (%)					
Pluton	**min**	**max**	**mean**	**std. dev.**	**n**
Carnmenellis	0.00	1.42	0.88	0.33	60
St. Austell	0.72	1.28	1.02	0.10	20
Cligga	0.00	12.02	4.45	3.95	13
Land's End	0.00	6.01	2.13	1.45	38
Tregonning-Godolphin	1.03	19.02	6.22	4.48	24
Intrinsic Permeability (m²)					
Pluton	**min**	**max**	**mean**	**std. dev.**	**n**
Carnmenellis	1.93E-18	7.64E-15	1.05E-15	2.2E-15	15
St. Austell	5.63E-18	6.12E-18	5.87E-18	2.5E-19	3
Cligga	2.65E-17	3.06E-14	1.50E-14	1.6E-14	6
Land's End	6.91E-19	1.90E-03	1.90E-04	5.9E-04	20
Tregonning-Godolphin	1.68E-18	4.32E-14	1.32E-14	1.3E-14	10

Table 21: Statistical evaluation of the thermophysical properties thermal conductivity, thermal diffusivity and specific heat capacity of the different granitic plutons of the Cornubian Batholite.

Thermal Conductivity (W/(m·K))					
Pluton	**min**	**max**	**mean**	**std. dev.**	**n**
Carnmenellis	2.23	3.30	2.82	0.25	68
St. Austell	2.21	3.91	3.00	0.51	17
Cligga	3.06	3.46	2.94	0.00	1
Land's End	2.18	5.24	3.07	0.85	36
Tregonning-Godolphin	1.23	4.49	2.10	0.61	22
Thermal Diffusivity (m²/s)					
Pluton	**min**	**max**	**mean**	**std. dev.**	**n**
Carnmenellis	0.00E+00	1.98E-06	1.07E-06	5.85E-07	89
St. Austell	1.13E-06	1.78E-06	1.51E-06	2.21E-07	17
Cligga	1.27E-06	1.84E-06	1.39E-06	1.62E-07	16
Land's End	1.02E-06	2.87E-06	1.63E-06	5.69E-07	30
Tregonning-Godolphin	7.61E-07	3.03E-06	1.11E-06	4.34E-07	23
Specific Heat Capacity (J/(kg·K))					
Pluton	**min**	**max**	**mean**	**std. dev.**	**n**
Carnmenellis	475	1066	809	104	42
St. Austell					
Cligga			766	0	1
Land's End					
Tregonning-Godolphin			572	0	1

Table 22: Statistical evaluation of the mechanical properties P- and S-wave velocity, uniaxial compressive strength, dynamic Young's modulus and dynamic Poisson's ratio of the different granitic plutons of the Cornubian Batholite.

P-wave Velocity (m/s)					
Pluton	**min**	**max**	**mean**	**std. dev.**	**n**
Carnmenellis	2920	6619	4716	896	86
St. Austell	1714	7174	4396	1477	20
Cligga	3367	5340	4044	595	13
Land's End	3048	8305	4999	1171	46
Tregonning-Godolphin	2038	6308	3170	1372	23
S- wave Velocity (m/s)					
Pluton	**min**	**max**	**mean**	**std. dev.**	**n**
Carnmenellis	1879	4718	2941	570	86
St. Austell	1024	4873	2724	1053	19
Cligga	2153	3389	2455	322	13
Land's End	1909	4377	2880	548	45
Tregonning-Godolphin	1174	3310	1825	593	23
Uniaxial Compressive Strength (MPa)					
Pluton	**min**	**max**	**mean**	**std. dev.**	**n**
Carnmenellis	105	192	152	33	13
St. Austell			216	0	1
Cligga					
Land's End					
Tregonning-Godolphin	209	253	230	22	3
Dynamic Young's Modulus (GPa)					
Pluton	**min**	**max**	**mean**	**std. dev.**	**n**
Carnmenellis	21	115	57	20	60
St. Austell	81	135	108	27	3
Cligga	28	65	46	18	3
Land's End	22	122	64	35	13
Tregonning-Godolphin	28	74	50	17	5
Dynamic Poisson's Ratio					
Pluton	min	max	mean	std. dev.	n
Carnmenellis	0.00	0.37	0.18	0.07	52
St. Austell	0.07	0.07	0.07	0.00	2
Cligga	0.16	0.31	0.22	0.08	3
Land's End	0.13	0.45	0.27	0.11	13
Tregonning-Godolphin	0.22	0.44	0.32	0.09	5

2.3.3 Variscan basement overlain by sedimentary basins: Paris and Aquitaine Basins

In the purpose of providing quantitative data for reservoir model parametrization, petrophysical parameters were measured on the various rock samples from the Variscan basement of the Paris and Aquitaine basins. Rock typing was chosen for rendering the data ranges associated to each potential reservoir rock. The statistical results are presented in tables and graphs.

Note that the impact of the amount of samples has to be taken into account. The statistical approach is quite limited for certain rock types since the number of collected samples for each lithology is not equivalent due to the amount of available material in the core storage shed.

The results of calcimetry are not shown in this part since the calcite content highly depends on the rock history and cannot be considered as a primary order petrophysical parameter for the characterization of rock types. Anyhow, it has to be expected that it influences the petrophysical properties considerably and is certainly of high interest for actual characterization at reservoir scale.

The petrographical analysis was performed on the thin-sections from Paris Variscan basement, which had a significant influence on the determination of main lithologies and mineral content, and further analysis of the ones from Aquitaine Variscan basement may affect the characteristics presented in this report.

Petrophysical parameters

Measurements of petrophysical properties were achieved on 57 different samples, some of which having been characterized by petrography. Ethanol porosity, bulk density and nitrogen-gas permeability has been performed (see Figure 55) and are presented below (Table 23)

Table 23: Statistical evaluation of ethanol porosity, permeability and bulk density performed on gneiss, quartzite and schists in the Variscan basements of Paris and Aquitaine basins.

Ethanol Porosity (%)					
Rock type	**Mean**	**Min.**	**Max.**	**Std.**	**n**
Gneiss	5.55	2.58	10.82	2.69	8
Quartzite	1.78	0	3.65	1.25	8
Schists	0.84	0.11	2.44	0.50	41
Permeability (m^2)					
Gneiss	1.06×10^{-15}	2.79×10^{-16}	2.98×10^{-15}	9.89×10^{-16}	6
Quartzite	1.82×10^{-15}	2.73×10^{-16}	9.22×10^{-15}	3.29×10^{-15}	7
Schists	1.32×10^{-15}	7.11×10^{-17}	2.12×10^{-14}	3.78×10^{-15}	32
Bulk Density (kg/m^3)					
Gneiss	2741.1	2660.3	2942.7	107.5	6
Quartzite	2673.0	2647.7	2710.3	28.8	5
Schists	2765.8	2014.2	3051.5	147.5	35

As one can see in the following graphs (Figure 55), several aspects can be pointed out:

- porosity seems to be partly determined by rock type since gneiss has much higher porosity than quartzite and schists;
- density profiles reproduce quite well the values commonly observed in nature (gneiss: 2600-2900 kg/m^3; schists: 2700-2800 kg/m^3; quartzite: 2600-2700 kg/m^3);
- permeability ranges are not highly influenced by lithology with low values measured in most of the samples.

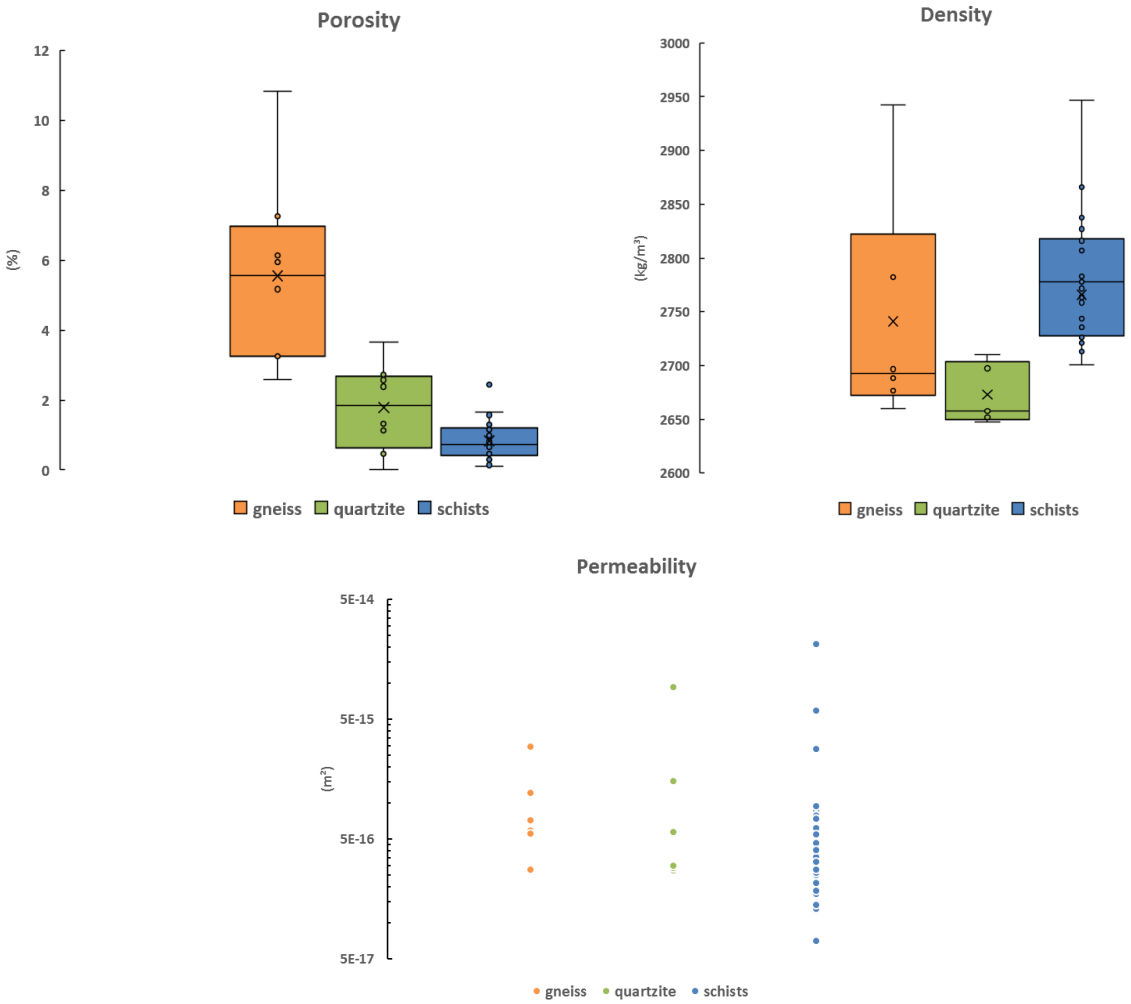

Figure 55: Results of petrophysical properties (porosity, bulk density and permeability) measured in gneiss, quartzite, and schists from the Variscan basements of the Paris and Aquitaine basins.

Magnetic properties

Measurements of magnetic susceptibility (see Figure 56) were achieved on 43 different samples, some of which having been characterized by petrography which can lead to further investigations to precise the influence of mineralogy on magnetic properties. The results are presented below (Table 24).

Table 24: Statistical evaluation of magnetic susceptibility performed on gneiss, quartzite and schists in the Variscan basements of Paris and Aquitaine basins.

Magnetic Susceptibility (SI)					
Rock type	**Mean**	**Min.**	**Max.**	**Std.**	**n**
Gneiss	1.62E-05	1.38E-05	1.88E-05	1.86E-06	5
Quartzite	1.76E-05	7.58E-06	4.82E-05	1.58E-05	6
Schists	3.76E-05	-9.05E-07	7.48E-05	1.95E-05	32

Figure 56 depicts the results of magnetic susceptibility obtained for the different rock types. Most of the samples are paramagnetic except one diamagnetic with negative data (lower value of the schists rock type). As explained in the part "Reservoir sample results", the contribution to the magnetic signal is mainly carried by the matrix, since $K < 30 \times 10^{-5}$ SI and that the principal mineralogy is made of phyllosilicates rocks (Rochette, 1987).

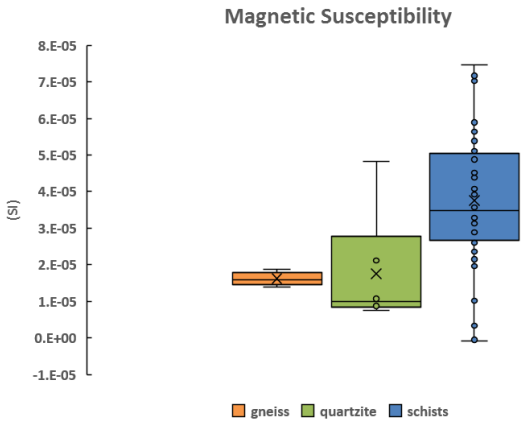

Figure 56: Results of magnetic susceptibility measured in gneiss, quartzite, and schists from the Variscan basements of the Paris and Aquitaine basins.

3. CONCLUSION AND OUTLOOK

The investigation and measurements of petrophysical and mechanical properties as presented here, focusses on the sample scale of centimeters to meters only. For further reservoir characterization, these results need to be combined with additional medium- to larger scale investigations as e.g. borehole geophysics, hydraulic well tests, structural and fracture network analyses in well logs and outcrops and finally geophysical surveys as e.g. 2D or 3D seismics, gravimetry, magnetics or resistivity (cf. Dezayes *et al.*, 2017).

In total 540 samples from the four Variscan demo sites and their respective outcrop analogue areas have been analyzed for their petrophysical properties summing up to 3770 measurements. The geochemical or mineralogical characteristics were determined with thin section analysis or XRD and XRF measurements on 264 of the abovementioned samples already. Further investigation is still ongoing.

The fracture network and its properties, which play a key role in EGS, can for example be analyzed from thin section to the decametric scale for all of the four main Variscan reservoir types. Deformation and the alteration processes determined by thin section analyses for the reservoir (and analogue samples) need to be confirmed at large scale by analysing:

- The fracture densities and their relation to the deformation process at thin section scale. Such a study will help to evaluate, if the deformation process and the alteration occurred in some areas are of significance at large scale.
- The fracture density, the impact of the structural heritage and its impact on petrophysical properties.

The results will be transposed to and compared with the respective demo-site reservoirs and their outcrop analogues. This serves to develop numerical models to quantify the capabilities of the envisaged geothermal reservoirs for improving or developing exploitation strategies, for estimating production rates and life cycles. Furthermore, the results help to better understand the reservoir rocks behavior and should be transferable to similar geological setting depending on the nature of the rock and the geological context.

The following deliverables of MEET will complete and reuse the results presented in this deliverable by focusing on:

- The construction of a 2D/3D models of fluid circulation for each sites and integrate petrophysical, petrographic (fluid/rock interaction) and mechanical data to these models (deliverable 5.6: *Static and dynamic geothermal models of the four Variscan reservoir types at reservoir scale or as conceptual models*, M40)
- The petrographic data, especially on the structural and geochemical (XRF, ICP-MS) nature of vein mineralizations should allow to adapt the stimulation measure which should be applied accordingly (deliverable 5.7: *Strategies and recommendations for stimulation operations for the four Variscan reservoir types*, M41).
- The fracture evolution by characterizing fault zones in term of petrophysical properties, petrographic properties (fluid/rock interaction) and deformation. Indeed fractures acting

initially as fluid pathways can due to ongoing mineralization evolve to a barrier and might change the whole behavior of the reservoir over time (deliverable 5.8: *Report on long-term sustainability of fractured rock system based on laboratory experiments*, M41).

The final deliverable (5.9: *Field-based characterization of the four reservoir types completed*, M41) will integrate the multiple scale datasets for each site to create comprehensive reservoir models. These models should include the fracture network characteristics with different fracture set and host rock properties and structural styles in which the fluids are expected to circulate. Ideally these characteristic datasets will be validated by hydraulic reservoir tests.

4. REFERENCES

Achtziger-Zupančic, P., Loew, S., Mariéthoz, G (2017): A new global database to improve predictions of permeability distribution in crystalline rocks at site scale. J. Geophys. Res. Solid Earth, 122, 3513–3539, doi:10.1002/2017JB014106.

Aretz, A., Bär, K., Götz, A.E., Sass, I. (2015): Outcrop analogue study of Permocarboniferous geothermal sandstone reservoir formations (northern Upper Rhine Graben, Germany): Impact of mineral content, depositional environment and diagenesis on petrophysical properties, Int. J. Earth Sci. (Geol. Rundsch.), 135, 1431–1452, http://dx.doi.org/10.1007/s00531-015-1263-2.

ASTM D2664-04 (2004): Standard Test Method for Triaxial Compressive Strength of Undrained Rock Core Specimens Without Pore Pressure Measurements (Withdrawn 2005), ASTM International, West Conshohocken, PA, 4 pp., DOI: 10.1520/D2664-04.

ASTM D2845-08 (2008): Standard Test Method for Laboratory Determination of Pulse Velocities and Ultrasonic Elastic Constants 730 of Rock, ASTM International, West Conshohocken, PA, USA, 7 pp., DOI: 10.1520/D2845-08.

ASTM D3148-02 (2002): Standard Test Method for Elastic Moduli of Intact Rock Core Specimens in Uniaxial Compression, ASTM International, West Conshohocken, PA, USA, 6 pp., DOI:10.1520/D3148-02.

ASTM D3967-16 (2016). Standard Test Method for Splitting Tensile Strength of Intact Rock Core Specimens, ASTM International, West Conshohocken, PA, USA, 5 pp., DOI:10.1520/D3967-16.

ASTM D4525-13e2 (2013): Standard Test Method for Permeability of Rocks by Flowing Air, ASTM International, West Conshohocken, PA, USA, 5 pp., DOI: 10.1520/D4525-13E02.

ASTM D4543-19 (2019): Standard Practices for Preparing Rock Core Specimens and Determining Dimensional and Shape Tolerances, ASTM International, West Conshohocken, PA, USA, 13 pp., DOI: 10.1520/D4543-19.

ASTM D6539-13 (2013): Standard Test Method for Measurement of the Permeability of Unsaturated Porous Materials by Flowing 745 Air , ASTM International, West Conshohocken, PA, 10 pp., DOI: 10.1520/D6539-13.

ASTM D7012-14 (2014): Test methods for compressive strength and elastic moduli of intact rock corespecimens under varying states of stress and temperatures, ASTM International, West Conshohocken, PA, USA, 9 pp., http://dx.doi.org/10.1520/D7012-14.

Autran, A., & Cogné, J. (1980). La zone interne de l'orogène varisque dans l'Ouest de la France et sa place dans le développement de la chaîne hercynienne. Mémoire du BRGM, (108), 191–202.

Autran *et al.*, in Keppie. (1994): Pre-Mesozoic Geology in France and related areas. (J. D. Keppie, J. Chantraine, J. Rolet, D. S. Santallier, & A. Piqué, Eds.). Springer-Verlag.

Baptiste, J., Martelet, G., Faure, M., Beccaletto, L., Reninger, P.-A., Perrin, J., & Chen, Y. (2016): Mapping of a buried basement combining aeromagnetic, gravity and petrophysical data: The substratum of southwest Paris Basin, France. Tectonophysics, 683, 333–348.

Bär, K. M.: Untersuchung der tiefengeothermischen Potenziale von Hessen. PhD Thesis, TU Darmstadt. http://nbn-resolving.de/urn:nbn:de:tuda-tuprints-30671, 2012.

Bär, K., Hintze, M., Weinert, S., Sippel, J., Freymark, J., Scheck-Wenderoth, M., Sass, I. (2016): Das Verbundprojekt Hessen 3D 2.0. Geothermische Energie 85(3): 24-25.

Bär, K., Reinsch, T., Bott, J. (2019a): P³ - PetroPhysical Property Database. V. 1.0. GFZ Data Services. Potsdam. http://dx.doi.org/10.5880/GFZ.4.8.2019.P3

Bär, K., Mielke, P., Knorz, K. (2019b): Petrographic classification table (Petrography): P³ - Petrography. V. 1.0. GFZ Data Services. Potsdam. http://dx.doi.org/10.5880/GFZ.4.8.2019.P3.p

Bär, K., Mielke, P. (2019): Stratigraphic classification table (Stratigraphy): P³ - Stratigraphy. V. 1.0. GFZ Data Services. Potsdam. http://dx.doi.org/10.5880/GFZ.4.8.2019.P3.s

Bates, R. L., Jackson, J. A. (1987): Glossary of geology, Third Edition, American Geological Institute, Alexandria, Virginia, USA.

Beyssac, O., Goffe, B., Chopin, C., & Rouzaud, J. N. (2002): Raman spectra of carbonaceous material in metasediments: a new geothermometer. Journal of Metamorphic Geology, 20(9), 859–871.

Beyssac, O., Goffé, B., Petitet, J.-P., Froigneux, E., Moreau, M., & Rouzaud, J.-N. (2003): On the characterization of disordered and heterogeneous carbonaceous materials by Raman spectroscopy. Spectrochimica Acta Part A: Molecular and Biomolecular Spectroscopy, 59(10), 2267–2276.

Bourrouilh, R. (2012): The Aquitaine Basin and the Pyrenees: geodynamical evolution and hydrocarbons. Regional Geology and Tectonics: Phanerozoic Passive Margins, Cratonic Basins and Global Tectonic Maps.

Brinckmann, J., Brüning, U. (Eds.) (1986): Das Bundesbohrprogramm im West-Harz, paläogeographische Ergebnisse (The federal drilling program in the Western Harz Mountains: paleogeographic results and five additional contributions to the geology of the Western Harz Mountains), Geol Jahrb Reihe D, Band D.

Buntebarth, G. (1980): Geothermie, Springer Berlin Heidelberg, 1, 156 pp., doi:10.1007/978-3-662-00910-9, 1980.

Burlet, Ch., Vanbrabant, Y., Piessens, K., Welkenhuysen, K., Verheyden, S. (2015): Niphargus: A silicon band-gap sensor temperature logger for High-precision environmental monitoring. Computers & Geosciences, 74, 54-59. DOI: 10.1016/j.cageo.2014.10.009

Cermak, V., Rybach, L. (1982): Thermal properties, in: Angenheister, G., Cermák, V., Hellwege, K.-H., Landolt, H. (Eds.), 310–314: Zahlenwerte und Funktionen aus Naturwissenschaft und Technik: Neue Serie. = Numerical Data and Functional Relationships in Science and Technology: New Series, c. Landolt-Börnstein - Group V Geophysics. Springer, Berlin.

Chamberlin, D., Boyce, R. (1974): Sequel: a structured English query language, Proceedings of the1974 ACM SIGFIDET(now SIGMOD) Workshop on Data Description, Access and Control, New York, 149–264.

Clauser, C., Huenges, E.: Thermal Conductivity of Rocks and Minerals. American Geophysical Union, 105 pp, http://dx.doi.org/10.1029/RF003p0105, 1995.

Clauser, C. & Huenges, E.: Thermal Conductivity of Rocks and Minerals. – Rock Physics and Phase Relations, A Handbook of Physical Constants. AGU Reference Shelf 3: 105-126, American Geophysical Union, Washington, 1995.

Clark, S. P. (1966): Handbook of physical constants (Bd. 97). Geological Society of America. doi: 10.1130/MEM97

Codd, E. F. (1970): A Relational Model of Data for Large Shared Data Banks, Communications of the ACM, 13, 377–387, doi:10.1145/362384.362685, http://dx.doi.org/10.1145/362384.362685

Cohen, K.M., Finney, S.C., Gibbard, P.L. & Fan, J.-X.(2013, updated): The ICS International Chronostratigraphic Chart, Episodes, 36: 199–204, 2013.

CrowdFlower, (2016): Data Scientist Report: https://visit.figure-eight.com/rs/416-ZBE-142/images/CrowdFlower_DataScienceReport_2016.pdf, 2016, last access: 26 February 2020.Descamps *et al.*, 2013,

Devaraju, A., Klump, J., Cox, S.J.D., Golodoniuc, P. (2016): Representing and publishing physical sample descriptions, Computers & Geosciences, 96, 1-10, http://dx.doi.org/10.1016/j.cageo.2016.07.018.

Dezayes, C. and the IMAGE working group (2017): Proposition for integrated exploration method in sedimentary basin context. Public deliverable IMAGE-D8.05 of the project IMAGE Integrated Methods for Advanced Geothermal Exploration Grant Agreement Number 608553.

DIN 18141-1:2014-05 (2014): Baugrund - Untersuchung von Gesteinsproben - Teil 1: Bestimmung der einaxialen Druckfestigkeit, Beuth, 14 pp., https://dx.doi.org/10.31030/2100323.

Enge, H.D., Buckley, S.J., Rotevatn, A., Howell, J.A. (2007): From outcrop to reservoir simulation model: workflow and procedures. Geosphere, 3, 469–490, http://dx.doi.org/10.1130/GES00099.1.

Filomena, C. M., Hornung, J., and Stollhofen, H. (2014): Assessing accuracy of gas-driven permeability measurements: a comparative study of diverse Hassler-cell and probe permeameter devices, Solid Earth, 5, 1–11, https://doi.org/10.5194/se-5-1-2014.

Fisher, R. V., Smith, G. A. (1991): Volcanism, tectonics and sedimentation, 1-5. Sedimentation in volcanic settings, Society for Sedimentary Geology, Special Publication No. 45.

Gard, M., Hasterock D., and Halpin, J. (2019): Global whole-rock geochemical database compilation, Earth Syst. Sci. Data, 11, 1553–1566, https://doi.org/10.5194/essd-11-1553-2019

Gard, M., Hasterok, D., and Halpin, J.: Global wholerock geochemical database compilation (Version 1.0.0), https://doi.org/10.5281/zenodo.2592823, 2019a.

Gillespie, M. R., Styles, M. T.: Classification of igneous rocks, BGS Rock Classification Scheme, Volume 1, British Geological Survey, Research Report Number RR 99-06, Nottingham, UK, 1999.

Grecksch, G., Ortiz, A. and Schellschmidt, R.: HDR project Soultz - thermophysical study of GPK2 and GPK3 granite samples. ZIP Vorhaben "Hot-Dry-Rock-Project Soultz - Hydrogeothermische Modellierung des HDR-Wärmetauschers" (Förderkennzeichen: 0327109B), "Hot Dry Rock Energy" (EC contract ENK5-CT-2000-00301), 2003.

Guillocheau, F., Robin, C., Allemand, P., Bourquin, S., Brault, N., Dromart, G., Grandjean, G. (2000): Meso-Cenozoic geodynamic evolution of the Paris Basin: 3D stratigraphic constraints. Geodinamica Acta, 13(4), 189–245.

Haffen, S., Geraud, Y., Diraison, M. and Dezayes, C.: Determination of fluid-flow zones in a geothermal sandstone reservoir using thermal conductivity and temperature logs. Geothermics, 46, 32-41. doi:10.1016/j.geothermics.2012.11.001, 2013.

Hallsworth, C. R., Knox, R. W. O'B. (1999): Classification of sediments and sedimentary rocks, BGS Rock Classification Scheme, Volume 3, British Geological Survey, Research Report Number RR 99-03, Nottingham, UK.

Hantschel, A.I. & Kauerauf, T. (2009): Fundamentals of Basin and Petroleum Systems Modeling, 476 pp, Springer Verlag, Berlin Heidelberg, http://dx.doi.org/10.1007/978-3-5-540-72318-9_1, 2009.

Hoffmann, H.R.A. (2015): Petrophysikalische Eigenschaften der Mitteldeutschen Kristallinschwelle im Bereich des Oberrheingrabens. unpubl. Masterthesis, TU Darmstadt, XVI + 150 pp., 55 fig., 34 Tab., 3 App.

Hornung, J. and Aigner, T. (2004): Sedimentäre Architektur und Poroperm-Analyse fluviatiler Sandsteine: Fallbeispiel Coburger 875 Sandstein, Franken, Hallesches Jahrb. Geowiss, Reihe B, Beiheft 18, 121–138.

International Society for Rock Mechanics Commission on Standardization of Laboratory and Field Tests (1978): Suggested Methods for Determining Tensile Strength of Rock Materials. Int J Rock Mech Min Sci & Geomech. Abstr. Vol 15, pp 99-103

Jaritz, R. (1999): Quantifizierung der Heterogenität einer Sandsteinmatrix am Beispiel des Stubensandstein (Mittlerer Keuper, Württemberg), Tübinger Geol. Abhandlungen, C, 48, 104 pp.

Klinkenberg, L. J. (1941): The permeability of porous media to liquids and gases, Drilling Production Practice, API, 200–213.

Kuschnir, A.R.L., Heap, M.J., Baud, P, Gilg, H.A., Reuschlé, T., Lerouge, C., Dezayes, C., Duringer, P., (2018): Characterizing the physical properties of rocks from the Paleozoic to Permo-Triassic transition in the Upper Rhine Graben. Geotherm Energy, 6, 16, https://doi.org/10.1186/s40517-018-0103-6

Landolt-Börnstein - Springer Materials: the Landolt-Börnstein database (www.springermaterials.com)

Lefort, J. P., & Agarwal, B. N. P. (1999): Of what is the centre of the Ibero-Armorican arc composed? Tectonophysics, 302(1–2), 71–81.

Lehnert, K., Vinayagamoorthy, S., Djapic, B., J. Klump (2006): The Digital Sample: Metadata, Unique Identification, and Links to Data and Publications, EOS, Transactions, American Geophysical Union, 87(52, Fall Meet. Suppl.), Abstract IN53C–07.

Le Bas, M. J., Streckeisen, A. L. (1991): The IUGS systematics of igneous rocks, J. Geol. Soc. London, 148, 825- 833.

Le Maitre, R.W., Streckeisen, A. (2003): Igneous rocks: a classification and glossary of terms – recommendations of the International Union of Geological Sciences Subcommission on the Systematics of Igneous Rocks. 2. Edition. Cambridge University Press, Cambridge.

LeDesert, B.: Fracturation et paléocirculations hydrothermales. Application au granite de Soultz-sous-Forêts. Ph.D. dissertation, 1993.

Lepique, M. (2008): Empfehlung Nr. 10 des Arbeitskreises 3.3 “Versuchstechnik Fels” der Deutschen Gesellschaft für Geotechnik e. V.: Indirekter Zugversuch an Gesteinsproben – Spaltzugversuch, Bautechnik, 85, 623–627, DOI: 10.1002/bate.200810048.

Lippmann, E. and Rauen, A. (2009): Measurements of Thermal Conductivity (TC) and Thermal Diffusivity (TD) by the Optical 930 Scanning Technology, Lippmann and Rauen GbR, Schaufling, Germany, 49 pp.

Liolios, P., and Exadaktylos, G. (2011): A relational rock mechanics database scheme with a hierarchical structure, Computers & Geosciences, 37: 1192-1204, http://dx.doi.org/10.1016/j.cageo.2011.02.014.

Louis, L., David, C., & Robion, P. (2003): Comparison of the anisotropic behaviour of undeformed sandstones under dry and saturated conditions. Tectonophysics, 370(1), 193–212.

Maire, R. (2014): Investigation of thermo-physical and mechanical parameters of crystalline geothermal reservoir rocks of the Upper Rhine Graben (Germany). – unpubl. Masterthesis, TU Darmstadt und Institute Polytechnique LaSalle Beauvais (Frankreich), 234 pp., 67 fig., 20 Tab., 10 App.

Matte, P., & Hirn, A. (1988): Seismic signature and tectonic cross section of the Variscan Crust in western France. Tectonics, 7(2), 141–155.

MEET Deliverable 3.4: Trullenque, G. (Ed.): Deliverable 3.4 - Evaluation of Crystalline Outcrop Aanalogue, WP3: Upscaling of Thermal Power Production and Optimized Operation of EGS Plants. Public Deliverable of the EU-H2020 Project MEET, 26 pp.

MEET Deliverable 5.2: Bär, K. (Ed.), Afshari Moein, M., Burlet, C., Leiss, B., Reinecker, J., Turan, A., Trullenque, G., Wagner, B., Vanbrabant, Y., Sosa, G., Ford, K., Rybacki, E., Milsch, H., Herrmann, J., Sengelen, X., Hébert, R., Ledésert, B.: Deliverable 5.2 – Sample Acquisition completed, WP5: Variscan Geothermal Reservoirs (Granitic and Metamorphic Rocks). Public Deliverable of the EU-H2020 project MEET, 31 pp.

MEET Deliverable 5.3: Reinecker, J. and Bär, K. (Eds.), Schulz, K., Genter, A., Hehn, R., Ravier, G., Dalmais, É.: Deliverable 5.3 – Strategy and Stimulation Design for Chemical Stimulation at UDDGP Project, WP5: Variscan Geothermal Reservoirs (Granitic and Metamorphic Rocks), Task 5.3: Demonstration of EGS Reservoir Stimulation at the UDDGP Project in Cornwall. Confidential Deliverable of the EU-H2020 project MEET, 25 pp.

MEET Deliverable 5.4: Trullenque, G. (Ed.), Bär, K., Turan, A., Schulz, K., Leiss, B., Ford, K., Reinecker, J., Vanbrabant, Y.: Deliverable 5.4 – Evaluation of Outcrop Analogues of the four Variscan Reservoir Types, WP5: Variscan Geothermal Reservoirs (Granitic and Metamorphic Rocks). Public Deliverable of the EU-H2020 project MEET, 47pp.

Mégnien, C. (1980): Synthèse géologique du bassin de Paris (Vol. 3). BRGM.

Mielke, P., Bär, K., Sass, I. (2017): Determining the relationship of thermal conductivity and compressional wave velocity of common rock types as a basis for reservoir characterization, J. Appl. Geophys., 140, 135-144, http://dx.doi.org/10.1016/j.jappgeo.2017.04.002.

Mortimer, N. (2005): PETLAB: New Zealand's rock and geoanalytical database. Geological Society of New Zealand Newsletter 136, 27–31.

Mutschler, T. (2004): Neufassung der Empfehlung Nr. 1 des Arbeitskreises "Versuchstechnik Fels" der Deutschen Gesellschaft für Geotechnik e. V.: Einaxiale Druckversuche an zylindrischen Gesteinsprüfkörpern, Bautechnik, 81, 825-834, doi: 10.1002/bate.200490194.

Paris, F. & Le Pochat, G., in Keppie (1994): Pre-Mesozoic Geology in France and related areas. (J. D. Keppie, J. Chantraine, J. Rolet, D. S. Santallier, & A. Piqué, Eds.). Springer-Verlag.

Paris, F., Le Pochat, G., & Pelhate, A. (1988): Le socle paléozoïque nord-aquitain : caractéristiques principales et implications géodynamiques. C. R. Acad. Sc. Paris, Série II, 306, 597–602.

Pei, L., Rühaak,W., Stegner, J., Bär, K., Homuth, S., Mielke, P., Sass, I. (2014): Thermo-Triax: an apparatus for testing petrophysical properties of rocks under simulated geothermal reservoir conditions. Geotech. Test. J. 38 (1):20140056. http://dx.doi.org/10.1520/GTJ20140056.

Popov, Y. A., Pribnow, D. F., Sass, J. H., Williams, C. F. and Burkhardt, H. (1999): Characterization of rock thermal conductivity by high-resolution optical scanning. Geothermics, 28, 253-276. doi:10.1016/S0375-6505(99)00007-3.

Popov, Y., Beardsmore, G, Clauser, C. and Roy, S. (2016): ISRM Suggested Methods for Determining Thermal Properties of Rocks from Laboratory Tests at Atmospheric Pressure, Rock Mech Rock Eng, 49, 4179-4207, https://doi.org/10.1007/s00603-016-1070-5.

Prijac, C., Doin, M. P., Gaulier, J. M., & Guillocheau, F. (2000): Subsidence of the Paris Basin and its bearing on the late Variscan lithosphere evolution: A comparison between Plate and Chablis models. Tectonophysics, 323(1–2), 1–38.

Ringrose, P., and Bentley, M. (2015): Reservoir Model Design, Springer Netherlands, 249 p., http://dx.doi.org/10.1007/978-94-007-5497-3.

Robardet, M., Bouyx, E., Lardeux, H., Herisse, A. L. E., Menn, J. L. E., Melou, M., … Weyant, M. (1993): Paléogéographie de l'Europe occidentale de l'Ordovicien au Dévonien. Bull. Soc. Géol. Fr., 164(5), 683–695.

Robertson S. (1999): Classification of metamorphic rocks, BGS Rock Classification Scheme, Volume 2, British Geological Survey, Research Report Number RR 99-02, Nottingham, UK.

Rochette, P. (1987): Magnetic susceptibility of the rock matrix related to magnetic fabric studies. Journal of Structural Geology, 9(8), 1015–1020.

Rosener, M.: Etude pétrophysique et modélisation des effets des transferts thermiques entre roche et fluide dans le contexte géothermique de Soultz-sous-Forêts. Ph.D. dissertation, Université Louis Pasteur-Strasbourg I. available at: https://tel.archives-ouvertes.fr/tel-00202959/, 2007.

Rosener, M., Géraud, Y. (2007): Using physical properties to understand the porosity network geometry evolution in gradually altered granites in damage zones. Geol. Soc. Lond. Spec. Publ. 284, 175–184. https://doi.org/10.1144/SP284.12

Rühaak, W. Guadagnini, A., Geiger, S., Bär, K., Gu, Y., Aretz, A., Homuth, S., Sass, I. (2015): Upscaling thermal conductivities of sedimentary formations for geothermal exploration, Geothermics 58, 49-61, http://dx.doi.org/10.1016/j.geothermics.2015.08.004.

Rummel, F.: Physical properties of the rock in the granitic section of borehole GPK1, Soultz-sousforets. Geothermal Energy in Europe: The Soultz Hot Dry Rock Project, 199-216, 1992

Rummel, F. and Schreiber, D.: Physical properties of the core K21, borehole GPK1, Soultz-sous-Forêts, depth interval 3522.58-3525.88 m. Yellow Report 12, Ruhr-Universität Bochum, 1993.

Rybach, L., Bassetti, S., Baumgärtner, R., Rohner, E. and Schärli, U. (2003): Projekt Drahtloser Minidatenlogger für Temperaturmessungen in Erdwärmesonden. Schlussbericht.

Sanjuan, B., Millot, R., Innocent, Ch., Dezayes, Ch., Schiber, J., Brach, M. (2016): Major geochemical characteristics of geothermal brines from the Upper rhine Graben granitic basement with constraints on temperature and circulation. – Chemical Geology 428, 27-47. http://dx.doi.org/10.1016/j.chemgeo.2016.02.021

Scheidegger, A. E. (1974): The Physics of Flow Through Porous Media, 3rd ed., Univ. of Toronto Press, Toronto, Ont., Canada, 1000 372 pp.

Schmid, R. (1981): Descriptive nomenclature and classification of pyroclastic deposits and fragments: Recommendations of the IUGS Subcommission on the Systematics of Igneous Rocks, Geology, 9, 41- 43, 1981.

Schön, J.H. (2004): Physical Properties of Rocks: Fundamentals and Principles of Petrophysics, In: Handbook of Geophysical Explorations, Section I, Seismic Exploration: V.18. - Redwood Books, Trowbridge.

Schön, J.H. (2011): Physical Properties of Rocks: A Workbook, In: Handbook of Petroleum Exploration and Production.

Schön, J.H. (Ed.) (2015): Physical properties of rocks: Fundamentals and principles of petrophysics, Developments in petroleum science, 65. Elsevier, Amsterdam Netherlands, 1 online resource.

Schulz, K. (2020): Analysis of permeability enhancement by chemical treatment in fractured granite (Cornubian Batholith) for the United Downs Deep Geothermal Power project. Unpublished M.Sc. thesis Technical University of Darmstadt. 151 p.

Scibek, J. (2020): Multidisciplinary database of permeability of fault zones and surrounding protolith rocks at world-wide sites. Scientific Data, 7:95. https://doi.org/10.1038/s41597-020-0435-5

Setaram Instrumentation (2009): K/C80-1A C80 Commissioning, Setaram Instrumentation KEP Technologies, Caluire, France:, 52 pp.

Simons, B., Shail, R., Andersen, J. (2016): The petrogenesis of the Early Permian Variscan granites of the Cornubian Batholith: Lower plate post-collisional peraluminous magmatism in the Rhenohercynian Zone of SW England. Lithos(260), 76-94. https://doi.org/10.1016/j.lithos.2016.05.010

Sizun, J. P.:Modification des structures de porosité de grès lors de transformations petrographiques dans la diagenese et l'hydrothermalisme. Ph.D. dissertation, Institut de Geologie Strasbourg, Université Louis Pasteur, Strasbourg, France, 1995.

Stober, I. & Jodocy, M. (2011): Hydrochemie der Tiefenwässer im Oberrheingraben - Eine Basisinforma-tion für geothermische Nutzungssysteme. - Z. geol. Wiss., 39: 39-57. Berlin.

Stober, I.; Bucher, K. (2015): Hydraulic and hydrochemical properties of deep sedimentary reservoirs of the Upper Rhine Graben, Europe. Geofluids 15, 464–482.

Strong, D., Turnbull, R., Haubrock, S., and Mortimer, N. (2016): Petlab: New Zealand's national rock catalogue and geoanalytical database, New Zealand J. Geol. Geophys., 53, 475–481, http://dx.doi.org/10.1080/00288306.2016.1157086.

Surma, F.: Détermination de la porosité des zones endommagées autour des failles et rôle de l'état du matériau sur les propriétés d'echange fluides-roches: minéralogie, structures de porosité, caractéristiques mécaniques. Ph.D. dissertation, Université Louis Pasteur (Strasbourg), 2003.

Surma, F., Geraud, Y. (2003): Porosity and Thermal Conductivity of the Soultz-sous-Forêts Granite. Pure Appl. Geophys. 160, 1125–1136. https://doi.org/10.1007/PL00012564

Tanikawa, W., and Shimamoto, T. (2008): Comparison of Klinkenberg corrected gas permeability and water permeability in sedimentary rocks, Int. J. Rock Mech. Min. Sci., 46, 229–238, doi:10.1016/j.ijrmms.2008.03.004.

Vernoux, J. F. and Lambert, M.: Rapport BRGM SGN/IRG ARG 93 T37. Tech. rep., BRGM, 1993.

Vernoux, J. F., Genter, A., Razin, P., Vinchon, C., Orléans, B. R. and Nord-Pas de Calais, B. R.: Geological and petrophysical parameters of a deep fractured sandstone formation as applied to geothermal exploitation. BRGM Report, 38622, 70. available at: http://infoterre.brgm.fr/rapports/RR-38622-FR.pdf, 1995.

Villeneuve, M., Heap, M.J., Kushnir, A.R.L., Qin, T., Baud, P., Zhou, G., Xu, T. (2018): Estimating in situ rock mass strength and elastic modulus of granite from the Soultz-sous-Forêts geothermal reservoir (France). Geotherm Energy 6, 11. https://doi.org/10.1186/s40517-018-0096-1

Weinert, S., Bär, K., Sass, I. (2020, in review): Petrophysical Properties of the Mid-German Crystalline High: A Database for Bavarian, Hessian, Rhineland-Palatinate and Thuringian Outcrops. TUDatalib

Welsch, B., Bär, K., Rühaak, W., Sass, I. (2014): An Outcrop Analogue Study on the Suitability of Crystalline Rocks as Heat Storage Media. In: Röhling, H-G., Zulauf, G. (ed.) – GeoFrankfurt 2014 – Dynamik des Systems Erde / Earth Systems Dynamics, Abstract Volume. Schriftenreihe der Deutschen Gesellschaft für Geowissenschaften, Heft 85, p.546

Weydt, L.M., Ramírez-Guzmán, Á,A., Pola, A., Lepillier, B., Kummerow, J., Mandrone, G., Comina, C., Deb, P., Norini, G., Gonzalez-Partida, E., Avellán, D.R., Macías, J-L., Bär, K., Sass, I. (2020): Petrophysical and mechanical rock property database of the Los Humeros and Acoculco geothermal fields (Mexico). ESSD Discussions, essd-2020-139. (submitted)

Wilkinson, M., Dumontier, M., Aalbersberg, I. *et al.*: The FAIR Guiding Principles for scientific data management and stewardship. Sci Data 3, 160018 doi: 10.1038/sdata.2016.18, 2016.

Zoback, M.D. (2011): Reservoir geomechanics, 5. Cambridge Univ. Press, Cambridge, 449 pp.

5. APPENDIX

5.1 LIST OF NOBLE HILLS OUTCROP ANALOGUE SAMPLES (DIGITAL ONLY)

5.2 LIST OF CORNWALL OUTCROP ANALOGUE SAMPLES (DIGITAL ONLY)

5.3 P³2MEET DATABASE (DIGITAL ONLY)

Imprint

Project Lead	ES-Géothermie 26 boulevard du Président Wilson 67932 Strasbourg Cedex 9, FRANCE https://geothermie.es.fr/en/	
Project Coordinator	Dr Albert Genter albert.genter@es.fr	Eléonore Dalmais eleonore.dalmais@es.fr
Scientific Manager	Dr Ghislain Trullenque Ghislain.TRULLENQUE@unilasalle.fr	
Project Manager	Dr Jean Herisson jherisson@ayming.com	
Project Website	https://www.meet-h2020.com/	
LinkedIn page	https://www.linkedin.com/in/meet-eu-project/	
Report Authorship	Bär K., Arbarim R., Turan A., Schulz K., Mahmoodpour S. (TUDa), Leiss B. (UEG, UGOE), Wagner B. (UGOE, UEG), Sosa G. (UGOE), Ford K. (UGOE), Trullenque G. (ULS), Klee J. (ULS), Vanbrabant Y. (GSB), Rybacki E., Milsch H., Herrmann J., Wang W. (GFZ), Sengelen X., Hébert R., Ledésert B. (CYU), (2020). Database of petrophysical and fluid properties and recommendations for model parametrization of the four Variscan reservoir types, MEET report, Deliverable D5.5, June 2020, 110 pp.	

Liability claim